Modelling and experimental verification of lizards' flexible trunks' effects on energetically efficient locomotion

GU XIAOYI

NATIONAL UNIVERSITY OF SINGAPORE

2015

Modelling and experimental verification of lizards' flexible trunks' effects on energetically efficient locomotion

GU XIAOYI

(B.Eng**)**

A THESIS SUBMITTED

FOR THE DEGREE OF MASTER OF ENGINEERING

DEPARTMENT OF BIOMEDICAL ENGINEERING

NATIONAL UNIVERSITY OF SINGAPORE

2015

Declaration

DECLARATION

I hereby declare that the thesis is my original work and it has been written by me in its entirety. I have duly acknowledged all the sources of information which have been used in the thesis.

This thesis has also not been submitted for any degree in any university previously.

Gu Xiaoyi

GU XIAOYI

17 April 2015

Acknowledgement

Foremost, I would like to express my sincere gratitude to my supervisor, Assit. Prof Yu Haoyong, for the continuous support of my master study and research, for his patience, motivation, enthusiasm and immense knowledge. His guidance helped me throughout the process to carry out the work successfully.

Besides that, I would like to thank following people for their assistance and encouragements during the process of implementing this research.

1). Dr Guo Zhao and Dr Peng Yuxin, research fellows in our group, shared their rich experience in the field of robotics with me and provided me an insightful knowledge in both master studies and robotic research.

2). Mr Chen Gong, PhD student in our group, helped me adapt to the new environment quickly and gave me a lot of suggestions to perfect this research in terms of hardware and software.

3). Mr Kyung-Ryoul Moon and Mr Francisco Anaya, PhD students in our group, taught me to use the experimental facilities and tirelessly assisted me in collecting data. Without their help, I can’t complete the research.

Contents

Summary

Compliant and flexible trunks play an important role in animals' elegant and efficient locomotion, which is neglected by most existing mobile robots. Getting inspiration from lizards, this research investigates effects of compliant and flexible trunks on improving robots' energy efficiency.

A simplified lizard model with a flexible trunk has been established. And simulations based on this model have been carried out to study the effects of the flexible trunk on the motor power. The simulation results indicate that this kind of flexible trunks can improve robots' energy efficiency in terms of reducing the peak power of the motor. The stiffness of the trunk and the frequency of the locomotion are two critical factors, which affect the peak power of the motor. The optimized stiffness and the optimized frequency under different conditions have been discussed. Additionally, by comparing velocities and accelerations of the model with different trunks, we can find that flexible trunks have influence on reducing the amplitude of both the velocity and the acceleration of the model, which eventually results in the decrease of the peak power.

A robot which has similar gait pattern to lizards has been designed on the principle of cost-effectiveness. This robot has been used as a test bed to verify the hypothesis and some simulation results.

Experiments have been conducted using the motion capture system. The displacement of the robot with different trunks has been recorded. Velocities, accelerations and motor powers of the robot have been calculated and analysed. Experiments have been conducted firstly to evaluate the performance of the robot. This robot has been proved to be able to follow a desired trajectory and move along a straight line when the velocity is uniform. When the velocity is variable, the robot can only perform well at the frequency of 1Hz. As a result, experiments about kinetic analysis have been conducted at the frequency of 1Hz. Experimental results suggest that flexible trunks do have effects on reducing the peak power of the motor. Besides that, trunks with different stiffness can result in different reduction rates of the peak power and flexible trunks have greater influence on the acceleration, which are consistent with simulation results.

List of Tables

List of Figures

List of Symbols

α_1 : The maximum rotational angle of the leg when the trunk is rigid.

α_2 : The maximum rotational angle of the leg when the trunk is flexible.

β : The angle between the leg and the trunk.

m, m_1, m_2 : Mass coefficient

k, k_1, k_2 : Stiffness coefficient

b_1, b_2 : Damping coefficient

x_1 : Displacement of the front part of the robot

x_2 : Displacement of the rear part of the robot

$v_1(\dot{x}_1)$: Velocity of the front part of the robot

$v_2(\dot{x}_2)$: Velocity of the rear part of the robot

$a_1(\ddot{x}_1)$: Velocity of the front part of the robot

$a_2(\ddot{x}_2)$: Velocity of the rear part of the robot

F : Force which is generated by the motor that actuate the robot

P : Motor power that is used for actuating the robot

Chapter 1: Introduction

1.1 Motivation

Nature is recognized as the best designer who has created a great diversity of biological systems which have the ability to survive in a world that is full of rapid changes and high uncertainties in a most harmonious and efficient way[1]. These biological systems are believed to have great potentials to provide abundant inspirations for engineers to design novel mechanisms or improve existing systems[2].

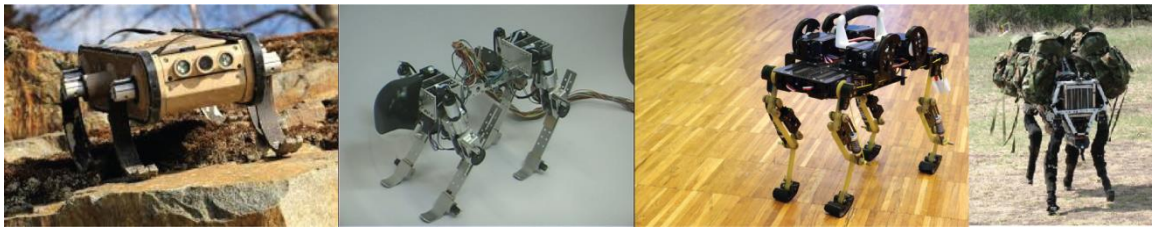

Figure 1.1 Mobile robots

In the field of robotics, bio-inspired mobile robots have been a hot topic for a long time due to its great application prospects in exploration, rescue, and military. By mimicking animals' gait or their control strategies, a large number of different bio-inspired mobile robots have been developed, e.g. RHex[3], Tekken[4], Cheetah-cup[5], BigDog, etc. These robots can walk, run, and crawl in a maneuverable manner and complete pre-defined tasks. However, in most cases, these robots are energetically inefficient compared with animals. Additionally, they are still not able to adopt the agile and elegant postures as real animals[1]. One of the most obvious reasons is that almost all researches about bio-inspired mobile robots are centered on perfecting legs' configurations or using complicated control trajectories to make robots achieve statistical and dynamical stability. Little attention has been paid to investigating the trunks' functions on robots' performance. For animals, their harmonious and energetically efficient locomotion is the outcome of the movements of both legs and trunks[6]. Their flexible and compliant trunks play a significantly important role in energetically efficient locomotion which should not be neglected. As a result, conferring flexibility and compliance on robots' trunks is believed to be a novel and reasonable avenue to improve existing mobile robots' performance.

The object of this research is lizard. The phenomenon that lizards bend their flexible trunks while moving has been validated by many biologists. As early as 1952, Snyder mentioned

that the trunk of the lizard moved horizontally to the same side as the hind legs moved when he concluded the locomotion of lizards [9]. In 1992, Ritter found that different lizards could generate different waves of bending in the trunk during locomotion[7]. In 1995, Eilam conducted a survey about the comparative morphology of locomotion in vertebrates and got the conclusion that lizards adopted diverse combinations of lateral movements and stepping [6].

Getting inspiration from lizards, this research focuses on investigating the effects of flexible trunks on energetically efficient locomotion and exploring potential applications of this feature in robot design.

1.2 Objective

The core of this research is to study effects of flexible trunks on improving mobile robots' energy efficiency. Both simulation analysis and experimental verification are required to complete this research. As a result, following objectives are needed to be achieved.

⑴. Understanding the functions of lizards' flexible trunks from a biological point of view;

⑵. Having a systematical overview of researches about bio-inspired lizard robots and robots with a flexible trunk;

⑶. Establishing a simplified lizard model which contains common characteristics of lizards;

⑷. Doing simulations on this lizard model to study the effects of flexible trunks on energy efficiency;

⑸. Designing a bio-inspired lizard robot based on the lizard model;

⑹. Carrying out experiments using the designed robot to verify the hypothesis and simulation results.

1.3 Outline

The entire research can be divided into four parts: theoretical study, modeling and simulation analysis, robot design, and experimental verification. Each part will be presented by one chapter in this thesis.

In chapter 2, the effects of lizards' flexible trunks are summarized from the aspect of biology. And the basic gait pattern of lizards is introduced. Both of them are the foundation of the following research. Studies about existing bio-inspired robots and robots with flexible trunks are summarized and compared to highlight the importance of this research.

In chapter 3, a simplified lizard model, which is adapted from other quadruped models, has been established. Based on this model, a series of simulations are performed. Simulation results are presented and analyzed. In addition, optimized results under different conditions are discussed.

In chapter 4, several designs are compared and the one which is the most consistent with the simulation model is selected to be the final version. All components of the robot are chosen based on the principle of cost-effectiveness. Both the hardware structure and the software structure are illustrated in this chapter.

In chapter 5, Experimental setups and procedures are introduced. Experiments have been conducted to test the performance of the designed robot and verify the hypothesis and part of simulation results. Experimental results under different conditions are presented and discussed.

In chapter 6, the whole research is summarized. All results and conclusions are discussed in this chapter. Additionally, some recommendations are put forward for the purpose of the further improvement of this research.

`

Chapter 2 Literature review

In this chapter, some useful biological background information about the functions of flexible trunks and the gait pattern of lizards is briefly summarized, which is the foundation of the entire research. The state of the art of bio-inspired lizard robots and robots with a flexible trunk is reviewed and introduced by listing some typical robots.

2.1 Biological background

2.1.1 Functions of flexible trunks

Generally, the flexible trunks of lizards are believed to have two fundamental functions: increasing the speed of locomotion and improving the energy efficiency.

In order to escape from predators or catch preys, almost all kind of animals need high speed of locomotion. Generally, there are two methods to achieve high velocity: (a) by increasing the stepping frequency and (b) by increasing the step length. The stepping frequency is limited by the restricted capacity of the muscles to retract and contract repeatedly[6]. Most animals choose the latter method---by increasing the step length to increase the velocity. For those animals whose body sizes are large, e.g. horse, cheetah, they can increase step length with longer legs and shorter support phase; for other animals whose body sizes are small, e.g. lizard, they rely on flexible trunks to increase the step length.

The role played by compliant and flexible trunks in increasing the step length can be interpreted from the aspect of morphology. Figure 2.1 illustrates the different step lengths resulted from trunks with different flexibility. In both figure 2.1 (a) and (b), the limit rotational angle β between the leg and the trunk keeps the same. In figure 2.1 (a), the trunk is rigid and cannot move laterally. The maximum rotational angle of the leg is α_1. In figure 2.1 (b), the trunk is flexible and is able to bend laterally, which leads to the further rotation of the leg. [8, 9] So the maximum rotational angle of the leg α_2 integrates this further rotation and α_1, which is obviously larger than α_1. In the case that the length of the leg is the same, the longest step length that can be achieved is only proportional to the maximum rotational angle. As a result, the step length in figure 2.1(b), whose trunk can bend laterally, is longer than the step length in figure 2.1 (a).

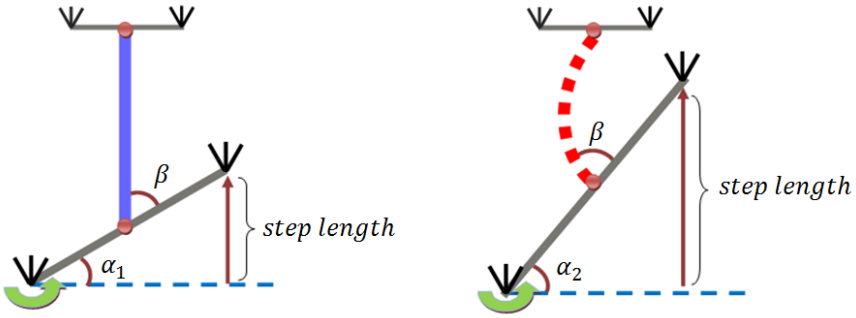

Figure 2.1 Diagram of the step length under different conditions

As for the function of lizards' flexible trunks in improving energy efficiency, there is no particular research about it. However, nearly all the biomechanical adaptations aim at achieving similar forms of locomotion in a manner that the energy efficiency is optimum[6]. Different animals adopt different methods. Lizards are believed to make use of their flexible trunks to achieve energy optimization, which is the core of this research.

2.1.2 The gait pattern of lizards [6, 10-13]

The basic pattern of movement for lizards' legs can be illustrated by a hind leg. A complete locomotion cycle of one hind leg consists of two strokes: the propulsive stroke and the recovery stroke.

The propulsive stroke (see figure 2.2):

1) It begins when the foot strikes the ground;
2) As the cycle proceeds, the leg moves backward while the foot adheres to the ground. As a result, the body would be pushed forward;
3) The stroke ends when the foot leaves the ground.

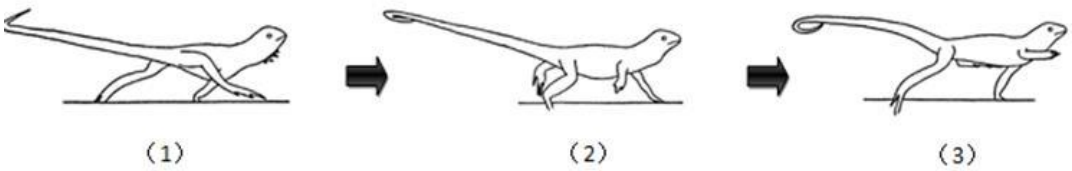

Figure 2.2 Process of the propulsive stroke

The recovery stroke (see figure 2.3):

1) It begins when the propulsive stroke ends;
2) During this stroke, the leg moves forward and the foot is lifted clear of the ground.
3) When the foot strikes the ground, the recovery stroke ends.

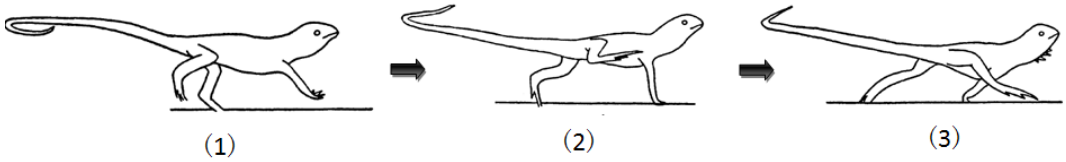

Figure 2.3 Process of the recovery stroke

2.2 State of the art

2.2.1 Bio-inspired lizard robots

Lizards have been a popular bionic object for many years because of some distinct characteristics. And some researchers have succeeded in applying these characteristics in robot design and making several prototypes.

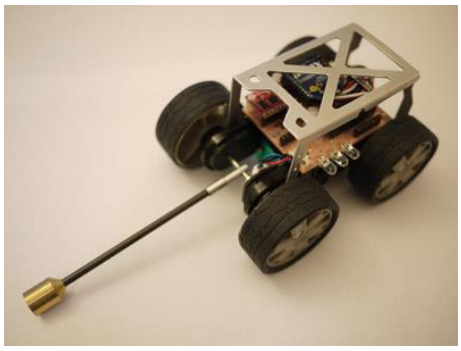

Figure 2.4 Tailbot

The most famous bio-inspired lizard robot should be the terrestrial robot, Tailbot (see figure 2.4), which was developed by researchers in University of California Berkeley [14-16]. Tailbot, which was inspired by the tail function of lizards, is able to rapidly adjust its attitude and achieve dynamic stabilization in mid-air by using an active tail and an inertial sensor. This active tail improves mobile robots' survivability in a fall and increases their abilities to cross complex terrains, which has great significance for the development of mobile robots.

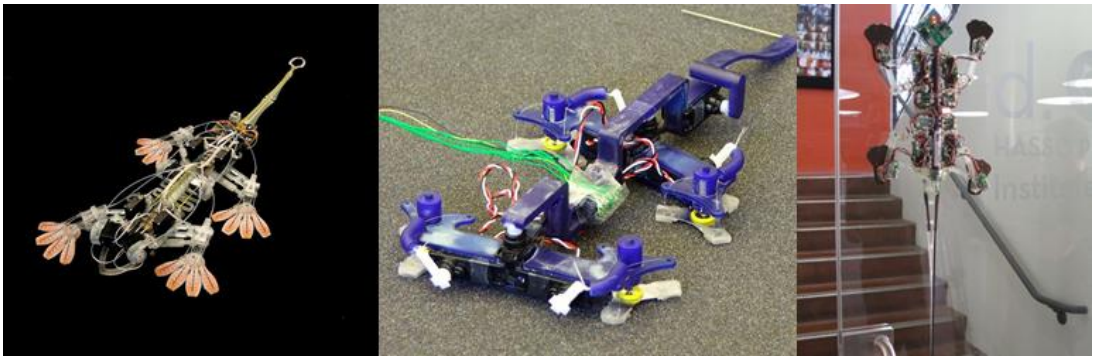

Figure 2.5 Several gecko inspired climbing robots

Designing a gecko inspired climbing robot is another very popular topic. Traditional attachment mechanisms e.g. suction adhesion, magnetic adhesion, and grasping technique, all have serious defects, which limit the development of climbing robots. The novel mechanism of the elastomer adhesive pads, which is utilized by geckos, overcomes these limitations and has been applied in several prototypes (see figure 2.5) [17-19]. These robots have been proved to be capable of climbing vertical and overhanging surfaces. This kind of climbing robots has great application prospects in many areas, e.g. inspection, repair, cleaning, and exploration.

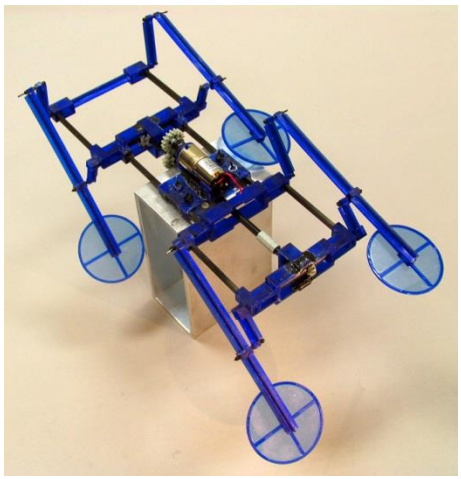

Figure 2.6 Lizard inspired water running robot

Researchers from Carnegie Mellon University have designed and developed a bio-inspired lizard robot (see figure 2.6) that can mimic the water running ability of the basilisk lizard[20, 21]. In this robot design, four bar mechanism was used as legs and a computer simulation model was created to predict the performance of the robot. In order to improve the performance of the robot, several critical parameters have been put forward and varied in both the computer model and the fabricated model. This robot is proved to be able to run on

open water. This work opens the door for development of novel legged robots which run on the water instead of traditional methods like floating or swimming.

Figure 2.7 Sand-walking robot

Based on the study of desert lizards, researchers from Georgia Institute of Technology have designed a sand-walking robot (see figure 2.7) [22-24]. Getting inspirations from desert lizards, people have equipped the robot with six C-shaped legs, which allows the robot to move on the deformable terrain. In addition, stride frequencies were optimized using mathematical models, which ensure that the robot is capable of running across the sandy ground rapidly and effectively. Their work lays fundamentals for designing robots that can move on loose terrain.

2.2.2 Robots with flexible trunks

In recent years, more and more people are aware of the importance of flexible trunks in animals' stable and effective locomotion. Some studies have been carried out to understand the role of the flexible trunks in improving stability and energy efficiency of the quadruped [25-32]. Some attempts have been made to equip quadruped robots with flexible trunks. All such studies can be divided into two main categories: the flexible trunk is passive or the flexible trunk is active.

In order to study effects of passive flexible trunks on robots' performance, researchers from University of Tehran have designed two robots [25-27]. Figure 2.8 illustrates a tiger robot, whose trunk is flexible and passive. This robot is able to mimic the gait pattern of tigers. Both simulation and experimental results show that flexible trunks increase the robot's stability, adaptability, and mobility.

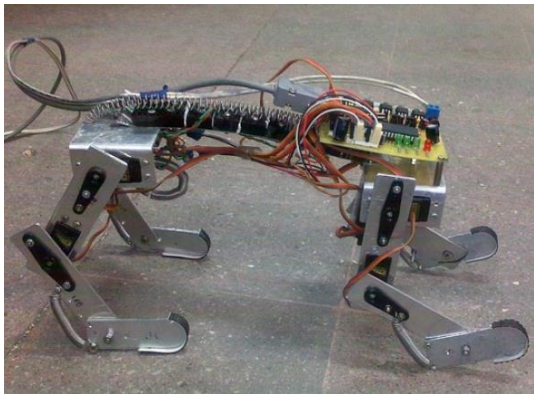

Figure 2.8 Tiger robot

As shown in figure 2.9, this crawling robot has a passive piecewise linear trunk that connects the two parts[25]. Experiments results suggest that the piecewise linear trunk enhances the robot's robust ability to respond to changes of the load. Additionally, the piecewise linear helps the robot to achieve speed-energy efficiency trade-off in motion.

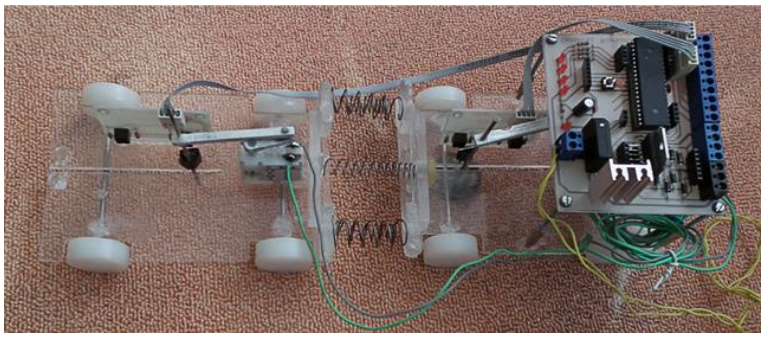

Figure 2.9 Crawling robot

For the active flexible trunks, most of the studies are conducted by simulation analysis. The simulation model presented in figure 2.10 has been widely used to study the effects of the active flexible trunks [28-30]. Simulation results indicate that active flexible trunks can enable robots to obtain higher speed and additional maneuverability.

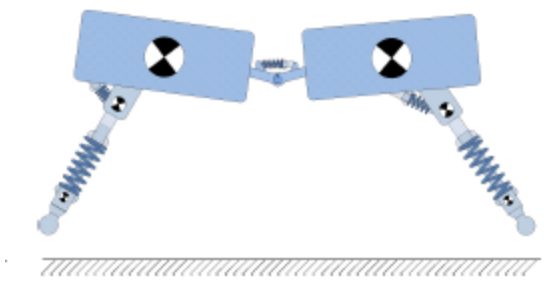

Figure 2.10 Simulation model

Based on this simulation model, a compliant quadruped robot with an active trunk, Bobcat robot, has been designed (see figure 2.11) [5, 31]. Comparing experimental results of the robot with an active flexible trunk with the results of the robot with a fixed trunk, we can find that the active flexible trunk makes the robot move much faster and more stable compared with the robot with a fixed trunk. However, there is no obvious improvement in the energy efficiency of this robot.

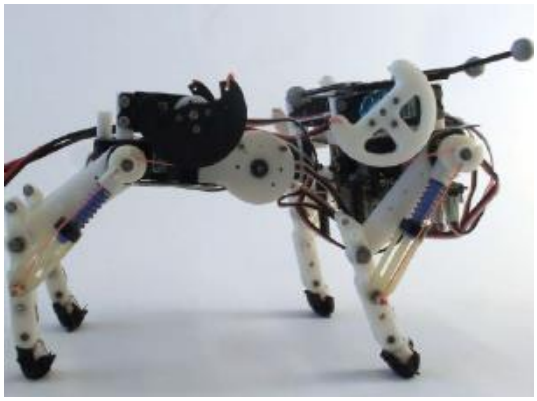

Figure 2.11 Bobcat robot

Robots with more complex trunks have also been studied[32]. A quadruped robot equipped with an active series-elastic trunk (see figure 2.12) was established in the simulation software. This robot has been tested in four cases: the trunk is rigid, the trunk is flexible and passive, the trunk is flexible and active, and the trunk is active and series-elastic. Experimental results indicate that the robot with an active and series-elastic trunk has the best performance. It run faster and consumed less energy. Besides that, the pattern of this robot was also more similar to actual fast animals.

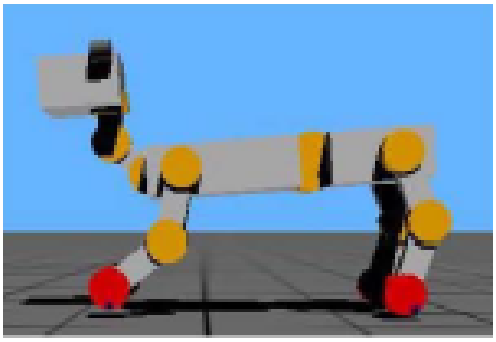

Figure 2.12 Quadruped robot

2.3 Conclusion

It is obvious that lizards' flexible trunks can increase their stride lengths. The function of flexible trunks on energy efficiency has not been studied, which is the core of this research. The introduction of the gait pattern makes preparations for the robot design. After viewing existing bio-inspired lizard robots, we can find that attentions of these researches are all paid to appendages of lizards. No research involves lizards' flexible trunks. Robots or simulation models used for investigating effects of flexible trunks on locomotion are all inspired by mammals, e.g. dogs, tigers, cheetahs, horses, etc. And all these robots and models mimic bounding gait and bend their trunks in the sagittal plane. The object of this research, lizard, is a reptile, which has a crawling gait and bends its flexible trunk in the horizontal plane. Thus, this research is distinct with previous studies and has practical significance for the development of robots.

Chapter 3: Modelling and Simulation

In this chapter, a simplified lizard model is presented and simulation results under different conditions are illustrated to verify the hypothesis: to achieve the same locomotion, a compliant and flexible trunk is capable of improving the energy efficiency of the model in terms of reducing the peak power of the motor. The optimized stiffness and the optimized frequency under different conditions are discussed. Additionally, how flexible trunks affect the motor power is analysed.

3.1 Modelling

Generally, biological systems are of great complexity. In the case of a biological locomotion system, it involves complex interplay among a great quantity of muscles, bones and a lot of other body parts like ligaments and tendons. In order to apply biological principles in dealing with engineering issues, it is necessary to establish simplified models which should retain the desired fundamental properties of real biological systems.

So far, there have been no models particularly describing natural properties of lizards' compliant and flexible trunks. There are some quadrupeds models which can be used for reference. Ijspeert and Buchli [33] have devised a simple mechanical model which could mimic the basic locomotion of quadrupeds and reflect dynamic functions of their compliant and flexible trunks (see fig 3.1). This model consists of two masses that were connected by two springs k_1 and k_2.This mechanical system has been proved that is suitable for the study of effects of compliant and flexible trunks on quadruped animals[25].

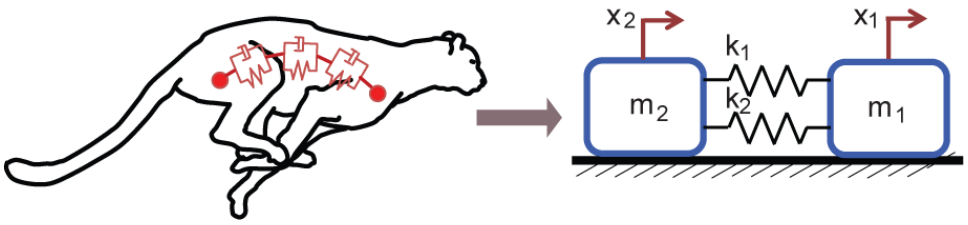

Figure 3.1 A simple mechanical model of the quadruped

Lizards possess some common characteristics like other quadrupeds, e.g. trunks are compliant and flexible, tendons serve as effective biological springs, muscle-tendon units have viscoelastic properties[34, 35]. As a result, the simplified lizard system can be established based on this simple mechanical model. However, lizards have some distinct

characteristics. Some adaptations and a few reasonable assumptions should be made to make the system more explicit and accurate for mimicking desired biological properties of lizards.

Lizards have following characteristics:

a) Lizards bend their trunks laterally, while most mammals bend their trunks up and down.
b) For most lizards, their hind legs are longer and stronger than their forelegs. And in some cases, lizards can even move forwards only by a pair of hind legs (bipedal locomotion)[11]. So hind legs of lizards play a more important role than forelegs in pushing the whole systems forward.
c) As mentioned in the fore chapter, legs only contact the ground in the propulsive strike. Therefore, friction force only exists in the propulsive strike and its direction is consistent with the forward direction of lizards.

Based on these characteristics, I made following adaptations and assumptions:

1) The lizard model moves on the horizontal plane and has only one dimension.
2) The hind legs take charge of generating propulsive force, and the fore legs take charge of supporting the whole model.
3) Static friction generated in the propulsive strike by hind legs and the ground works as the propulsive force. No sliding friction exists.
4) Only linear springs are considered in this research, nonlinear or further complicated conditions will be conducted in future research.

Integrating these adaptations and assumptions, the simplified lizard model has been constructed and is presented in figure 3.2.

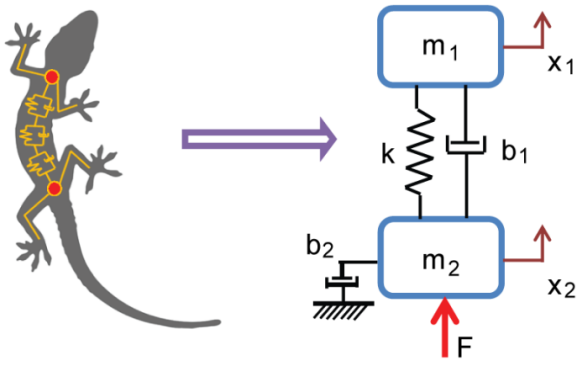

Figure 3.2 A simplified lizard model

As shown in figure 3.2, the simplified lizard system is composed of two masses $m_1$and m_2 and one linear spring k. x_1 and x_2 are displacements of $m_1$and m_2. b_1 is the coefficient of the damping between two masses. b_2 is the coefficient of the motor damping. F is the propulsive force generated by the motor in the mass 2. Since the lizard model has been established, simulation analysis of the effect of lizards' complanit and flexible trunk on energy effciency can been carried out.

3.2 Simulation

For the sake of high accuracy and high efficiency of the simulation analysis, I utilized MATLAB\Simulink as the simulation tool.

MATLAB\Simulink, which is a data flow graphical programming language tool to MATLAB and has great superiorities in modelling, simulating and analysing multi-domain dynamic systems, has been widely used in various fields.

In order to systematically and comprehensively analyse this lizard model, I performed simulations in three cases:

1) Lizard model with a rigid trunk(the rigid model);
2) Lizard model with a compliant and flexible trunk, but without any damping(the ideal model);
3) Lizard model with a compliant and flexible trunk and two kinds of damping (the complete model).

The desired locomotion of the system was given as follows:

$$x_1 = (-\frac{1}{3}\sin(2\pi ft) + \frac{2}{3}\pi\text{ft}) \times 0.07 \times \frac{\sqrt{3}}{2} \quad (3\text{-}1)$$

$$v_1 = (-\frac{2}{3}\pi f\cos(2\pi ft) + \frac{2}{3}\pi\text{f}) \times 0.07 \times \frac{\sqrt{3}}{2} \quad (3\text{-}2)$$

$$a_1 = (\frac{4}{3}\pi^2 f^2 \sin(2\pi ft)) \times 0.07 \times \frac{\sqrt{3}}{2} \quad (3\text{-}3)$$

Where x_1 is the desired displacement of the model, v_1 is the desired velocity of the model, a_1 is the desired acceleration of the model, and f is the frequency of the desired locomotion.

Figure 3.3 shows the desired displacement, the desired velocity and the desired acceleration of the model when the frequency is 1 Hz.

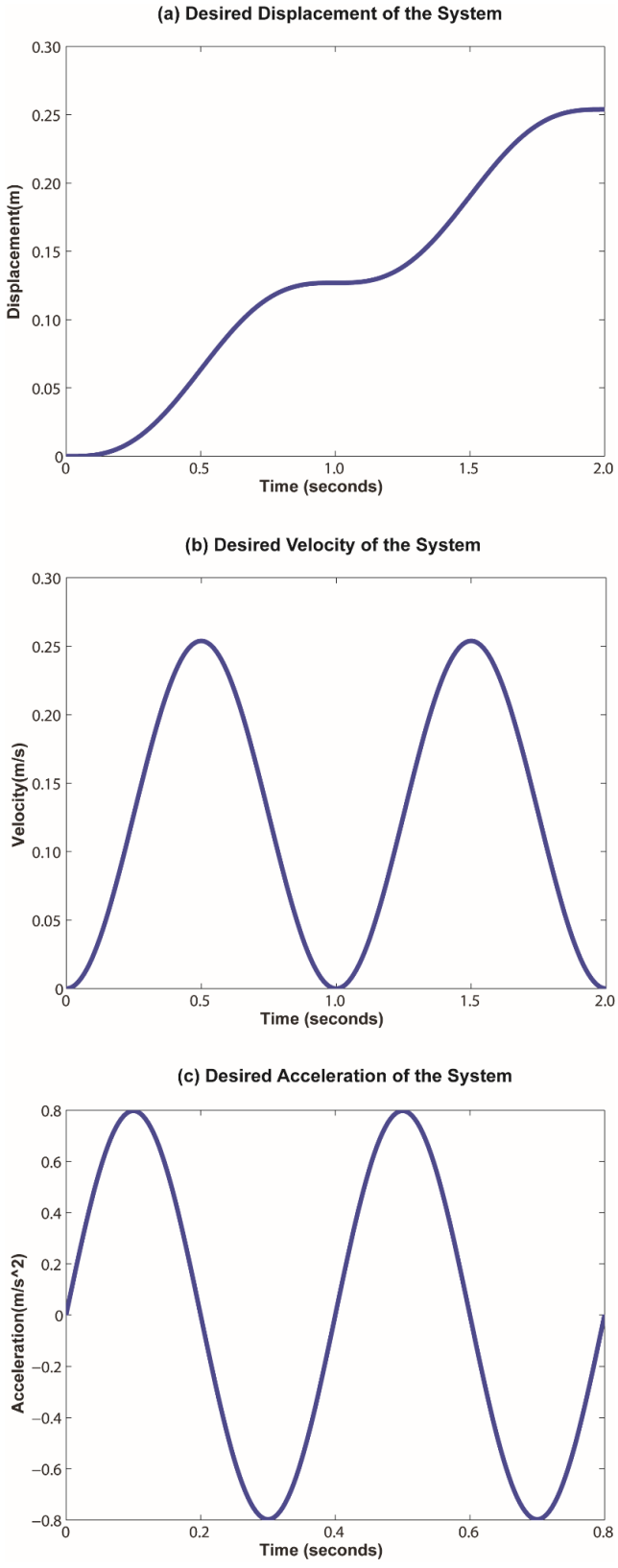

Figure 3.3 Desired locomotion of the model

The motor power which is utilized to actuate the model can be calculated using the following equation:

$$P_{motor} = F \times v_2 \tag{3-4}$$

where F is the force generated by the motor, and v_2 is the velocity of the mass 2.

3.2.1 Simulation of the rigid model

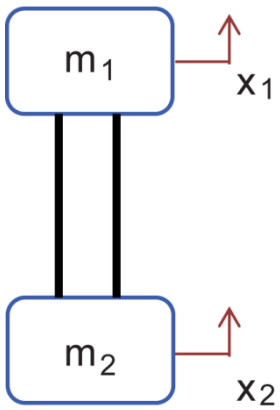

Figure 3.4 The rigid model

As illustrated in figure 3.4, for the rigid model, two masses are connected by rigid joints. The locomotion of the mass 1 represents the desired locomotion of the model. The simulation model of the rigid model established in Simulink is illustrated in Fig 3.5.

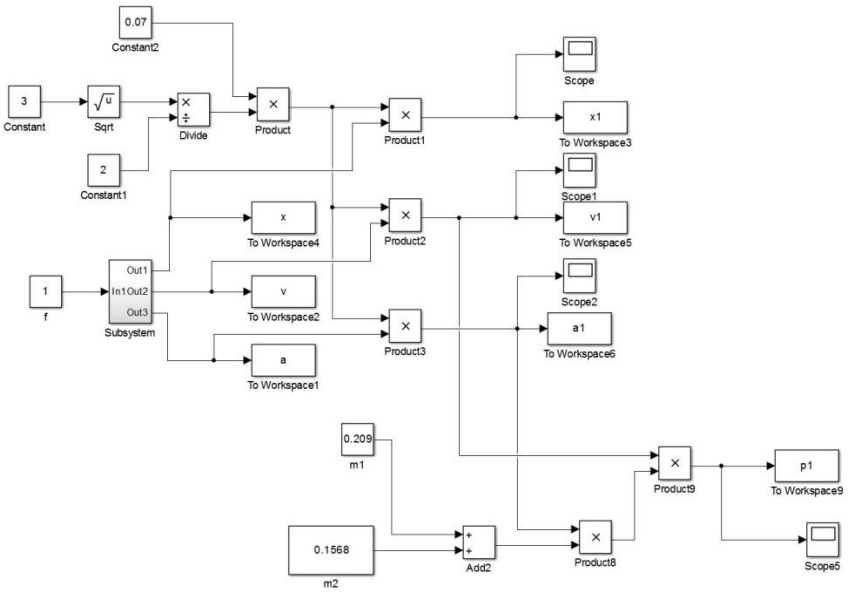

Figure 3.5 Simulink model of the rigid model

The locomotion of two masses is identical. Therefore, the motor power of this model can be calculated using the equation (3-5).

$$p_1 = \mathrm{F} \times v_2 = (m_1 + m_2) \times a_1 \times v_1 \tag{3-5}$$

Setting $m_1 = 0.209kg,\ m_2 = 0.1568kg$, we can get the motor power of this model (see figure 3.6).

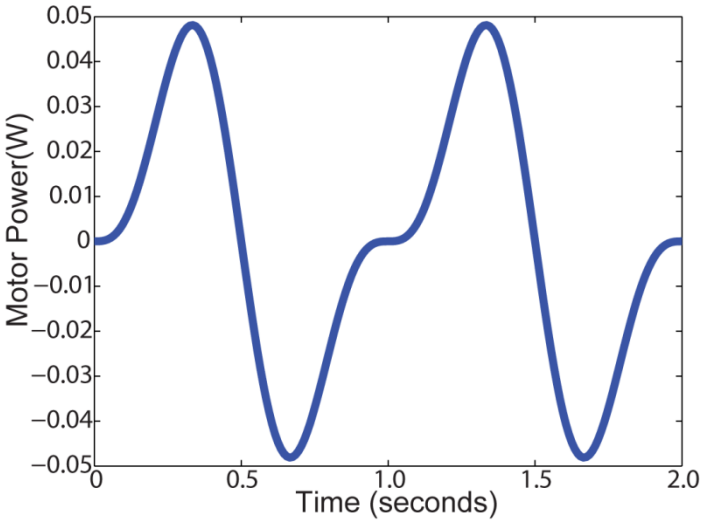

Figure 3.6 Motor power of the rigid model

3.2.2 Simulation of the ideal model

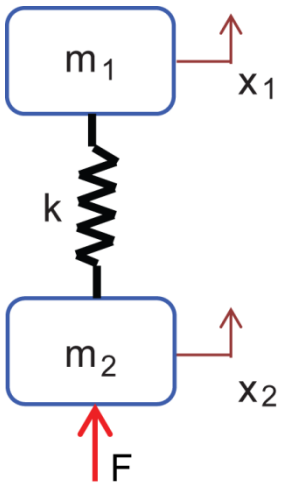

Figure 3.7 The ideal model

As illustrated in figure 3.7, for the ideal model, two masses are connected by linear springs with all the damping neglected.

The ideal model can be written as follows

$$m_1\ddot{x}_1 = k(x_2 - x_1) \tag{3-6}$$

$$m_2\ddot{x}_2 = F - k(x_2 - x_1) \tag{3-7}$$

The simulation model established in Simulink is illustrated in Fig 3.8.

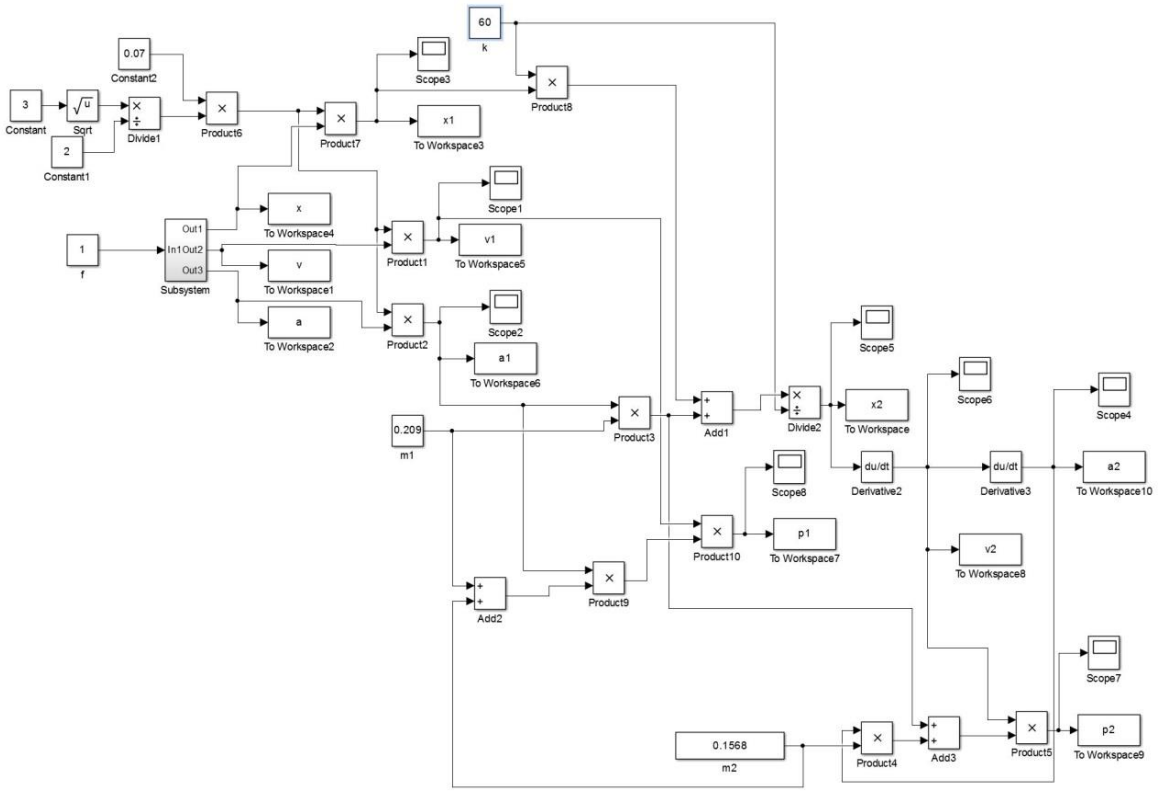

Figure 3.8 Simulink model of the ideal model

The locomotion of the mass 1 represents the desired locomotion of the model, which is already given. The locomotion of the mass 2 is unknown. But if the stiffness of the spring is given, the locomotion of the mass 2 can be calculated using the equation (3-6). Then the force utilized to actuate the system can be calculated by the equation (3-7).

Once knowing the locomotion of both masses and the propulsive force, the motor power utilized to actuate the ideal model can be calculated using the following equation:

$$P_2 = F \times v_2 = (m_1\ddot{x}_1 + m_2\ddot{x}_2) \times \dot{x}_2 \tag{3-8}$$

Arbitrarily choosing the stiffness of spring as 60 N/m, the motor power of the ideal model is shown in figure 3.9.

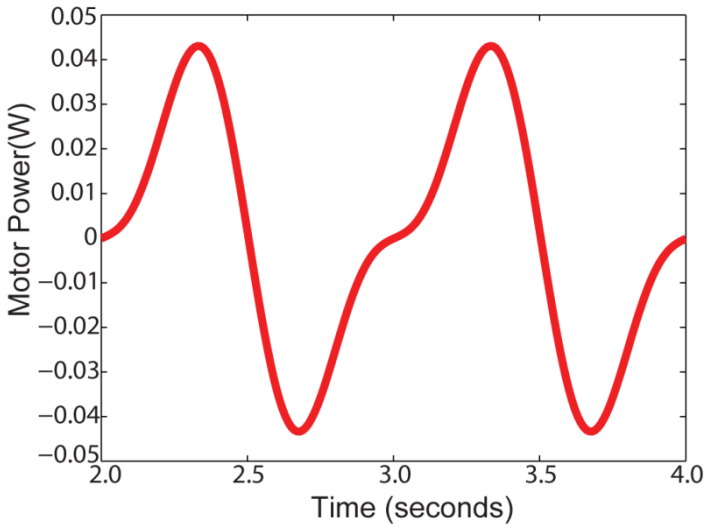

Figure 3.9 Motor power of the ideal model

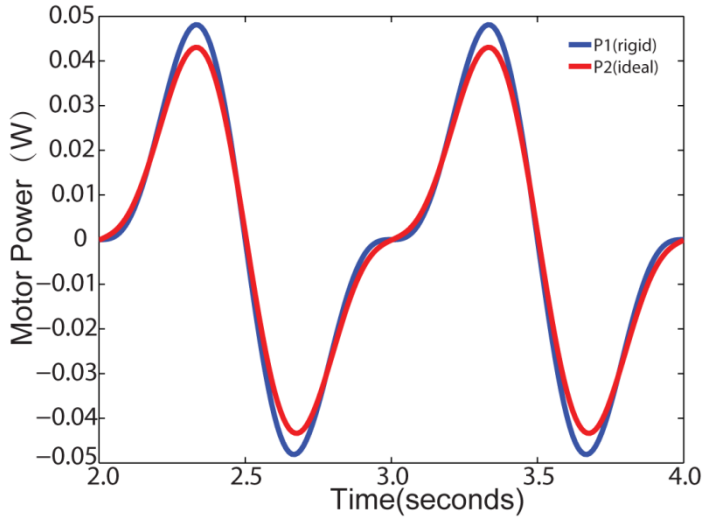

Figure 3.10 Comparison of motor powers

Comparing the motor power of the rigid model with that of the ideal model (see figure 3.10), it is obvious that the peak power of the motor is decreased, which verifies the hypothesis that a compliant and flexible trunk do have effect on improving the ideal model's energy efficiency in terms of reducing the peak power of the motor.

When the peak power is reduced to the minimum, the ideal model has the best energy efficiency. In order to do this optimization, we should find critical factors which can affect the motor power. From the equation (3-8), we can find that the motor power is determined by five parameters: m_1, $\ddot{x}_1$, m_2, $\dot{x}_2$, and $\ddot{x}_2$. Among these parameters, m_1, $\ddot{x}_1$, and m_2 are given conditions, $\dot{x}_2$, and $\ddot{x}_2$ are determined by x_2 which is related to the desired locomotion of the

model and the stiffness of the spring. As a result, the motor power is influenced by the desired locomotion of the model and the stiffness of the spring.

Keeping the desired locomotion of the ideal model unchanged, motor powers of the ideal model with different springs are illustrated in Fig 3.11.

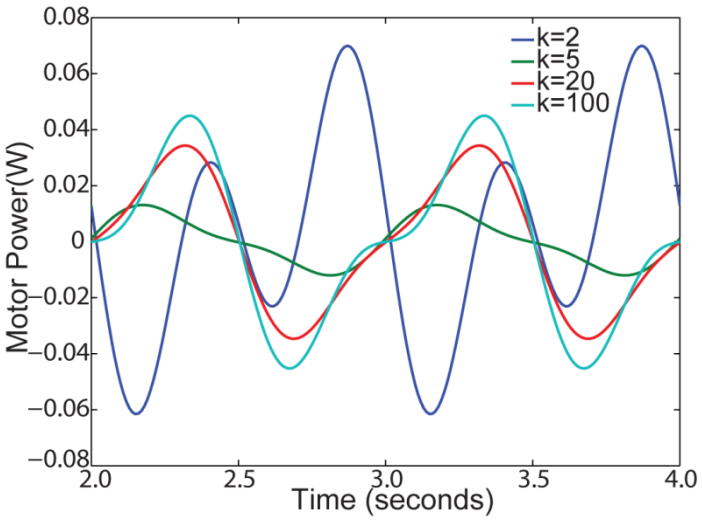

Figure 3.11 Motor powers of the ideal model with different trunks

As shown in figure 3.11, trunks with different springs can result in different motor powers. And the variation tendency is not simplex. In order to find out the relationship between the peak power of the motor and the stiffness of the trunk at the frequency of 1 Hz, I changed the stiffness of the spring from 0 to 100 N/m. Results are illustrated in figure 3.12.

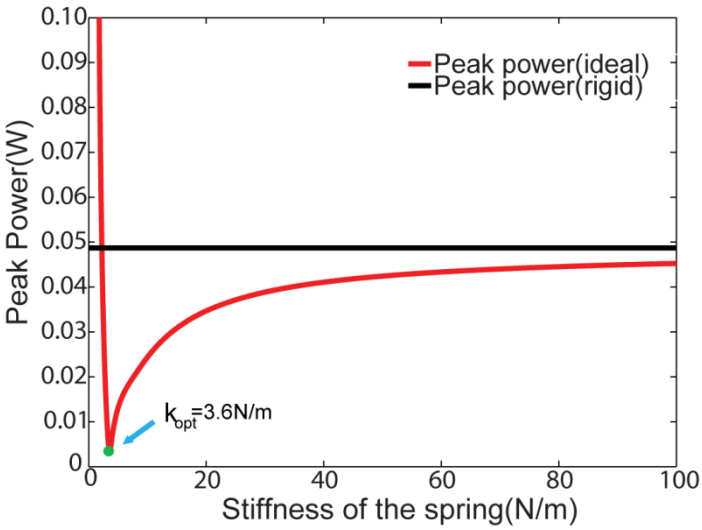

Figure 3.12 Relationship between the peak power of the motor and stiffness of the trunk

As shown in figure 3.12, when the spring is very soft, the peak power of the motor can be extremely large. With the increase of the stiffness, the peak power is sharply reduced to the minimum. Continuing increasing the stiffness, the peak power will rise again and approach a horizontal asymptote. When the stiffness equals 3.6 N/m, the peak power of the motor reaches the minimum. So 3.6 N/m is the optimized stiffness of the ideal model in the condition that the frequency of the desired locomotion is 1 Hz.

Increasing the frequency from 1 Hz to 2 Hz, the new desired locomotion can be written as follows:

$$x_1 = (-\frac{1}{3}\sin(4\pi t) + \frac{4}{3}\pi t) \times 0.07 \times \frac{\sqrt{3}}{2} \tag{3-9}$$

$$v_1 = (-\frac{4}{3}\pi\cos(4\pi t) + \frac{4}{3}\pi) \times 0.07 \times \frac{\sqrt{3}}{2} \tag{3-10}$$

$$a_1 = (\frac{16}{3}\pi^2\sin(4\pi f t)) \times 0.07 \times \frac{\sqrt{3}}{2} \tag{3-11}$$

The new motor power of the rigid model is illustrated in figure 3.13. Still choosing the stiffness of the spring equals 60N/m, motor powers of the different models are shown in figure 3.14.

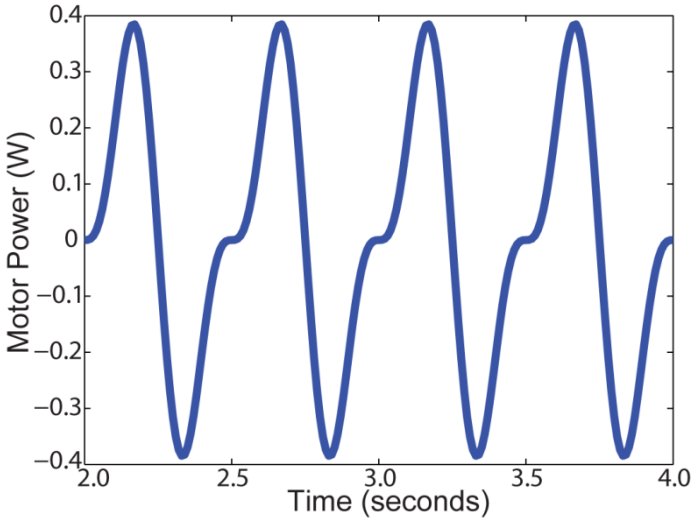

Figure 3.13 Motor power of the rigid model

Comparing motor powers of different models (see figure 3.14), we can get the same conclusion that a compliant and flexible trunk do have effect on improving the system's energy efficiency in terms of reducing the peak power of the motor.

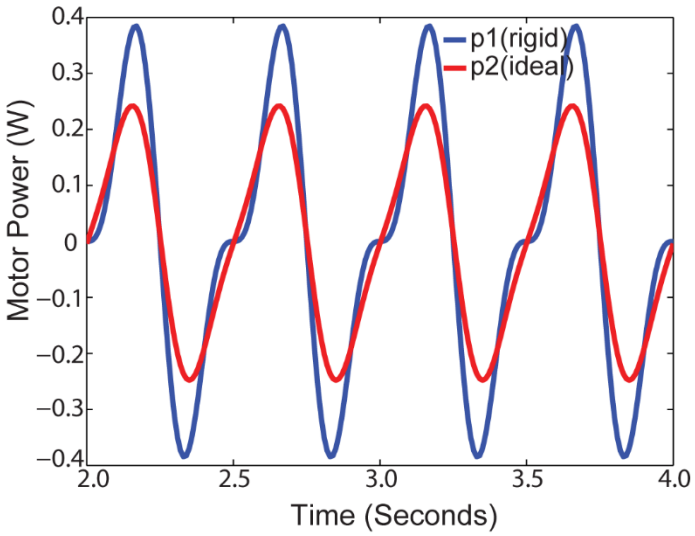

Figure 3.14 Motor Power of different models

Keeping the desired locomotion unchanged, motor powers of the ideal models with different springs at the frequency of 2 Hz are illustrated in figure 3.15.

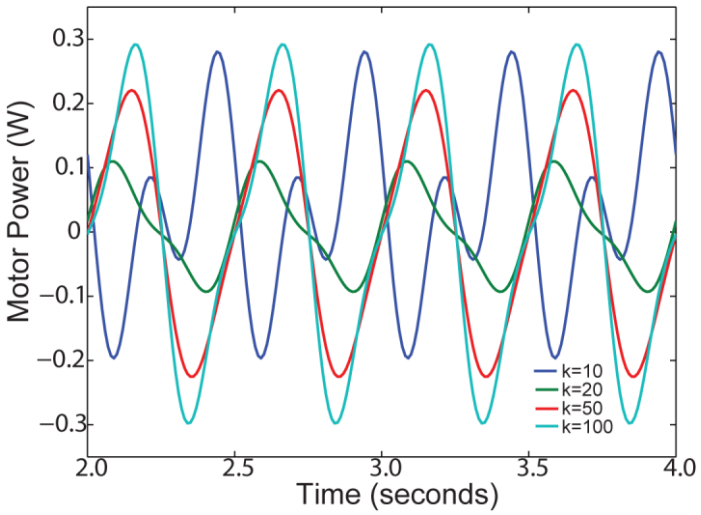

Figure 3.15 Motor powers of the ideal model with different trunks

As shown in figure 3.15, trunks with different springs result in different motor powers at the frequency of 2 Hz. And the variation tendency is not simplex. This conclusion is similar to that in the condition that the frequency of the desired locomotion equals 1 Hz. In order to find out the relationship between the peak power of the motor and the stiffness of the spring at the frequency of 2 Hz, I changed the stiffness of the spring from 0 to 100 N/. Results are illustrated in figure 3.16.

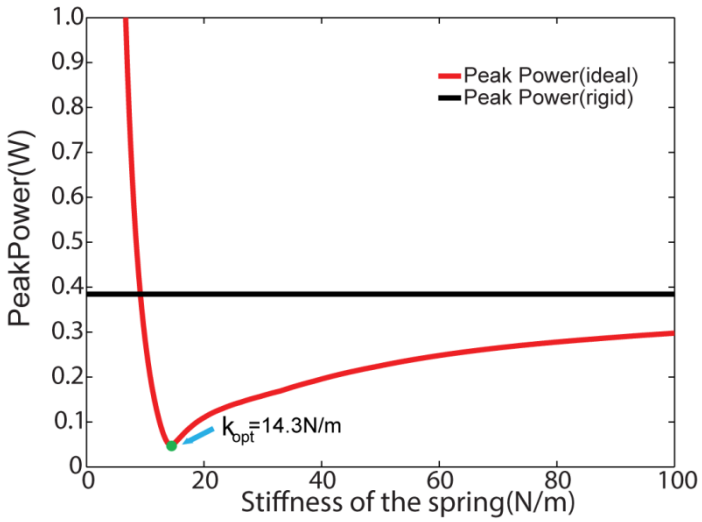

Figure 3.16 Relationship between the peak power of the motor and stiffness of the trunk

From figure 3.16 we can easily find the same variation tendency. When the stiffness of the spring is small, the peak power can be extremely large. As the stiffness increases, the peak power will shapely reduce to the minimum. Continuing increasing the stiffness, the peak power will rise and approach a horizontal asymptote. The optimized stiffness of the ideal model at the frequency of 2 Hz is 14.3 N/m.

Based on the above simulations, we can find that for each frequency, there should be an optimized stiffness. The optimized stiffness at some frequencies is listed in Table 3.1.

Table 3.1 Optimized stiffness of the ideal model at different frequencies

Frequency(Hz)	**0.5**	**1**	**1.5**	**2**	**2.5**	**3**	**3.5**
Optimized stiffness(N/m)	**0.9**	**3.6**	**8**	**14.3**	**22.6**	**32.8**	**45.5**

These points are plotted in figure 3.16, which are well fitted by one two-order polynomial:

$$k = 3.952 \times f^2 - 1.038 \times f + 0.5571 \quad (3\text{-}12)$$

where k denotes the optimized stiffness of the spring, f denotes the frequency of the desired locomotion of the model. Using equation (3-12), we can estimate the optimized stiffness of the ideal model if the frequency of the desired locomotion is given.

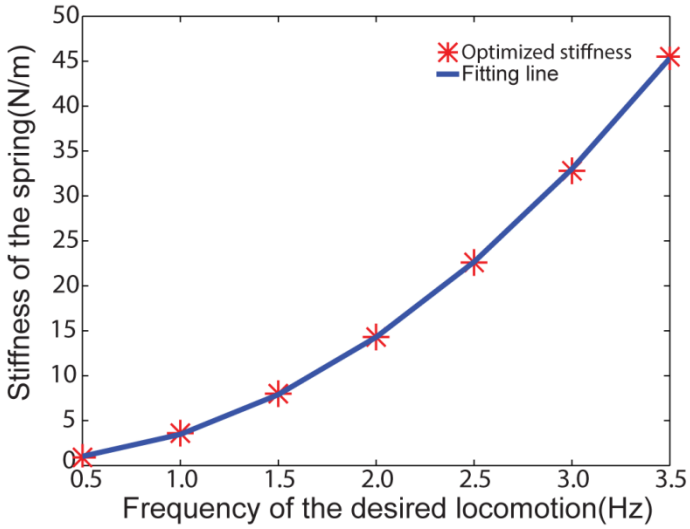

Figure 3.17 Relationship between the optimized stiffness and the frequency of the locomotion

In order to know influence of the frequency on the peak power, I fixed the stiffness at some specific values and changed the frequency from 0 Hz to 4 Hz. Simulation results are shown in figure 3.18. In figure 3.18, we can find that peak powers of ideal models with different trunks have similar variation tendency. At low frequencies, peak powers increase slowly with the increasing of the frequency. After reaching a certain value, peak powers will rapidly increase and even exceed the peak power of the rigid model at the same frequency. This certain value becomes larger if the stiffness of trunk is higher.

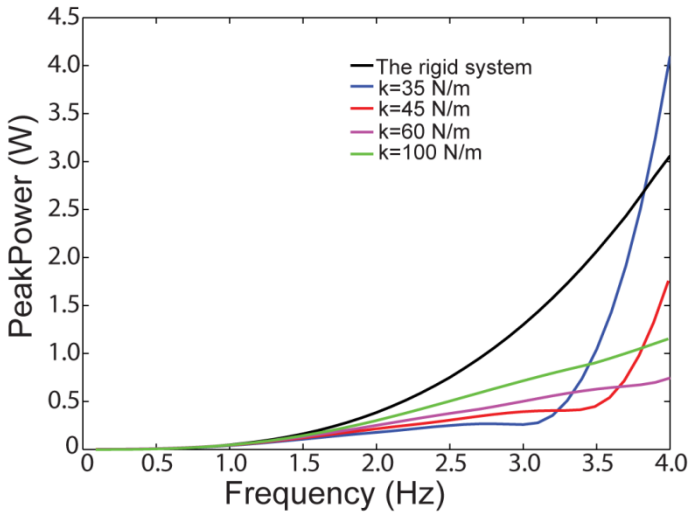

Figure 3.18 Peak powers under different frequencies

The reduction rate of the peak power under different conditions can be written by equation (3-13).

$$\text{Reduction rate} = \frac{P_m(rigid) - P_m(complete)}{P_m(rigid)} \times 100\% \quad (3\text{-}13)$$

As shown in figure 3.19, the variation tendencies of the reduction rate of ideal models with different trunks are similar. With the increasing of the frequency, the reducing increases to the maximum and then decreases. The optimized frequencies, at which the reduction rate reaches the maximum, are different for different stiffness.

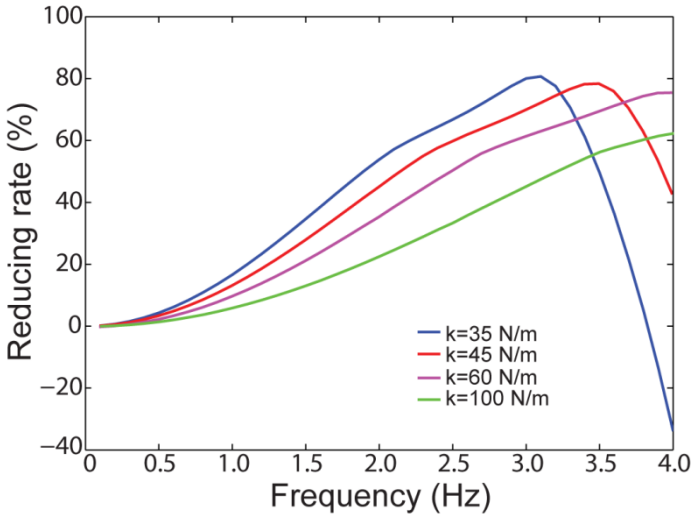

Figure 3.19 Reduction rate under different frequencies

3.2.3 Simulation of the complete model

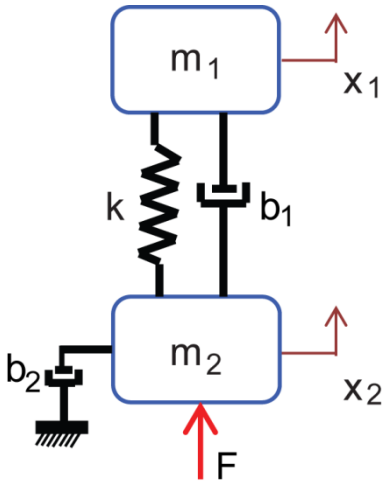

Figure 3.20 The complete model

Compared with the ideal model, the complete model (see figure 3.20) has two additional damping: the motor damping and the damping between the two masses. The new model can be written as floows:

$$m_1\ddot{x}_1 = k(x_2 - x_1) + b_1(\dot{x}_2 - \dot{x}_1) \quad (3\text{-}14)$$

$$m_2\ddot{x}_2 = F - k(x_2 - x_1) - b_1(\dot{x}_2 - \dot{x}_1) - b_2\dot{x}_2 \quad (3\text{-}15)$$

where the b_1 is the damping between the two masses and b_2 is the motor damping. In my simulation, I choose b_1 equals 1 $N/m \cdot s^{-1}$ and b_2 equals 0.01 $N/m \cdot s^{-1}$.

The simulation model established in Simulink is presented in figure 3.19. Setting the frequency of the desired locomotion of the model equal 1 Hz, the desired displacement, the desired velocity and the desired acceleration of the model are illustrated in figure 3.3. Making the stiffness of the spring equal 60 N/m, we can get the motor power of the complete model (see figure 3.22). As illustrated in the figture, the motor power of the complete model reduces when compared with the motor power of the rigid model.

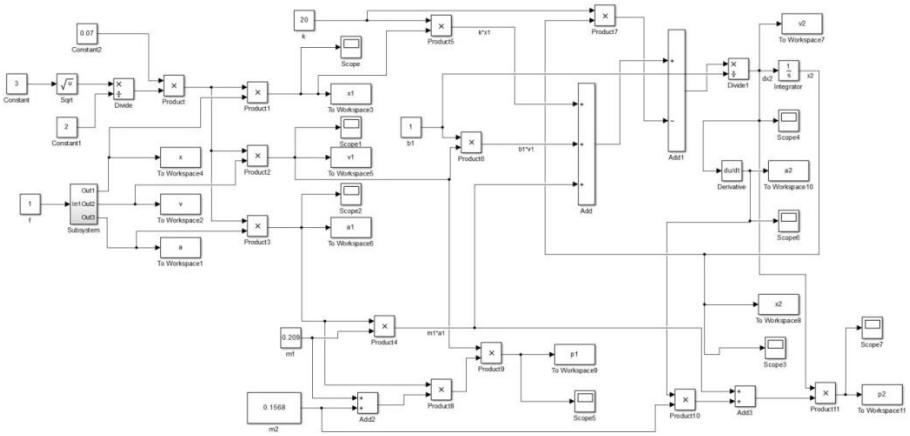

Figure 3.21 Simulink model of the complete model

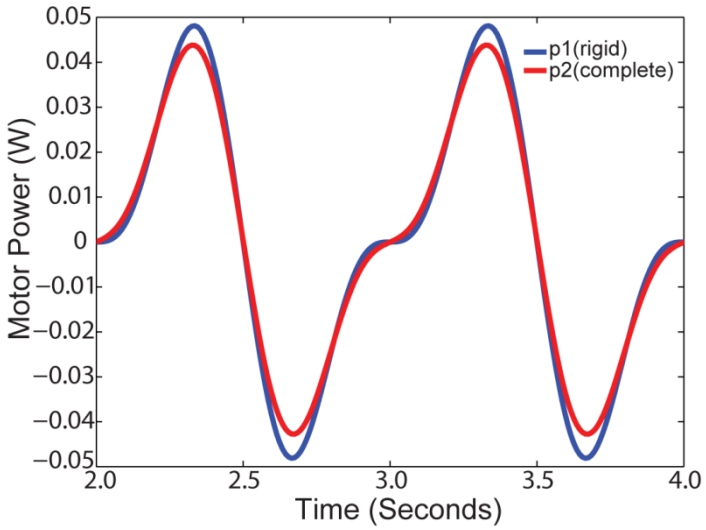

Figure 3.22 Motor powers of different systems

Choosing four springs (5 N/m, 20 N/m, 50 N/m, 100 N/m), motor powers of the complete model with these springs are illustrated in figure 3.23. As we can see, trunks with different springs result in different motor powers. And the variation tendency is not simplex. In order to find out the relationship between the peak power of the motor and the stiffness of the spring of the complete model at the frequency of 1 Hz, I kept the desired locmotion unchanged and increased the stiffness of the spring from 0 to 100N/m. Results are shown in figure 3.24. The variation tendency of the motor's peak power as the stiffness of the spring becoming larger is similar with that of the ideal model: when the spring is very soft, the peak power of the motor can be extremely large. With the increasing of the stiffness, the peak power is sharply reduced to the minimum. Continuing increasing the stiffness, the peak power will rise again and approach a horizontal asymptote.

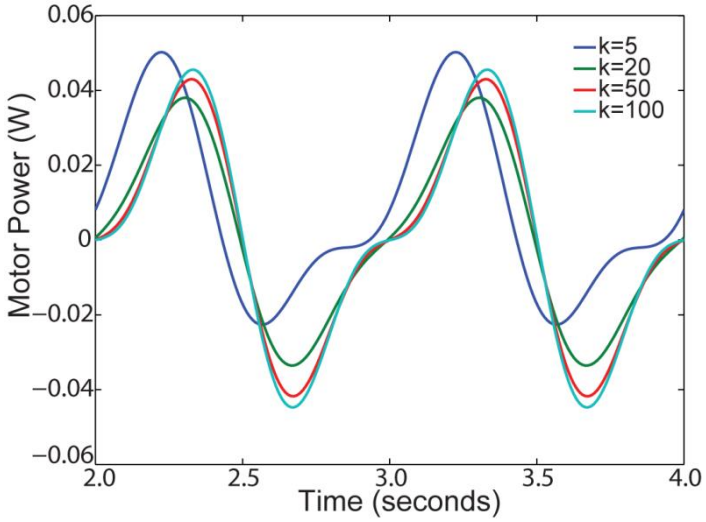

Figure 3.23 Motor powers of the complete model with different trunks

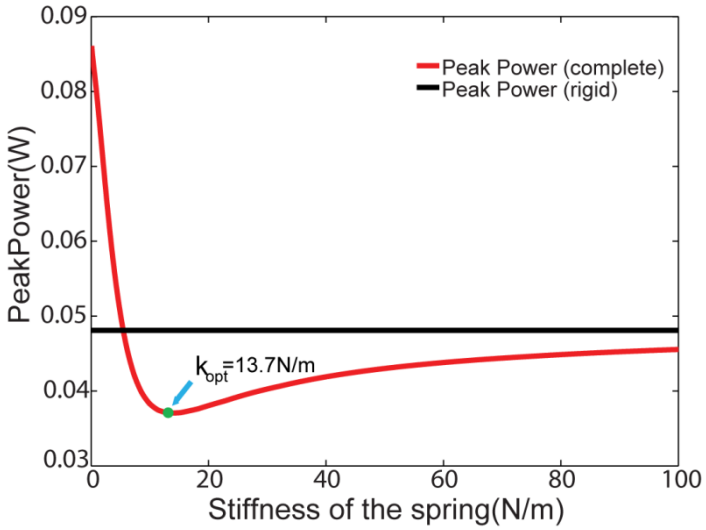

Figure 3.24 Relationship between the peak power of the motor and the stiffness of the trunk

In figure 3.24, we can easily find the optimized stiffness of the complete model at the frequency of 1 Hz, which equals 13.7 N/m. Letting the stiffness equal 13.7 N/m and plotting the motor power of both the rigid model and the complete model in one figure (see Fig 3.25), the motor's peak power of the rigid model is 0.0481 W, and the motor's peak power of the complete model is 0.0285 W. The peak power of the motor has been reduced by about 22.9 %.

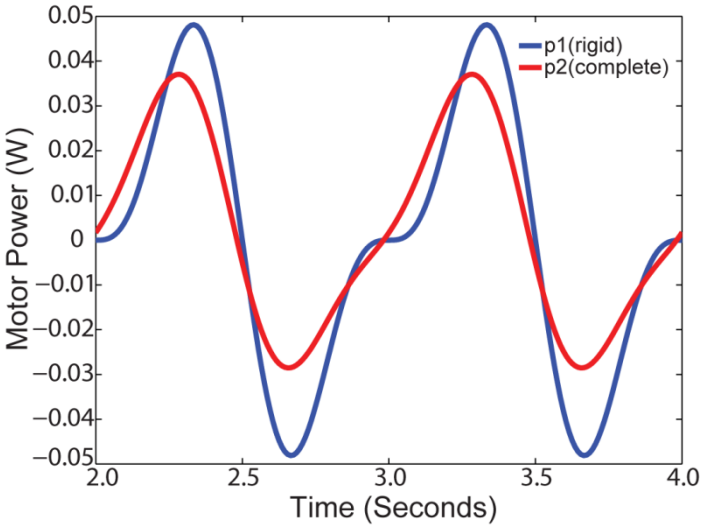

Figure 3.25 Motor powers of different models

Increasing the frequency of the desired locomotion to 2 Hz and still setting the stiffness of the spring equal 60 N/m, motor powers of both the rigid model and the complete model are illustrated in figure 3.26.

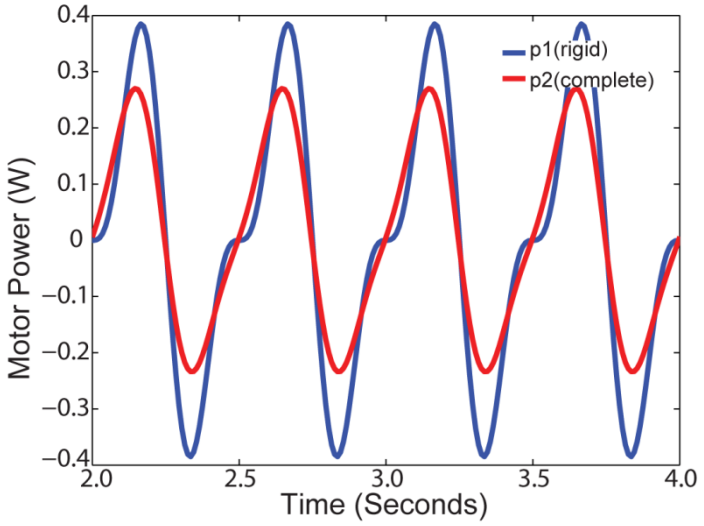

Figure 3.26 Motor powers of different models

As we can see from figure 3.26, the motor's peak power of the complete model is less than that of the rigid model. Choosing four different springs (10 N/m, 20 N/m, 50 N/m, 100N/m), simulation results are shown in figure 3.27. Trunks with different springs result in different motor powers at the same frequency. And the variation tendency is not simplex.

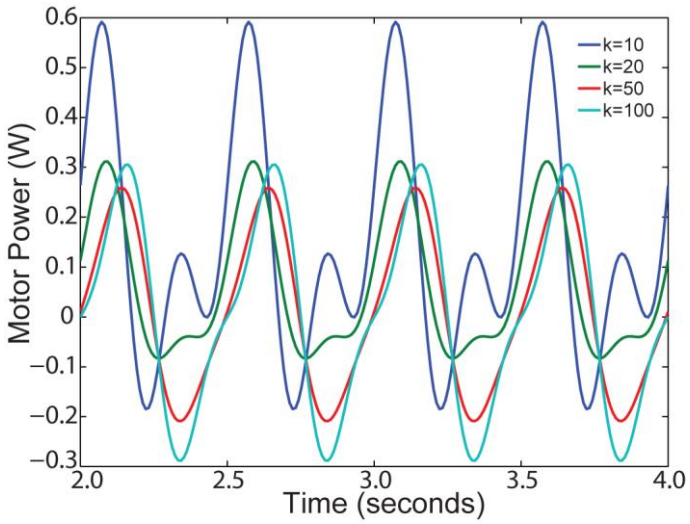

Figure 3.27 Motor powers of the complete model with different trunks

In order to find out the relationship between the peak power of the motor and the stiffness of the spring of the complete model at the frequency of 2 Hz, I kept the desired locmotion unchanged and increase the stiffness of the spring from 0 to 100N/m. Results are shown in figure 3.28. The variation tendency of the motor's peak power as the stiffness of the spring becoming larger is similar to that at the freqeucny of 1 Hz.

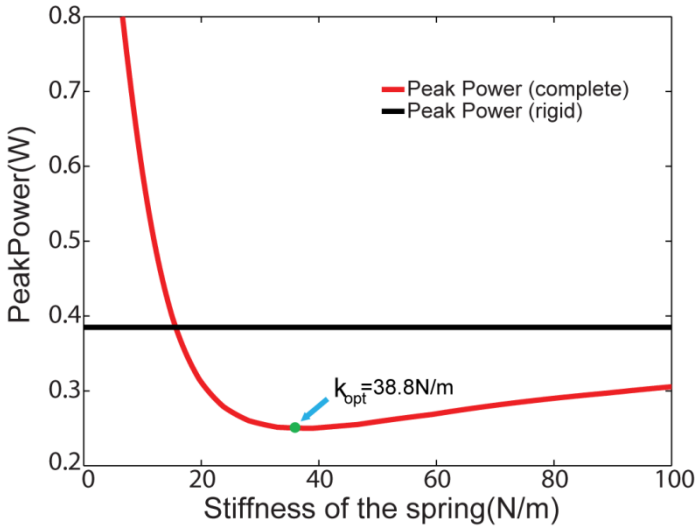

Figure 3.28 Relationship between the peak power of the motor and the stiffness of the trunk

When the frequency is 2 Hz and the stiffness is 38.8 N/m, the motor power of different models are illustrated in figure 3.29. The peak power of the model with a rigid trunk is 0.3849 W; while the peak power of the complete model is 0.2529 W. Achieving the same locomotion, the flexible and compliant trunk reduces the peak power of the motor by 35.1 %.

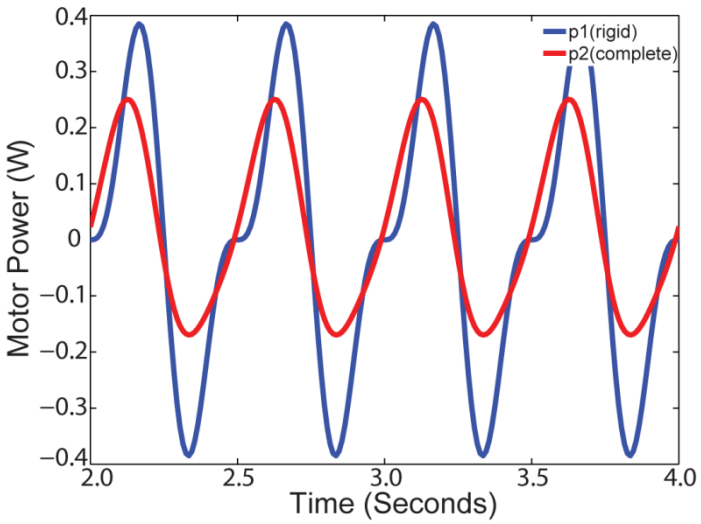

Fig 3.29 Motor powers of different models

Changing the frequency of the desired locomotion from 0.5 Hz to 3.5 Hz, we can observe the similar variation tendency and can always find an optimized stiffness at a specified frequency. Some frequencies and their relative optimized stiffness are listed in Table 3.2. The reduction rate can be calculated by equation (3-13).

Table 3.2 Optimized stiffness of the complete system at different frequencies

Frequency(Hz)	**0.5**	**1**	**1.5**	**2**	**2.5**	**3**	**3.5**
Optimized stiffness(N/m)	**5.8**	**13.7**	**24.3**	**38.8**	**52.9**	**68.1**	**89.1**
Reduction rate (%)	**13.3**	**22.9**	**29.9**	**35.1**	**38.9**	**42.0**	**44.5**

These points are plotted in figure 3.30, which are well fitted by one two-order polynomial:

$$k = 4.176 \times f^2 + 10.96 \times f - 0.9857 \quad (3\text{-}16)$$

where k denotes the optimized stiffness of the spring, f denotes the frequency of the desired locomotion of the system. Using equation (3-16), we can estimate the optimized stiffness of the complete system if the frequency of the desired locomotion is given.

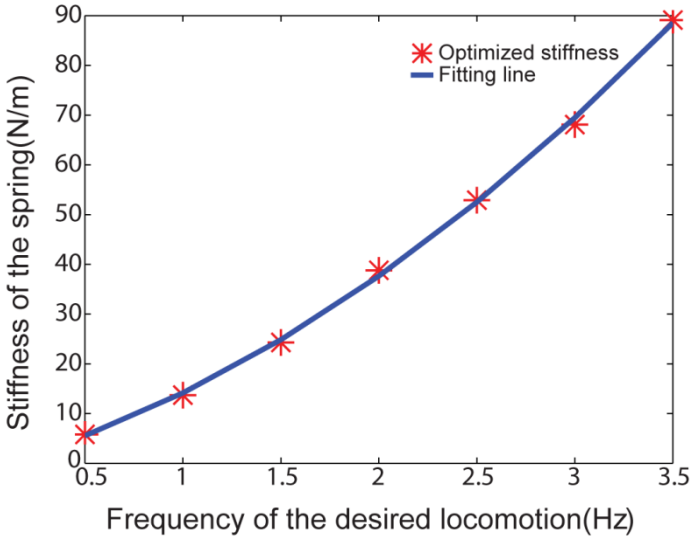

Fig 3.30 Relationship between the optimized stiffness and the frequency of the locomotion

I fixed the stiffness at some specific values and changed the frequency from 0 Hz to 4 Hz. Simulation results are shown in figure 3.31. In figure 3.31, we can find that peak powers of ideal models with different trunks have similar variation tendency. With the increasing of the frequency, peak powers will become larger. However, the frequency, at which the peak power of the complete model exceeds the peak power of the rigid model, is different for different trunks. This specific frequency will become larger if the stiffness becomes higher.

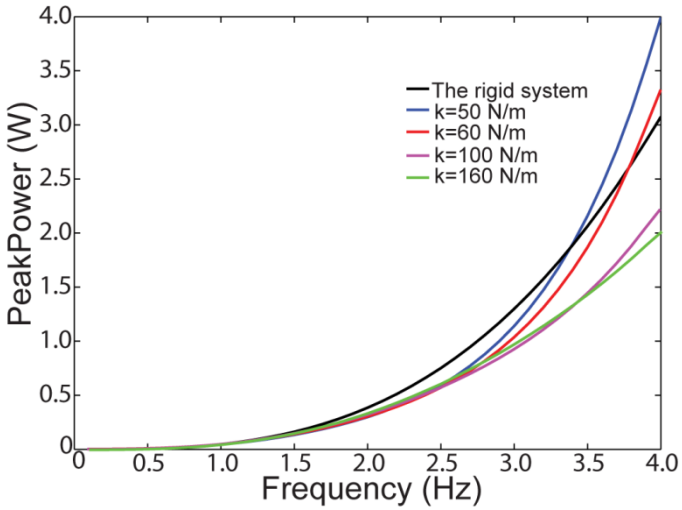

Figure 3.31 Peak powers at different frequencies

Reduction rates of the peak power of the complete model with different trunks are shown in figure 3.32. With the increasing of the stiffness, both the optimized frequency, at which the reduction rate reaches the maximum, and the maximum reduction rate become larger.

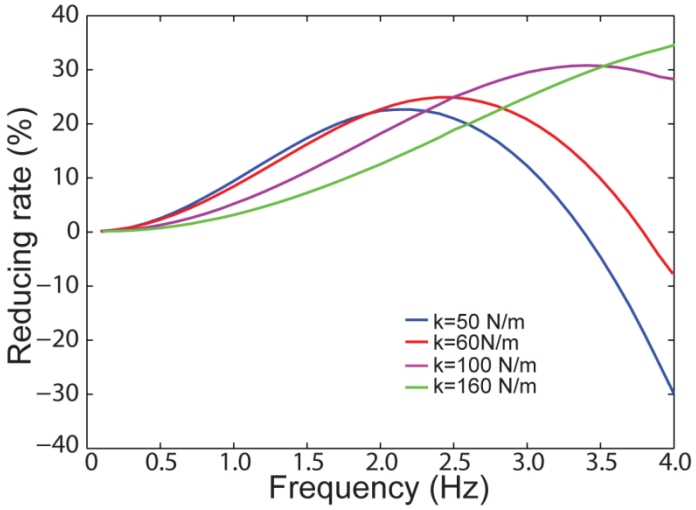

Figure 3.32 Reduction rate at different frequencies

3.3 Analysis

The functions of the compliant and flexible trunk on improving energy efficiency in terms of reducing the peak power of the motor can be explained from the aspect of kinematics. The motor power of the rigid model can be calculated based on the displacement of mass 1. And the motor power of the flexible model can be calculated based on the displacement of mass 2. By comparing kinematics of two masses, we can know how flexible trunks affect the motor power. Conducting the simulation when the frequency of the desired locomotion equals 2 Hz and the stiffness of the spring equals 60 N/m, kinematics of both masses are illustrated in figure 3.33. As we can see from figure 3.33(a), within the same time, both masses move the same distance. However, their trajectories are not completely overlapped. In figure 3.33 (b), the blue curve denotes the velocity of the mass 1 and the red curve denotes the velocity of the mass 2. The amplitude of the red curve is much smaller compared to the blue curve. In Fig 3.33 (c), the blue curve denotes the acceleration of the mass 1 and the red curve denotes the acceleration of the mass 2. The amplitude of the red curve is much smaller compared with the blue curve. To achieve the same desired locomotion, the compliant and flexible trunk reduces the amplitude of both the velocity and the acceleration. In other words, kinematics of the mass 2 is “amplified” by the compliant and flexible trunk. The trunk works as an amplifier. The motor power is the product of velocities and accelerations. So the motor power is also

amplified by the trunk. The peak power of the motor is proportional to amplitudes of the velocity and the acceleration. Both amplitudes are determined by the stiffness of the trunk and the frequency of the desired locomotion. As a result, the reduction rate of the peak power of the motor is determined by the stiffness of the trunk and the frequency of the desired locomotion.

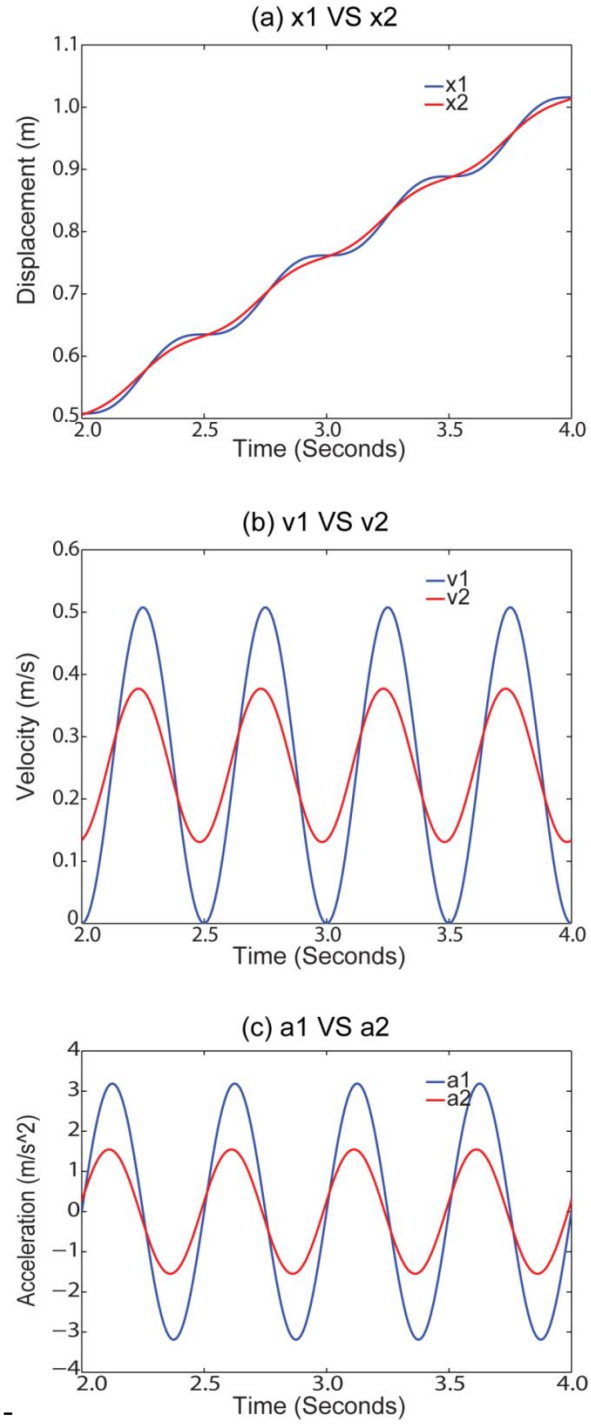

Fig 3.33 Comparison of kinematics of two parts of the robot

3.4 Conclusion

Simulation results based on the simplified lizard model indicate that compliant and flexible trunks do have effects on improving energy efficiency in terms of reducing the peak power of the motor. The frequency of the locomotion and the stiffness of the trunk are two critical factors. At a specific frequency, the variation tendency of the peak power when the stiffness of the trunk (spring) becomes larger is similar: With the increasing of the stiffness, the peak power will sharply decrease from an extremely large value to the minimum. Continuing increasing the stiffness, the peak power will rise again and approach a horizontal asymptote. For each frequency, there always exists an optimal stiffness, in which condition the peak power of the motor can be reduced to the minimum. When the stiffness is fixed, the peak power will become larger if the frequency of the locomotion becomes higher. At a certain frequency, the peak power of the model with flexible trunks will exceed the peak power of the rigid model. The reduction rate of the peak power will increase first and then decrease. For each trunk, there always exits an optimal frequency, at which the reduction rate of the peak power reaches the maximum. In additional, comparing the simulation results of the ideal model and the complete model, we can find that the damping does not change the variation tendency of the peak power. The damping only changes the magnitude of the optimal stiffness and the optimal frequency.

Chapter 4: Design and Fabrication

Our goal is to design a robot that is capable of mimicking the basic gait pattern of the lizard and can be used to verify the hypothesis and simulation results. In this chapter, three problems the design process of the robot is introduced. Several previous versions are presented and compared. Both hardware and software architectures are described in detail.

4.1 Design process

During the design process, there are three problems needed to work out. As mentioned in Chapter 2, legs of the robot should be lifted during the recovery stroke. How to lift legs while keeping the robot maintaining balance is the key problem in the design. As we can see from figure 3.33 (a), displacements of the front part and the rear part of the robot are different, which means the distance between these two parts is variable. How to connect two parts and ensure that the stiffness of the trunk can be changed easily and conveniently is another key problem in the design. The last but the most neglected problem is that how to make the robot move along a straight line. Different from running robot, the robot in this research employs the crawling gait, which means the thigh would sweep forward. If the length of the thigh is fixed, the midpoint, which determines the forward direction, will change all the time. Then the robot can't move along a straight line. If the length of the thing is variable, the robot will have more degrees of freedom, which will greatly increase the complexity of the design and fabrication of the robot. Solving these three problems is the key to ensure the feasibility of the designed robot.

4.1.1 Version I

The version I (see Figure 4.1) is the robot looks most like the lizard among all the designed robots. There are totally five motors. Four of them are equipped for actuating the robot. The left one is quipped for controlling the tail. Its trunk is divided into three parts. The spring can be stored in the middle part. The tail is designed for achieving balance during the locomotion of the robot.

While this robot looks like a lizard, it is a conceptual design. Its legs cannot be lifted while moving. And using tail to keep balance needs complicated control algorithms, which reduces its feasibility.

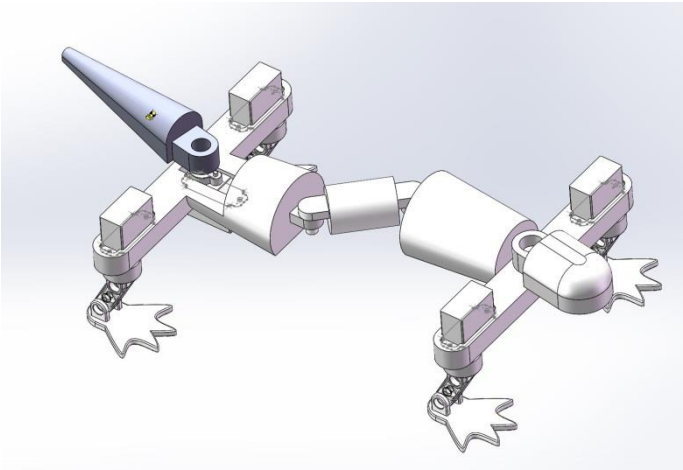

Figure 4.1 CAD model of the Version I

4.1.2 Version II

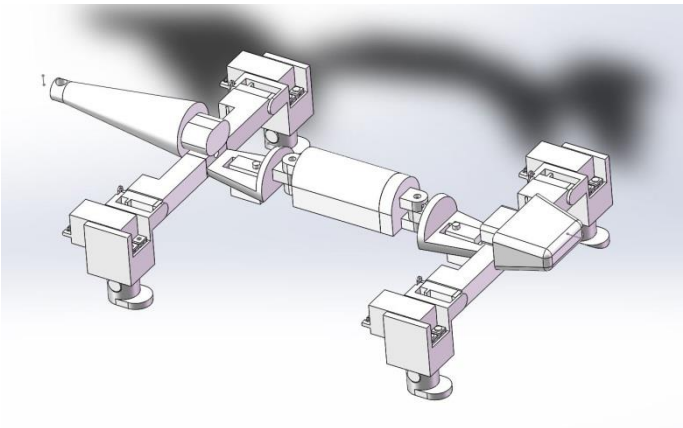

Figure 4.2 CAD model of the Version II

Based on the Version I, the Version II is the most complicated robot among all designed robots, which has maximum degrees of freedom. There are totally ten motors equipped for actuating the robot. Four of them are utilized for lifting legs. Four motors are utilized for rotating thighs. And the left two motors are utilized for changing the length of thighs during the locomotion of the robot to keep the robot move along a straight line. The spring is stored in the middle part, which can be replaced easily and conveniently. The function of the tail is unchanged, which is used to help robot achieve balance. But the tail is passive now and doesn't need a motor.

This robot seems to meet all the requirements and work out the problems mentioned above. It can move successfully and smoothly in SolidWorks. However, Moving well in the software doesn't mean it can move well practically. There are many unpredictable problems in practice.

Controlling ten motors synchronously and making them work concordantly with each other is not a simple thing. This robot is composed of so many parts. Most of these parts are actuated by motors. Therefore, this robot needs high precision assembly. Even a small assembly error may lead to breakdown. The manufacturing cost of this robot can be extremely high. Additionally, this robot cannot be used to verify the hypothesis. The function of the flexible and compliant trunk is not so obvious.

Both version I and version II are designed based on the imitation of the appearance of lizards. I try to control every degree of freedom, which makes the robot complicated and difficult to be fabricated. To make things even worse, these two robots cannot reflect the value of their flexible and compliant trunks. Actually, the goal of designing bio-inspired robots is not just to copy animals' appearance, but to investigate and study principles beyond the surface. And researchers try to explore potential applications of these principles. In this research, the most important thing is to design a robot which is consistent with our lizard model and can be utilized to verify the hypothesis. So the flexible and compliant trunk is the core of our robot. Other parts should be as simple as possible.

4.1.3 Version III

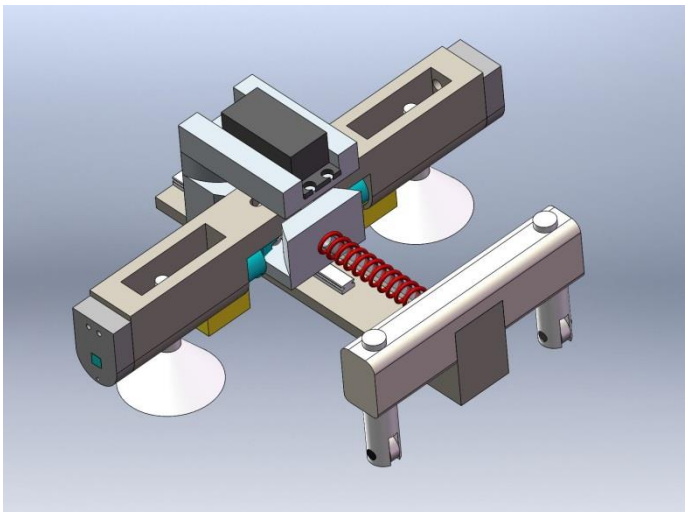

Figure 4.3 CAD model of the Version III

Version III is totally different from previous two robots. Its front legs are replaced by a pair of passive wheels. The front part and the rear part are connected by a linear guide. The front part is passive. And the robot is actuated by the rear part. This is consistent with our lizard model. There are three motors mounted in the rear part. One larger motor is utilized for

rotating the thigh and two smaller motors are utilized for lifting two legs. When the rear part is actuated, it will compress the spring. The compressed spring then will generate force to push the front part move forward.

(a) stationary state

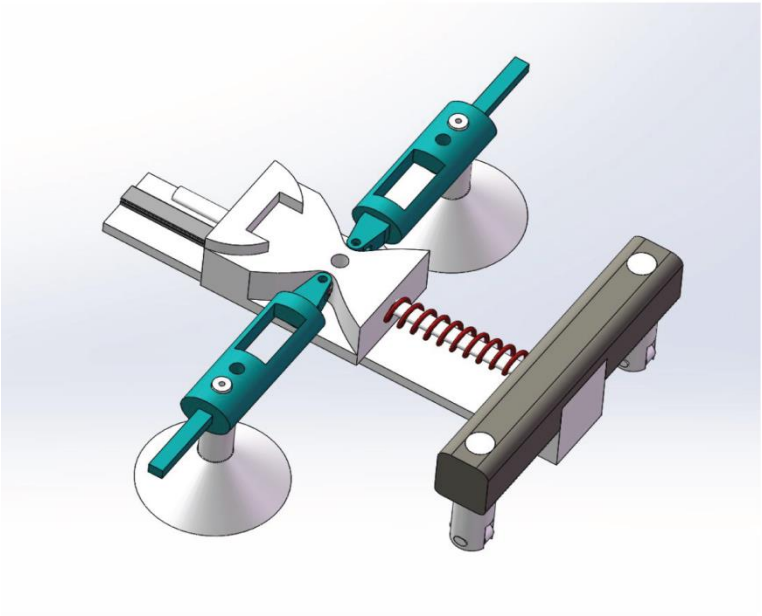

(b) motion state

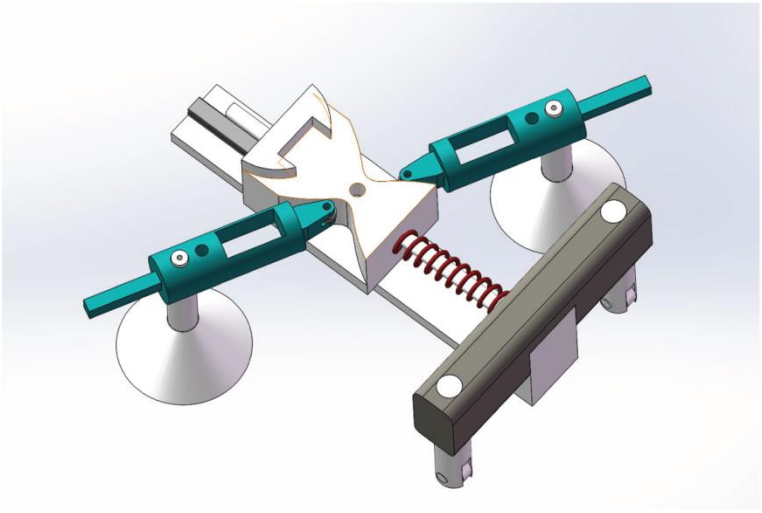

Figure 4.4 Schematic diagram of the rear part of the robot

The highlight of this robot is how it controls the length of the thigh. The length of the thigh is only related to its rotation angle. The relationship between them can be written down by an equation. For this reason, I take advantage of the principle of the cam to design the rear part and two thighs of the robot. As we can see from Figure 4.4, the length of the thigh can change automatically without additional motors because of the structure.

While the structure is novel and reduces the number of motors, it requires small manufacturing errors. We use a 3D printer to make our prototype, whose precision is limited and can't meet the requirement.

4.1.4 Version IV

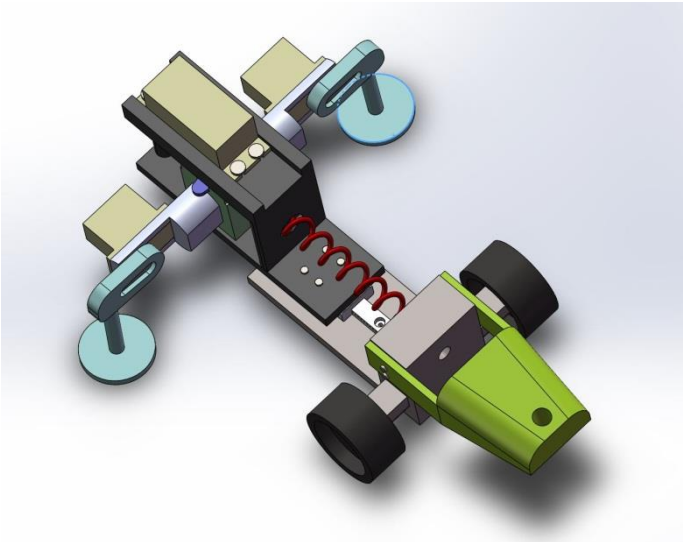

Figure 4.5 CAD model of the Version IV

Version IV is the final version. This robot is similar to the third robot. There are three motors equipped in the robot. One of them is utilized to rotate the thigh. The other two motors are utilized for lifting hind legs. Similarly, the rear part is connected to the front part by a linear guide. When the rear part is actuated, it will compress the spring. The compressed spring then push the front part forward. The spring can be replaced easily and conveniently. Front legs are replaced by a pair of passive wheels. This robot has been proved to be able to move along a straight line.

Compared with the first and second robots, this robot simplifies the configuration of legs in order to emphasize the role of the compliant and flexible trunk in the robot's locomotion. It has fewer motors. Therefore, controlling this robot doesn't need complicated control algorithms. Compared with the third robot, this robot doesn't need high precision machining. So using 3D printing to make the prototype meets the accuracy requirement.

4.2 Mechanical design

(a) CAD drawing

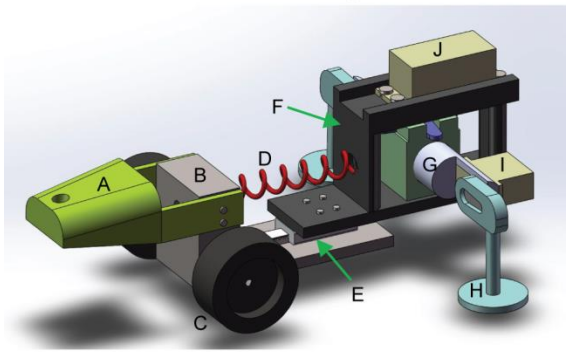

(b) Prototype

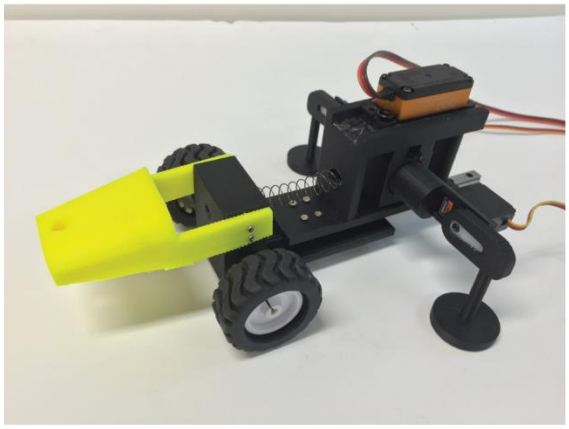

Figure 4.6 A lizard inspired robot

The robot is composed of following components: (A) head; (B) front body; (C) front leg (passive wheel); (D) spring; (E) linear guide; (F) rear body; (G) thigh; (H) hind leg; (I) servo motor; (J) servo motor.

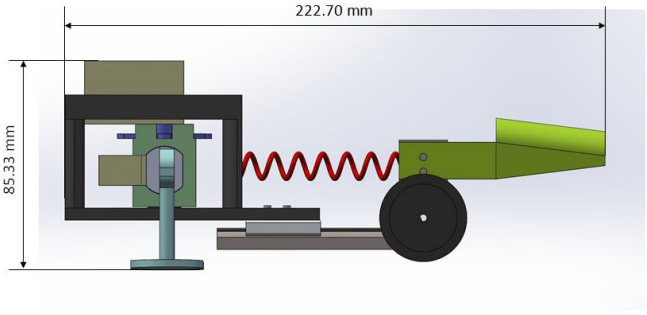

Figure 4.7 Side view of the robot

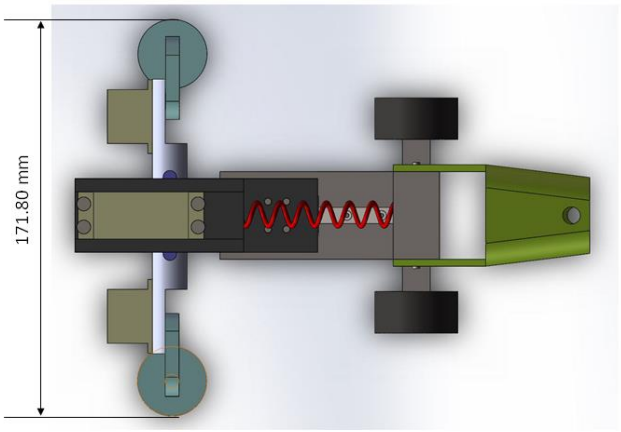

Figure 4.8 Top view of the robot

As shown in figure 4.7 and figure 4.8, the dimension of robot is 222.17mm (L), 171.80mm (W) and 85.33mm (H). The total weight of the robot is 365.8 grams. Details about the mechanical design of the robot will be introduced from the front part to the rear part.

4.2.1 Head

In addition to increasing the beauty, the head plays an important role in maintaining balance. As we can see from figure 4.6, all motors are mounted in the rear part. Obviously, the rear part is heavier than the front part. So the center of gravity of the robot will approach the rear part. In that case, when one hind leg is lifted, the robot can't keep balance. The function of the head is to shift then center of gravity forward by changing its weight. As shown in figure 4.9, there is a threaded hole in the head. By changing the number of bolts and nuts, we can easily change the weight of the head.

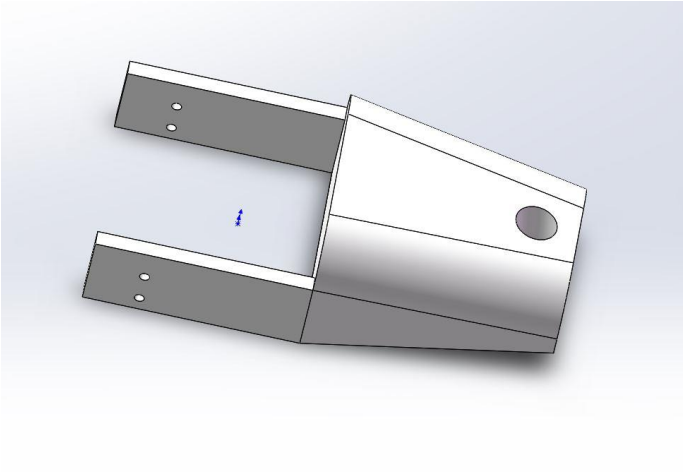

Figure 4.9 Diagram of the head

However, if the head is too heavy, hind legs cannot touch the ground closely. Then they can't generate enough friction. The robot will slip on the ground easily. By trial and error, I find that the closer the center of gravity near the axle of front legs, the better performance the robot has. Eventually, the weight of the head is determined as 90.8 grams.

4.2.2 Front legs

In my design, one function of front legs is to support the front part of the robot. And according to my simulation model, there should be no sliding friction between the front legs and the ground. As a result, I choose a pair of passive wheels as the front legs of my robot. Another important function of the front legs is to keep the robot move along a straight line. To achieve this goal, these two wheels are designed to work synchronously.

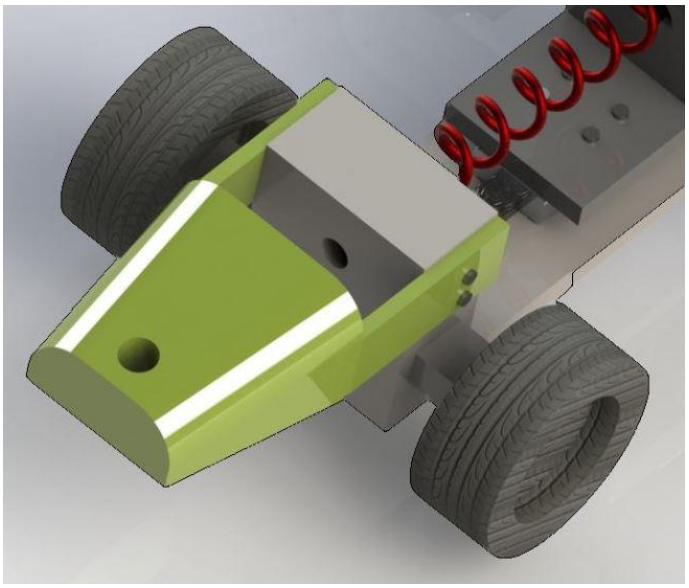

Figure 4.10 Diagram of the front legs

4.2.3 Trunk (linear guide and linear spring)

The trunk is the key part of my robot. The trunk of my robot is composed of a linear guide and a linear spring. According to my simulation model, displacements of the front part and the rear part are different. There should be no any friction between two parts and both parts should move towards the same direction. Using one spring is not enough. So I use one linear guide to connect these two parts. As shown in figure 4.11, the rear part is connected to the block and the front part is connected to the linear guide. The spring between two parts is linear and can be replaced easily and conveniently.

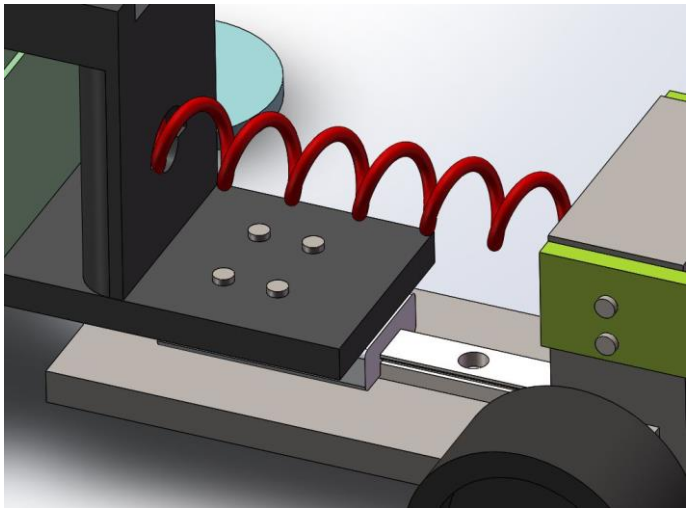

Figure 4.11 Diagram of the trunk

4.2.4 Rear part

The rear part takes charge of actuating the whole robot, which is the most important and the most difficult part in the design. As illustrated in figure 4.12, the rear part is composed of following components: one main body, one connecting part, one servo arm, one thigh, two hind legs, three servo motors and some crews.

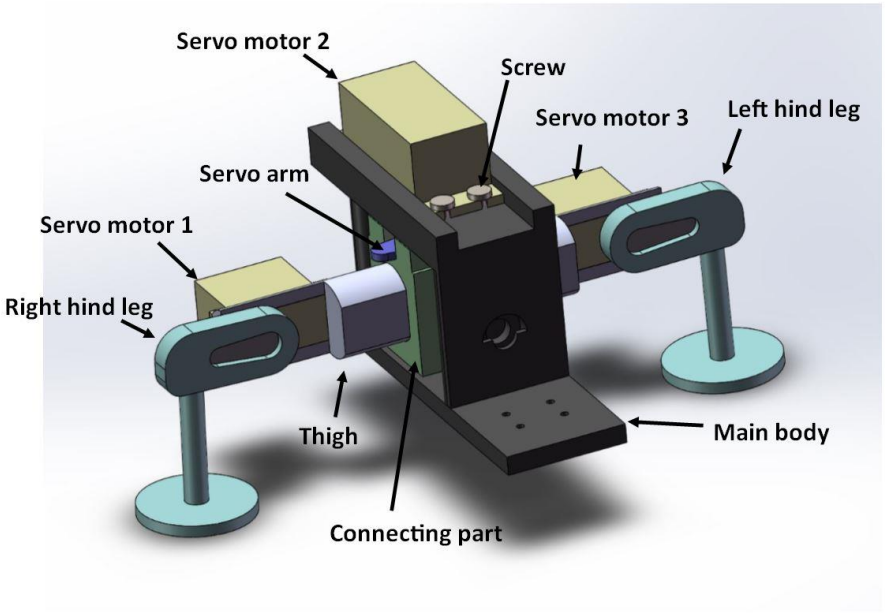

Figure 4.12 Schematic diagram of the rear part

The forward force is generated by the servo motor 2. The servo motor is mounted in the main body by screws. It rotates the connecting part by the servo arm. The connecting part rotates

the thigh to push the robot move forward. Another two servo motors are utilized to lift two hind legs respectively.

There are some design details need to be noticed. As shown in figure 4.13, the cross-sectional shape of the thigh is not a complete circle. So the thigh can only move along one direction, which enhances the stability of the robot. The surface of the contact portion between the connecting part and the thigh is highly smooth (see figure 4.14). So the thigh can cross the connecting part easily and without any resistance.

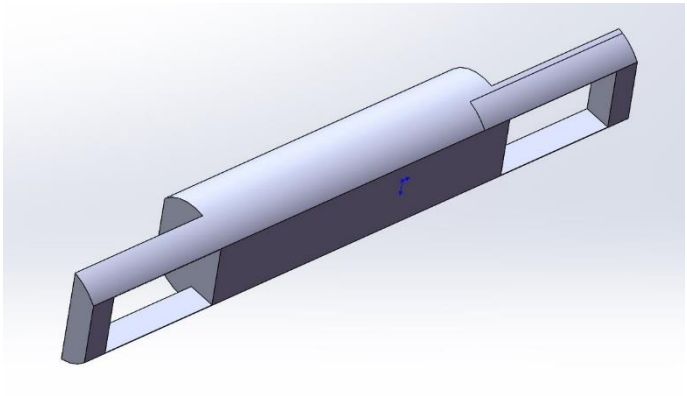

Figure 4.13 Diagram of the thigh

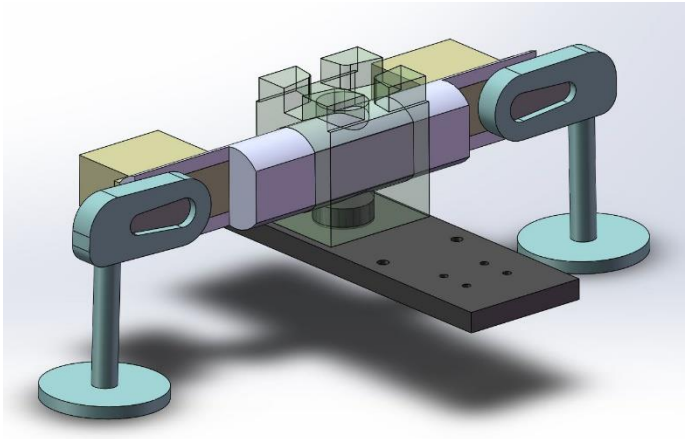

Figure 4.14 Diagram of the connecting part and the thigh

Figure 4.15 shows how the thigh changes its length passively and automatically. In this figure, the green dot denotes the middle point of the thigh and the yellow dotted line denotes the forward direction of the robot. Taking half cycle as an example. When the thigh rotates around its left hind leg, the robot lifts its right hind leg. At the beginning, the middle point of the thigh coincides with the forward direction. As the thigh rotates forward, the middle point of the thigh will gradually deviate from the forward direction and then gradually approach the

forward direction. At the end of the half cycle, the middle point of the thigh coincides with the forward direction again. The offset distance is determined by the length and the rotation angle of the thigh.

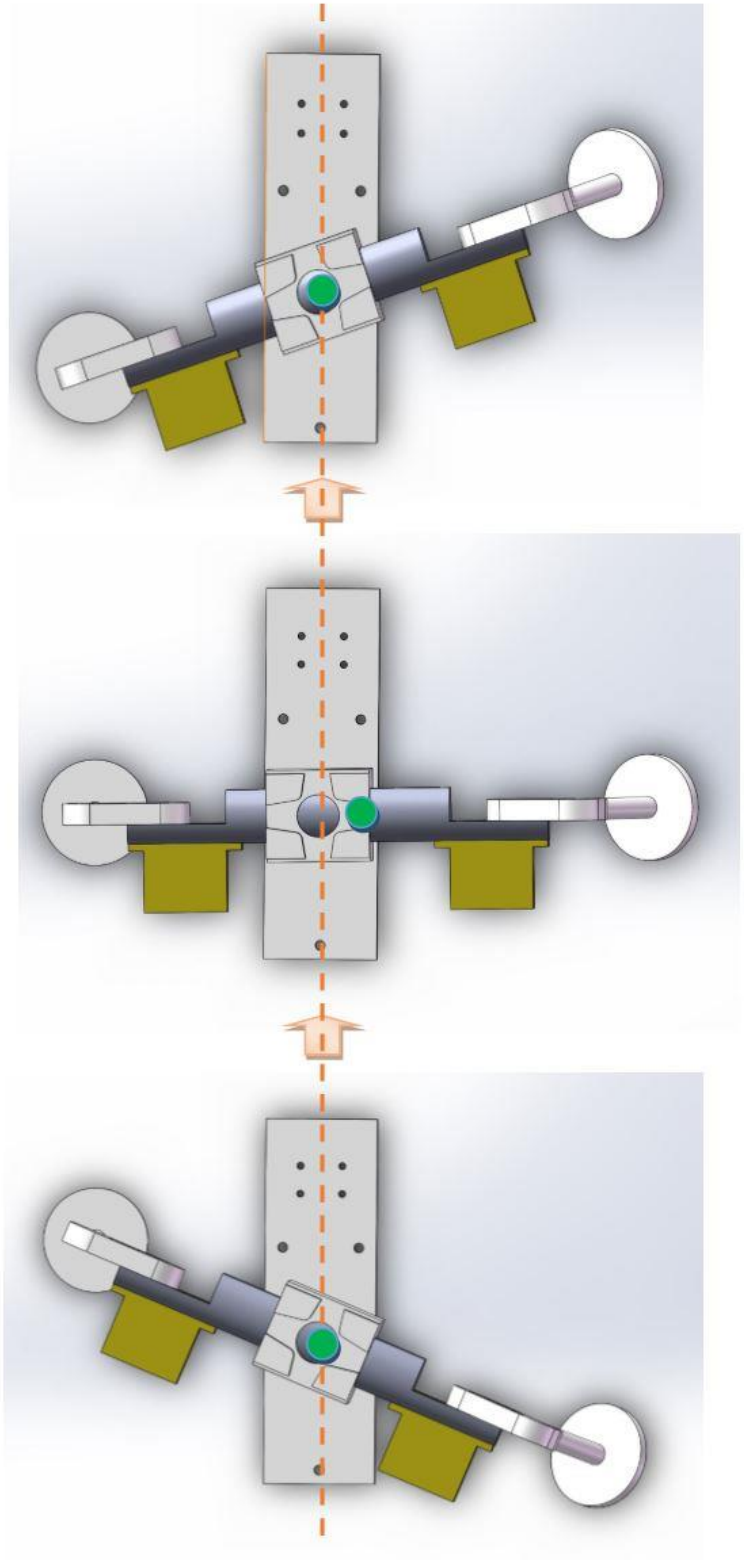

Figure 4.15 Schematic diagram of the thigh's movement

Figure 4.16 shows the explored view of one hind leg of the robot. For each hind leg, it consists of three components: a leg, a sole, and a screw. When the sole touches the ground, it should keep still. But the leg should rotate with the rotation of the thigh. That's why the leg and the sole should be separate.

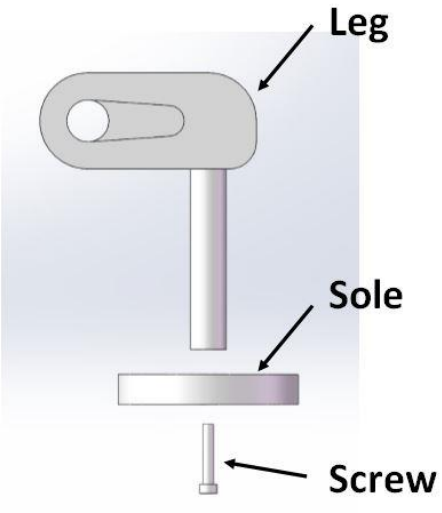

Figure 4.16 Explored view of one hind leg

4.3 Fabrication

4.3.1 Selection of the manufacturing method and materials

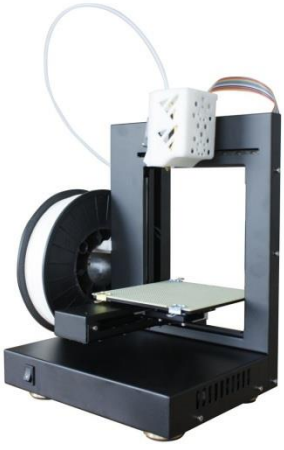

Figure 4.17 3D printer

Traditional metal manufacturing methods take a long time. Additionally, most of them are expensive. 3D printing, as a kind of new manufacturing method, is good at making fast

prototypes, which saves both time and money. The 3D printer I have used is UP! PLUS 2 (see figure 4.17), which is designed and produced by a US company, Tiertime corporation. The material I have used is acrylonitrile butadiene styrene (ABS). The resolution of this printer is 0.15 mm. Both the stiffness and the resolution meet requirements of my design.

4.3.2 Selection of servomotors

Figure 4.18 Servomotors

My robot needs three servomotors. Different tasks ask for different servomotors. The one, which is utilized for actuating the robot, should generate enough torque to rotate the thigh. The other two servomotors, which are utilized for lifting two hind legs respectively and don't need to generate large torque, should be light and small. Besides that, under the premise to meet all the requirements, we should choose the most economic servomotors. After comparing a number of different servomotors, I eventually choose following two types: SC-1251MG and ES09MD (see figure 4.18). SC-1251MG is chosen to actuate the robot and ES09MD is chosen to lift hind legs. Datasheets of these two types of servomotors are attached in appendix A.

4.3.3 Selection of the linear guide

The function of the linear guide is to combine the front part and the rear part together. There is not much force acting on the linear guide. To reduce the size and the weight of the robot, the linear guide should be small and light. Miniature linear guides are suitable for my robot. The type of the linear guide I choose is SSEBSZ8-100, which is manufactured by MISUMI

(see figure 4.19). The CAD drawing and dimensions of the linear guide are attached in appendix A.

Figure 4.19 Miniature linear guide

4.3.4 Selection of the spring

In Chapter 2, I have obtained the conclusion that stiffness of the spring has great effects on the energetically efficient locomotion of the robot. At a specific frequency, there should be an optimized stiffness. But most of the optimized stiffness is so small that springs with the optimized stiffness can't be bought from the market. As a result, in this research, I choose two springs. One of them is relatively soft, whose stiffness is 60 N/m. And the other one is relatively stiff, whose stiffness is 160N/m. Experiments will be performed based on these two springs (details about experiments will be introduced in the next chapter). Figure 4.21 shows the picture of them and parameters of both springs are attached in appendix A.

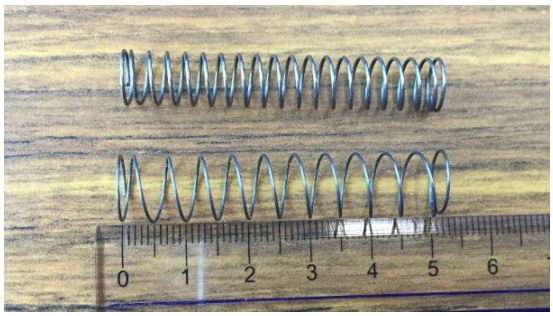

Figure 4.21 Linear springs

4.3.5 Selection of the controller

Servo motors are controlled by PWM (pulse width modification) signals. The controller used in this research should have the ability to generate PWM signals. And its weight and size should be small. Figure 4.23 shows the selected controller: Arduino Mega 2560. The Arduino Mega 2560 is a microcontroller board based on the ATmega2560. It has 54 digital

input/output pins (of which 15 can be used as PWM outputs), 16 analog inputs, 4 UARTs (hardware serial ports), a 16 MHz crystal oscillator, a USB connection, a power jack, an ICSP header, and a reset button.

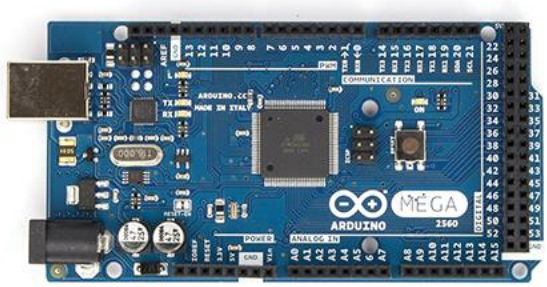

Figure 4.22 Arduino Mega 2560

4.3.6 Selection of the front legs (wheels)

In my design, the front legs are replaced by a pair of passive wheels. The wheels should work synchronously to ensure that robot can move along a straight line. To achieve this goal, I chose a pair of wheels whose axle is hexagonal (see figure 4.23).

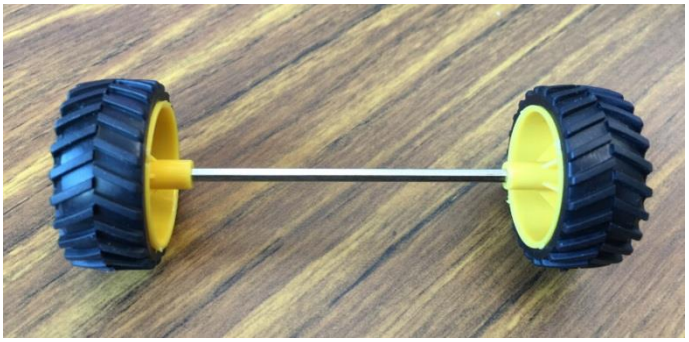

Figure 4.23 A pair of passive wheels

4.4 Hardware and software architecture

As shown in figure 4.24, the complete system includes a computer, a 5V DC power supply, a controller, a bread board, a robot and several wires. When the system is working, control programmes are compiled in the computer and then transferred to the controller. After receiving the programmes, the controller board will generate PWM signals. Motors in the robot will receive these signals and actuate the robot to follow the desired trajectory. The 5V

DC power supply provides power for motors and the controller. The whole process is illustrated in figure 4.25.

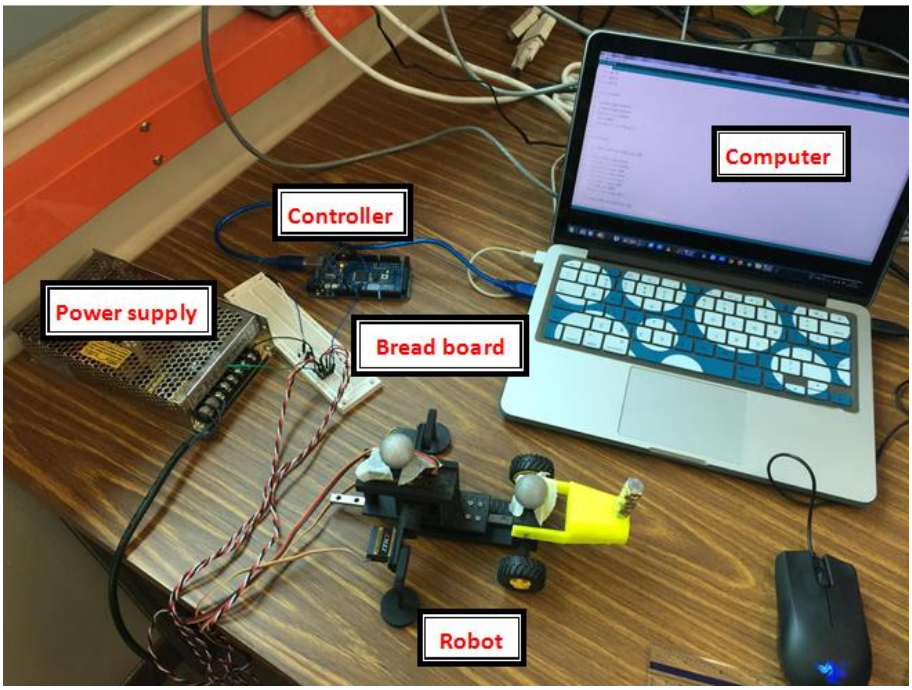

Figure4.24 Hardware architecture of the system

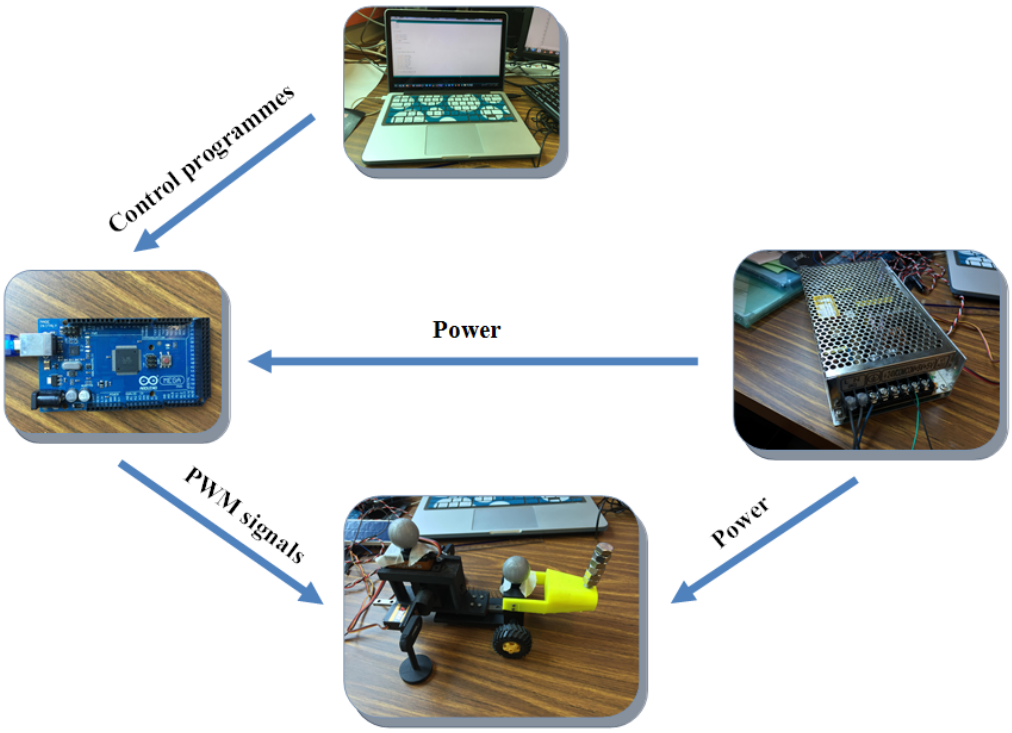

Figure 4.25 Software architecture of the system

4.5 Conclusion

Compared with previous several designs, the final design has advantages in feasibility, simplicity and similarity to the simulation model. 3D printing is selected as the manufacturing method to make the prototype. All the components are selected carefully based on the principle of cost-effect. Both hardware and software architectures have been established.

Chapter 5: Experiment

Experiments have been carried out aiming at testing the performance of the designed robot and verifying the hypothesis. In this chapter, experimental setups and procedures are introduced. Experimental results are illustrated and discussed.

5.1 Purpose of the experiment

The experiment has two goals. One is to test the performance of the designed robot including the ability to follow a desired trajectory and the ability to move along a straight line. The other is to verify my hypothesis that flexible trunks do have effects on improving robots' energy efficiency in terms of reducing motors' peak power. As mentioned in Chapter 3, motor power discussed in this research is the one that is utilized for actuating the robot, which can be calculated by equation (3-5) and equation (3-8). Therefore, displacements of the robot have been recorded under different conditions, which can be used to calculate velocities and accelerations of the robot. Once velocities and accelerations are obtained, the motor power can be analysed.

5.2 Experimental setup

In order to achieve these two goals, experiments were conducted on robots with different trunks (see figure 5.1). The rigid robot means two parts of the robot are connected rigidly using a bolt. The flexible robot can have different trunks by changing the stiffness of the spring. In this experiment, I chose two springs, one's stiffness is 60 N/m and the other's is 160N/m.

(a) The rigid robot

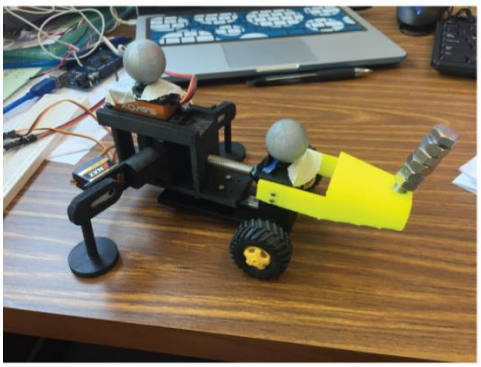

(b) The flexible robot

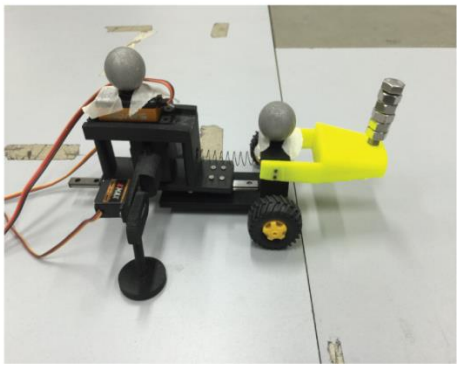

Figure 5.1 Robots used for experiments

All experiments were conducted in the gait lap of National University of Singapore, which is equipped with a Vicon motion capture system (see figure 5.2). A Vicon high speed motion capture system (Vicon, Oxford, UK) is able to capture 3D position of the each reflective marker with sampling frequency at 100Hz. 3D position of the markers can be collected using eight cameras. The raw kinematic data can be low-pass filtered via zero-lag 4th-order Butterworth filter with cut-off frequency of 6 Hz to remove motion artefacts and high random noise. The filtered data can be extracted and used for further analysis on kinetics.

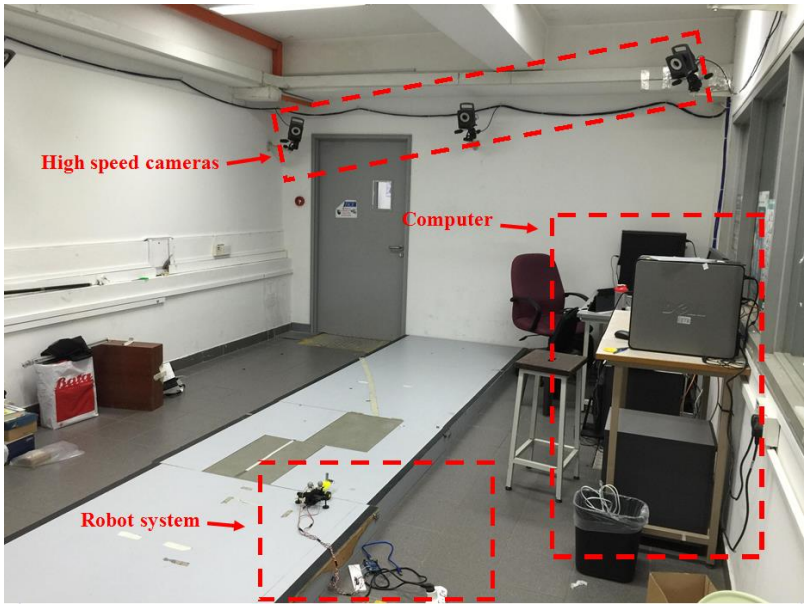

Figure 5.2 Experimental setup

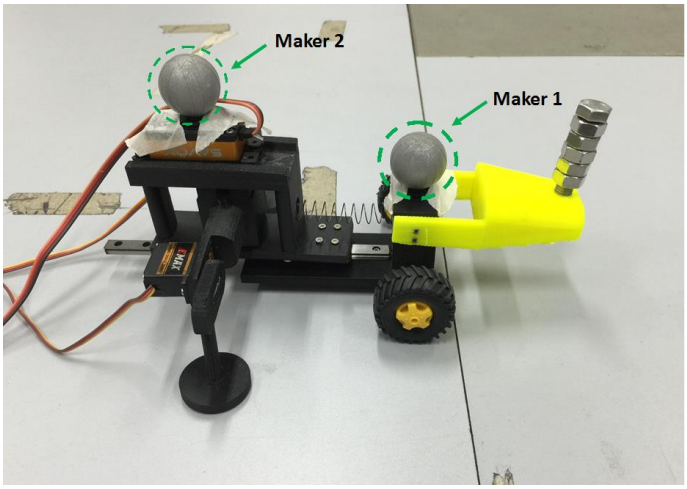

Figure 5.3 Robot with two markers

During the experiment, two makers have been respectively attached to two parts of the robot (see figure 5.3). Therefore, kinematic data (displacement, velocity and acceleration) of both

two parts were able to be recorded and analysed. Kinetic analysis can be performed based on these data. As illustrated in figure 5.4, displacements in both x-axis and y-axis have been recorded. Displacement in the y-axis direction was used for testing the robot's ability to follow the disred trajectory. The smaller the tracking error is, the better performance the robot has. Displacement in the x-axis was used for testing the robot's ability to move along a straight line. The smaller displacement in the x-axis means the robot has a better performance.

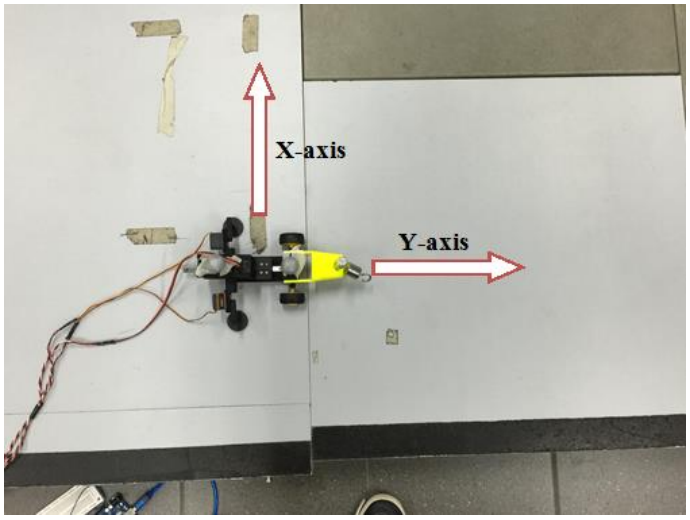

Figure 5.4 X-axis and Y-axis

5.3 Experimental procedure

The whole experiment can be divided into two parts: kinematics and kinetics. Experiments about kinematics were conducted for the purpose of evaluating the performance of the robot. Experiments about kinetics were conducted for the purpose of verifying the hypothesis.

For the purpose of testing the performance, the rigid robot was firstly programmed to follow uniform velocity trajectories at four different frequencies: 0.5Hz, 1Hz, 2Hz, and 3Hz. Then the rigid robot was programmed to follow variable velocity trajectories at three different frequencies: 1Hz, 2Hz, and 4Hz. During these experiments, displacement of the robot in both x-axis and y-axis has been recorded. And tracking errors in the y-axis and offset in the x-axis were calculated to evaluate the performance of the robot.

After measuring the performance of the robot, the robot with three different trunks was respectively programmed to follow a desired trajectory. Displacement of both parts of the robot in y-axis has been recorded. Tracking errors were obtained by comparing the desired trajectory and the actual trajectory. Velocities and accelerations were integrated from the

displacement. Once obtaining velocities and accelerations, the motor power was calculated based on the obtained velocities and accelerations. By comparing motor powers of different robots, my hypothesis can be verified.

5.4 Experimental results

5.4.1 Kinematics

Experiments on kinematics were conducted to evaluate the performance of the robot. And experiments of this part were only carried out on the rigid robot. The robot was programmed to follow two kinds of trajectories: uniform velocity and variable velocity.

5.4.1.1 Uniform velocity

For uniform velocities, the robot worked at four different frequencies: 0.5Hz, 1Hz, 2Hz, and 3Hz. In each case, the robot ran ten times. One of these ten results was selected and presented in the following part. Displacement in both indirections (x-axis and y-axis) was records and compared with the desired displacement. Tracking errors were analysed.

(1) 0.5Hz

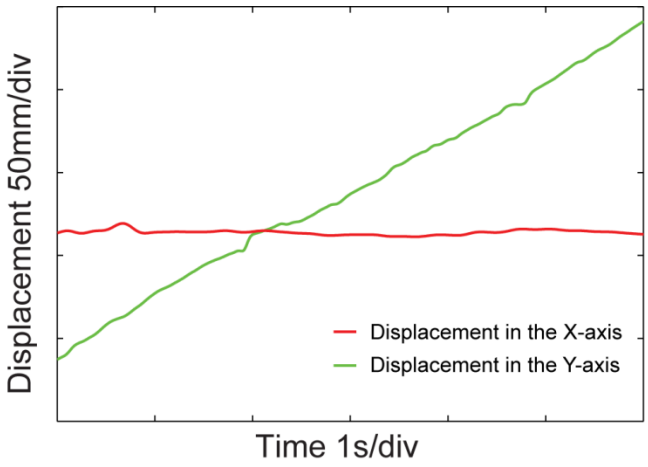

Figure 5.5 Displacement of the robot

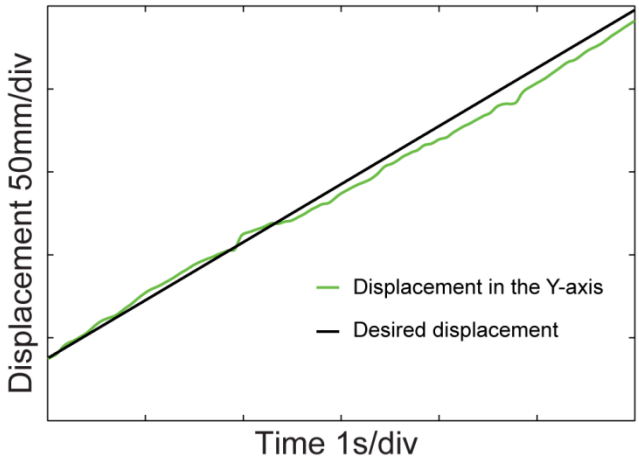

Figure 5.6 Comparison of the displacement in the Y-axis

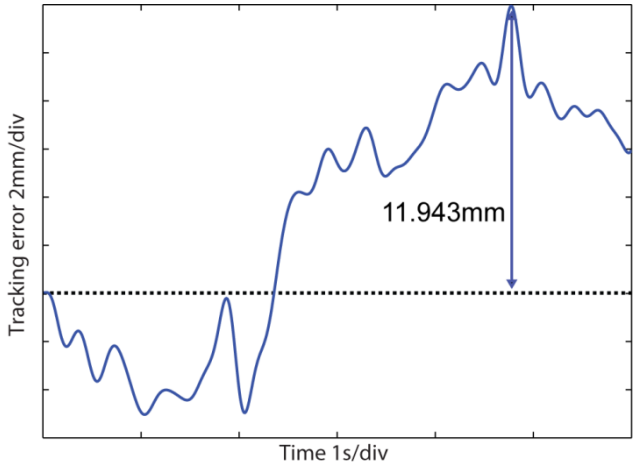

Figure 5.7 Tracking errors in the Y-axis

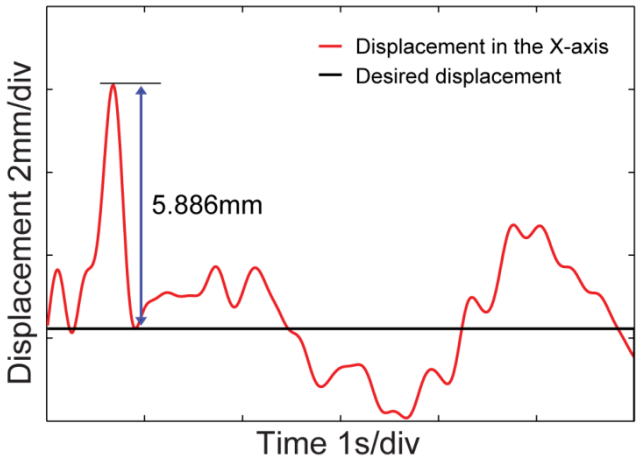

Figure 5.8 Comparison of the displacement in the X-axis

Figure 5.5 shows the actual displacement of the robot at the frequency of 0.5 Hz. The green curve denotes the displacement of the robot in the y-axis and the red curve denotes the displacement in the x-axis. The green curve is approximately linear and the red curve is an approximate horizontal straight line. In order to explicitly indicate the performance of the robot, the displacement of the robot in two directions were respectively compared with the desired displacement (see figure 5.6 and 5.8). The green curves denote the actual displacement of the robot and the black curves denote the desired displacement of the robot. Tracking errors are presented in figure 5.7. The maximum tracking error is 11.943 mm, which is 2.8% of the total displacement (420mm). The maximum offset in the x-axis is 5.886mm.

(2) 1Hz

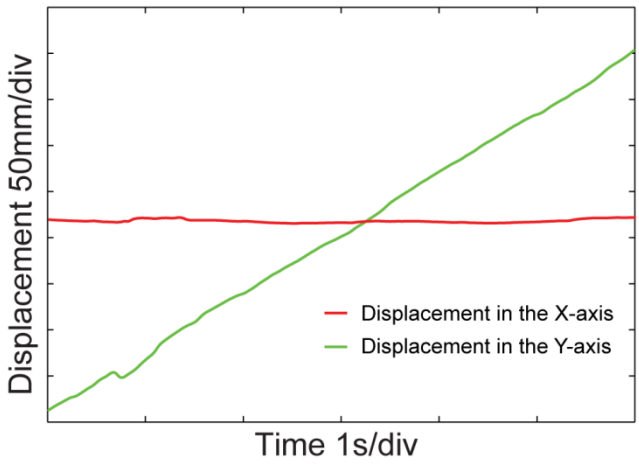

Figure 5.9 Displacement of the robot

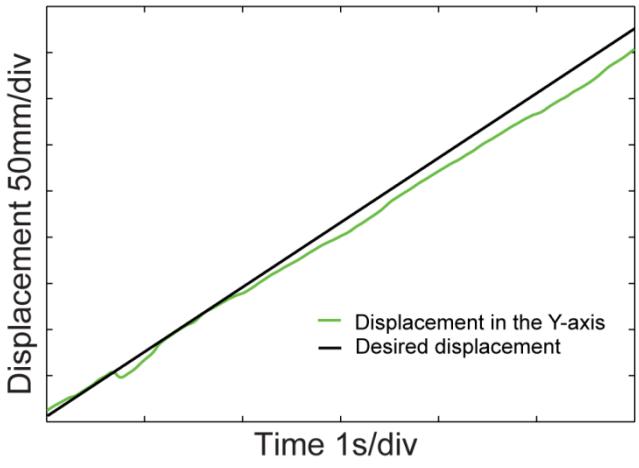

Figure 5.10 Comparison of the displacement in the Y-axis

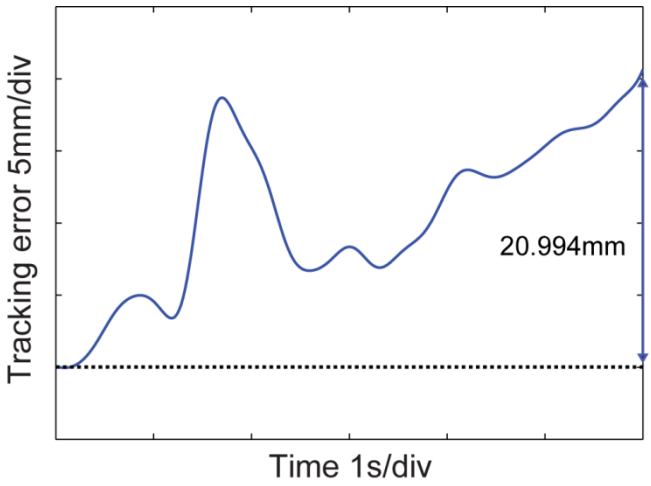

Figure 5.11 Tracking errors in the Y-axis

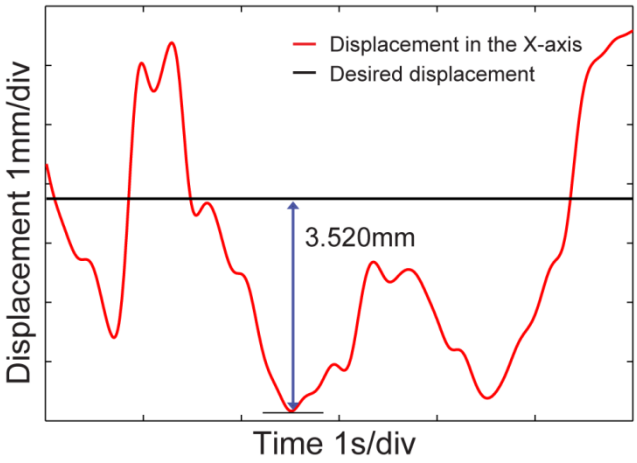

Figure 5.12 Comparison of the displacement in the X-axie

Figure 5.9 shows the actual displacement of the robot at the frequency of 1 Hz. The displacement of the robot in two directions is respectively compared with the desired displacement in figure 5.10 and 5.12. Tracking errors are presented in figure 5.11. The maximum tracking error is 20.994 mm, which is 2.5% of the total displacement (840mm). The maximum offset in the x-axis is 3.520 mm. The performance of the robot at the frequency of 1Hz is better than that at the frequency of 0.5Hz.

(3) 2Hz

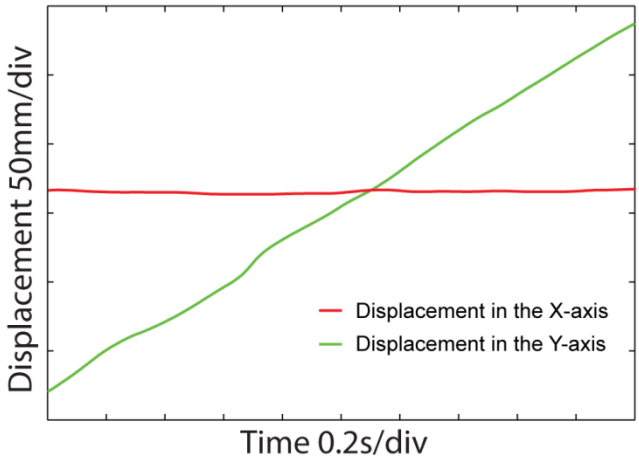

Figure 5.13 Displacement of the robot

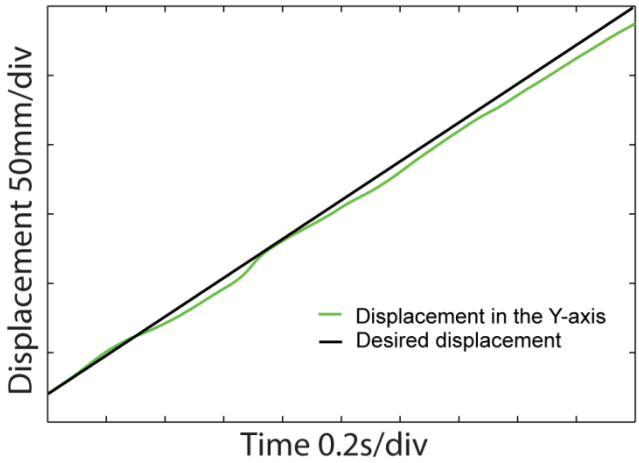

Figure 5.14 Comparison of the displacement in the Y-axis

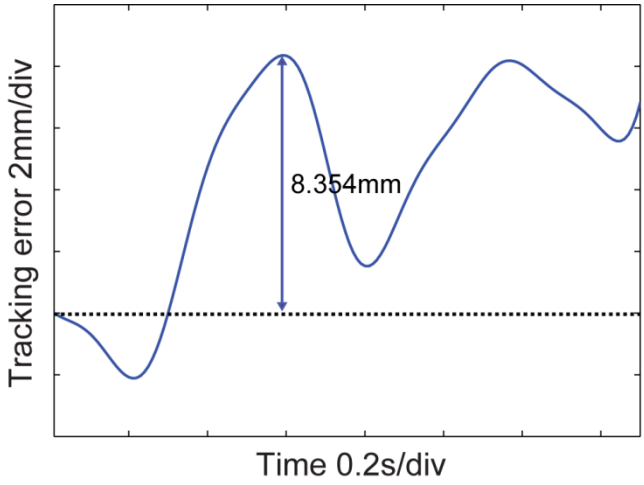

Figure 5.15 Tracking errors in the Y-axis

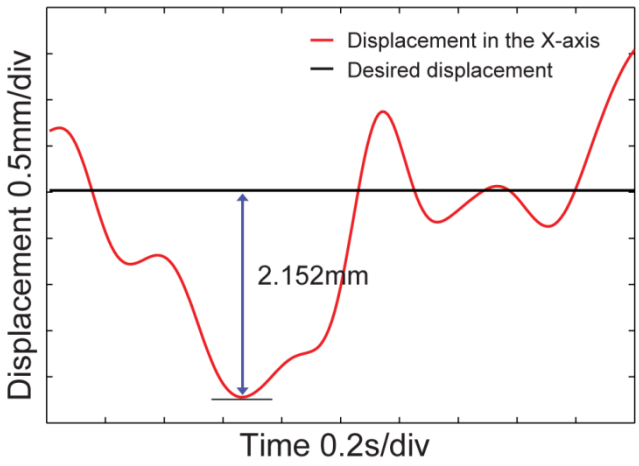

Figure 5.16 Comparison of the displacement in the X-axie

Figure 5.13 shows the actual displacement of the robot at the frequency of 2 Hz. The displacement of the robot in two directions is respectively compared with the desired displacement in figure 5.14 and 5.16. Tracking errors are presented in figure 5.15. The maximum tracking error is 8.354 mm, which is 1.5% of the total displacement (560mm). The maximum offset in the x-axis is 2.152 mm. The performance of the robot at the frequency of 2 Hz is better than previous two cases.

(4) 3Hz

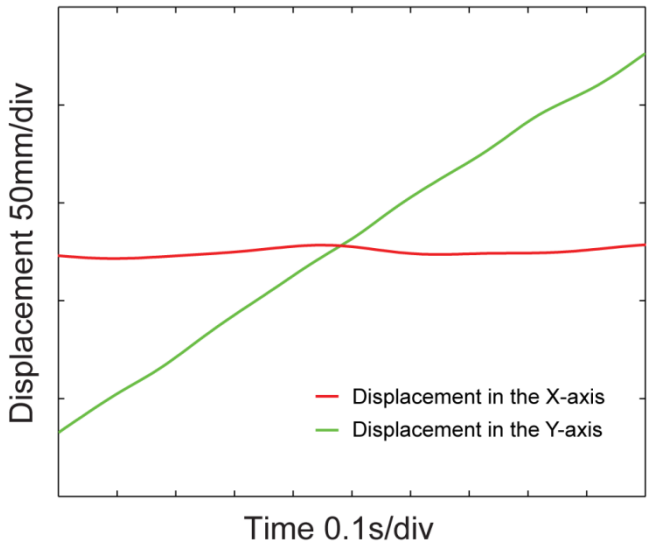

Figure 5.17 Displacement of the robot

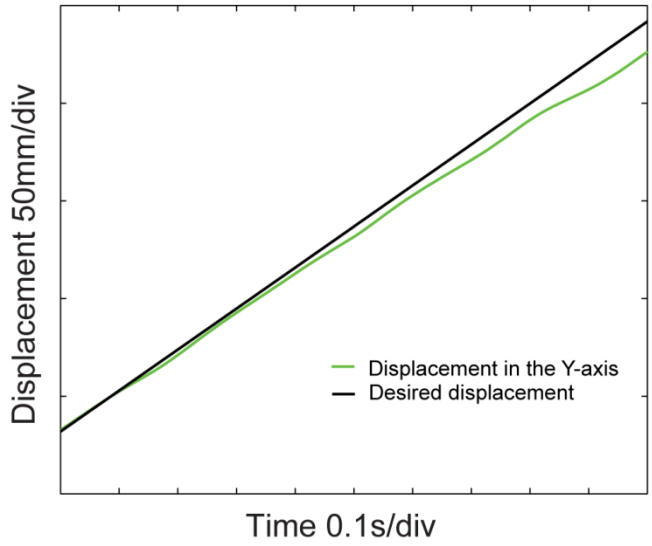

Figure 5.18 Comparison of the displacement in the Y-axis

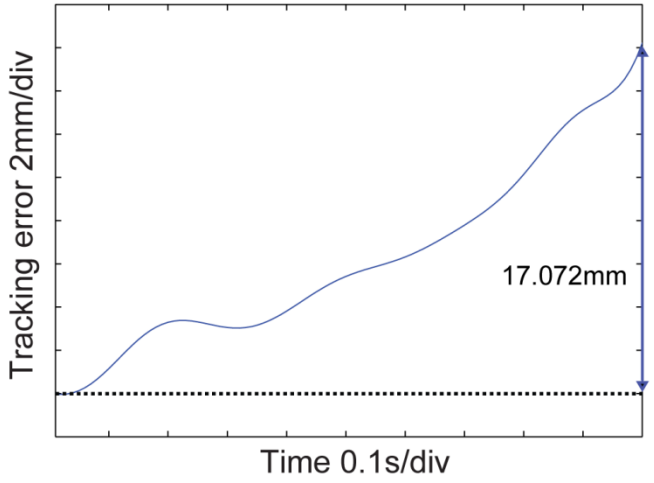

Figure 5.19 Tracking errors in the Y-axis

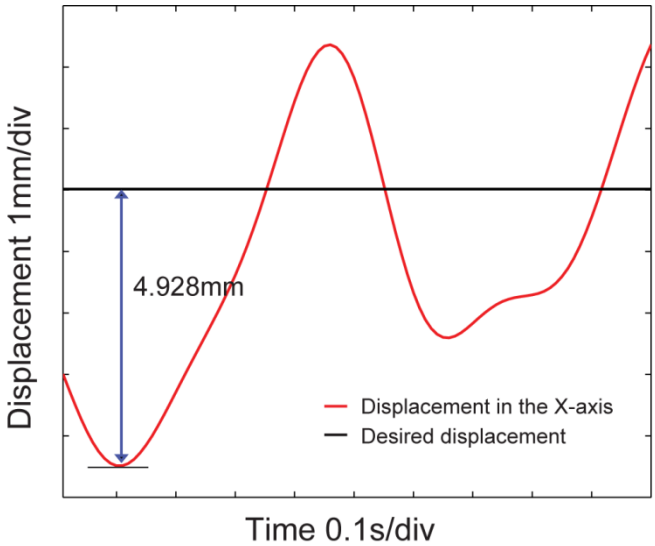

Figure 5.20 Comparison of the displacement in the X-axie

Figure 5.17 shows the actual displacement of the robot at the frequency of 3 Hz. The displacement of the robot in two directions is respectively compared with the desired displacement in figure 5.18 and 5.20. Tracking errors are presented in figure 5.19. The maximum tracking error is 17.072 mm, which is 4.1% of the total displacement (420mm). The maximum offset in the x-axis is 4.928 mm. The performance of the robot at the frequency of 3 Hz is the worst among all cases.

5.4.1.2Variable velocity

For variable velocities, the robot worked at three different frequencies: 1Hz, 2Hz, and 4Hz. Displacement in the y-axis was recorded and compared with the desired displacement. Tracking errors were analysed. In each case, the robot ran twenty times. Three sets of all results were selected and presented in the following part. For each set of results, the left figure illustrates the comparison between the actual displacement and the desired displacement. The right figure illustrates the tracking error.

Figure 5.21 shows the performance of the robot at the frequency of 1Hz. Compared with the desired displacement, the actual displacement has a similar variation tendency. The average maximum tracking error is 14.635 mm, which is 3.5% of the total displacement (420mm). Taking into account the assembly error, the performance of the robot at this frequency is acceptable.

Figure 5.22 shows the performance of the robot at the frequency of 2Hz. Compared with the desired displacement, the variation tendency of the actual displacement is not so obvious, which can be also indicated from the tracking errors. The fluctuation of the tracking errors is violent. The performance of the robot at this frequency is worse than that at the frequency of 1Hz.

Figure 5.22 shows the performance of the robot at the frequency of 4Hz. Compared with the desired displacement, the variation tendency of the actual displacement is more inconspicuous. The curve is approximately linear. The fluctuation of the tracking errors is more violent than that at the frequency of 2Hz. The performance of the robot is the worst among three cases.

(1) 1Hz

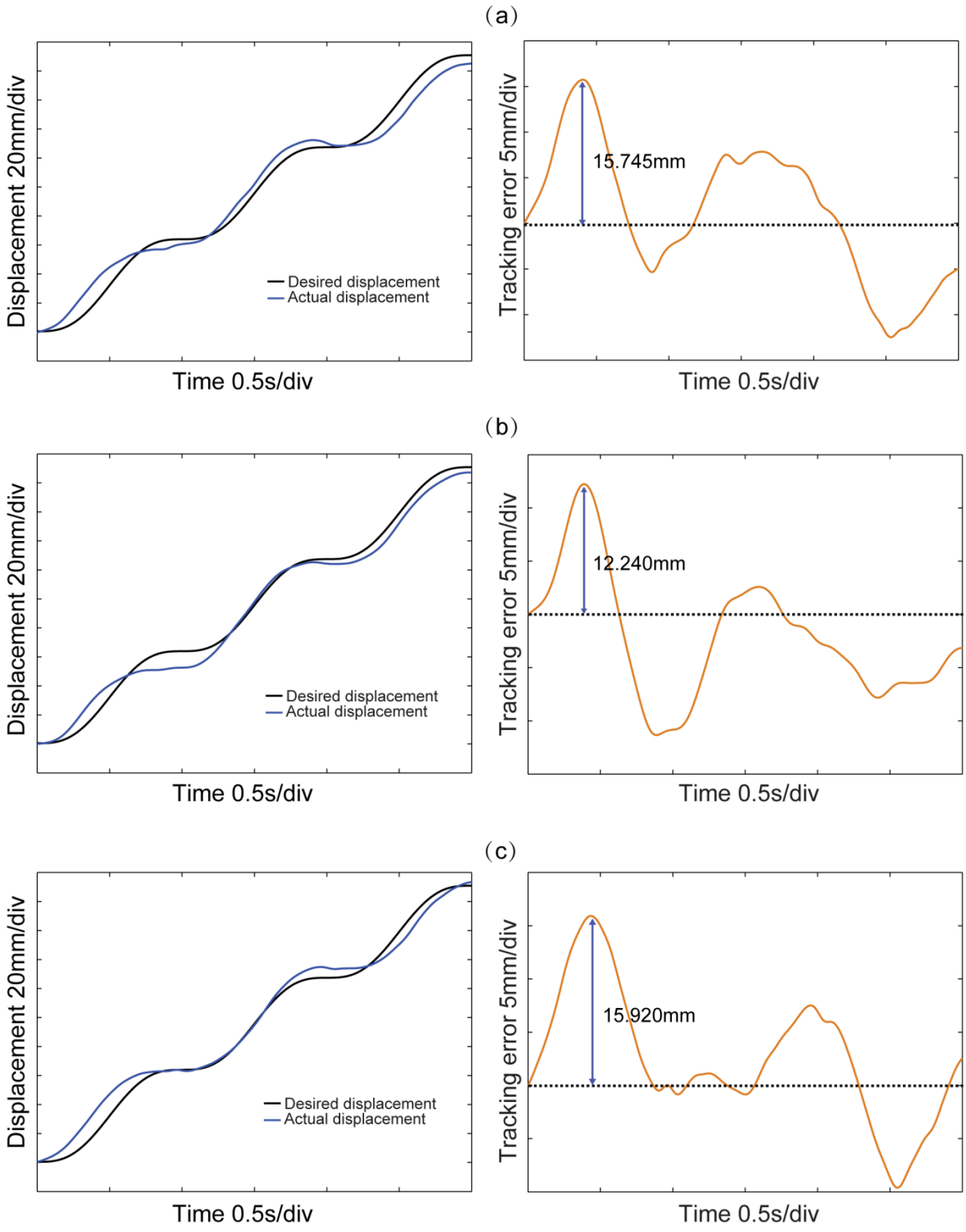

Figure 5.21 Performance of the robot at the frequency of 1Hz

(2) 2Hz

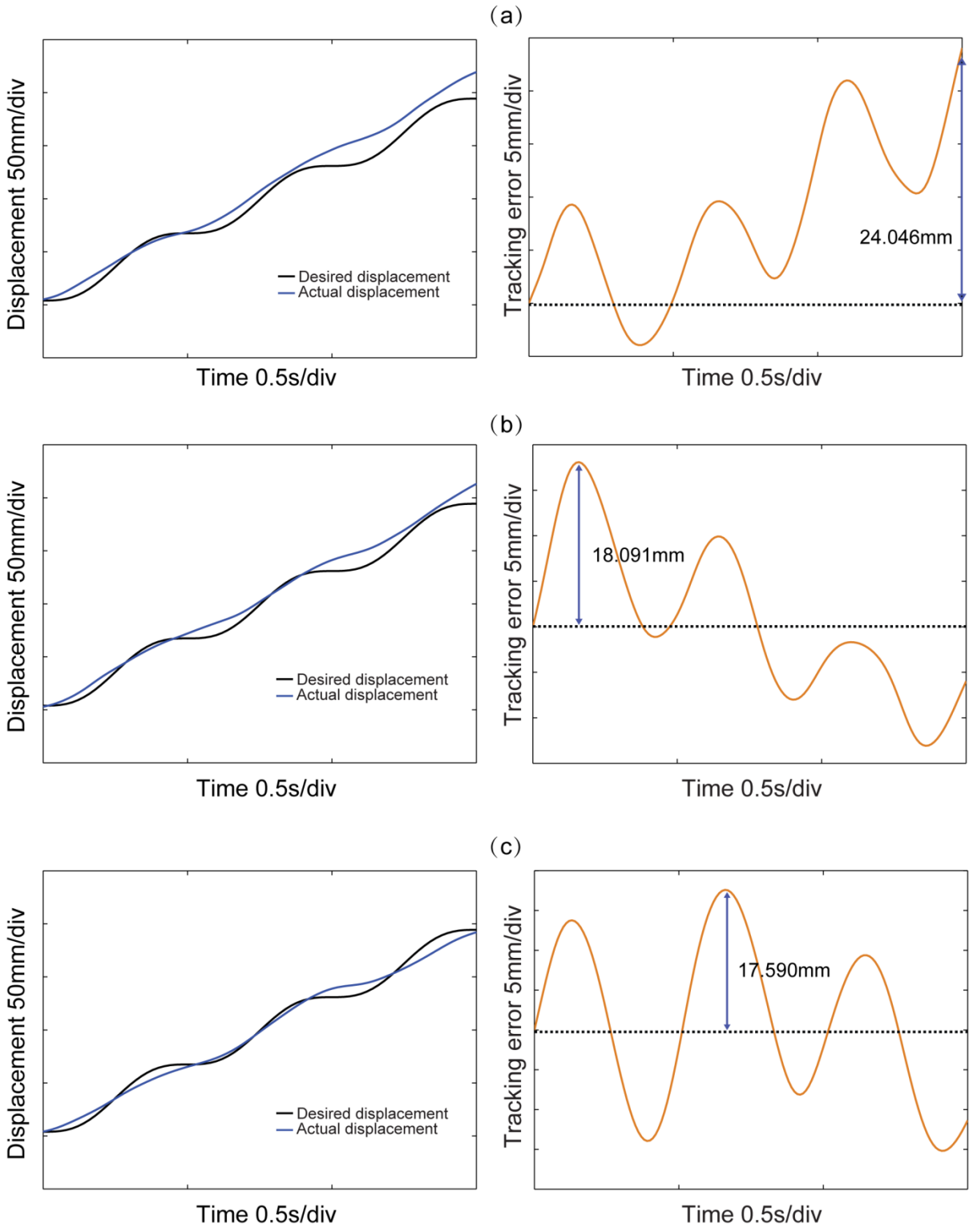

Figure 5.22 Performance of the robot at the frequency of 2Hz

(3) 4Hz

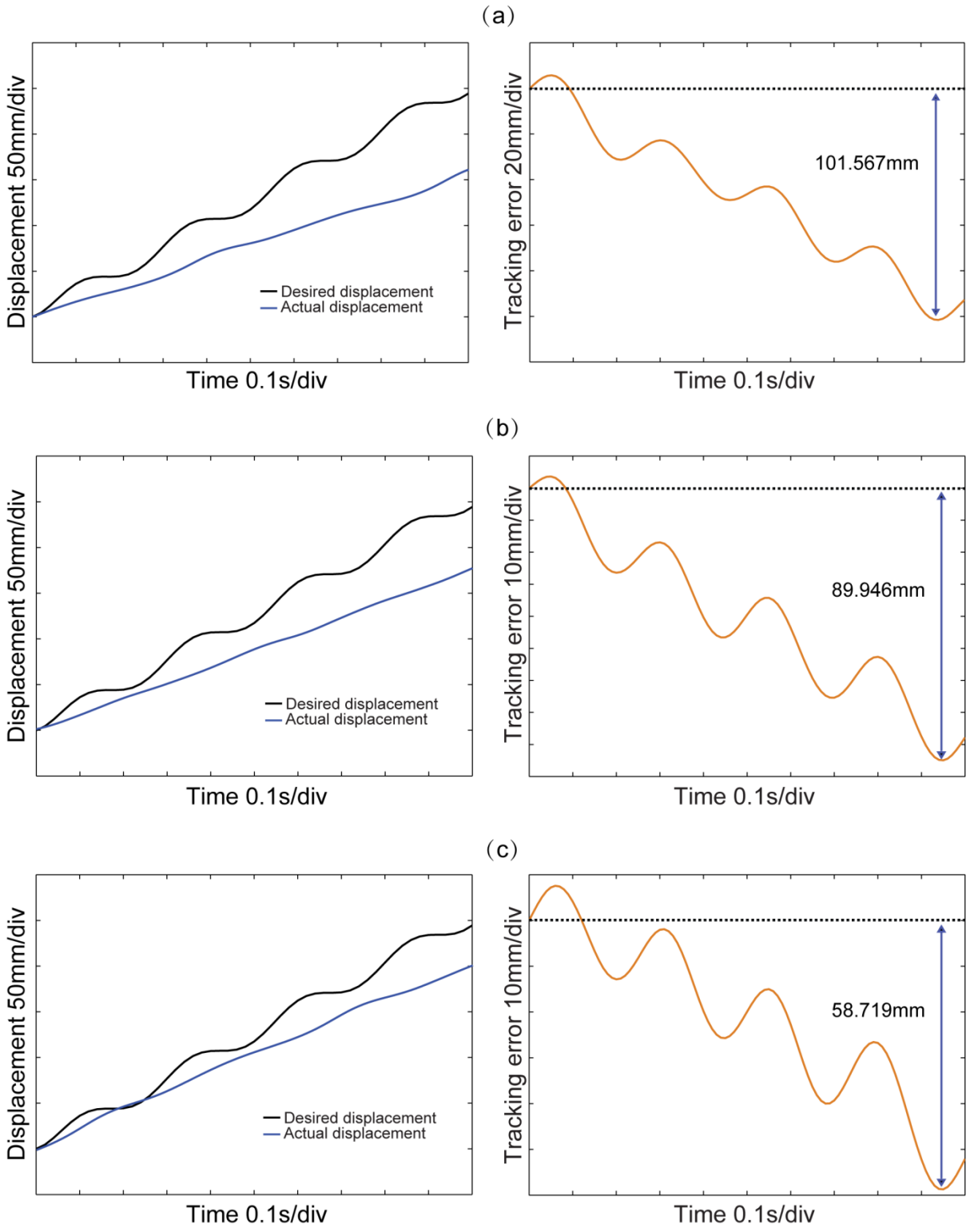

Figure 5.23 Performance of the robot at the frequency of 4Hz

5.4.2 Kinetics

Experiments on kinetics were conducted to verify the hypothesis that flexible trunks do have effects on energetically locomotion in terms of reducing motors' peak power. And experiments of this part were carried out on robots with three different trunks (rigid, stiffness equalled 60N/m, stiffness equalled 160N/m). From above results, we found that robots could have good performance when the velocity was uniform. In the case of variable velocities, the robot could only perform well at relatively low frequencies. However, simulations results indicated that the reducing of the peak power was not obvious if the frequency of the desired trajectory was too low. As a result, robots were programmed to follow a desired trajectory whose frequency was 1 Hz. For each robot, displacement of two parts was compared with the desired displacement. Velocities and accelerations of the rear part were calculated. The motor power that was utilized for actuating the robot was obtained to verify the hypothesis and part of simulation results.

5.4.2.1 The rigid robot

The rigid robot was programmed to follow a desired trajectory at the frequency of 1Hz. For the rigid robot, the displacement of the rear part was recorded. Figure 5.24 illustrates the comparison of the actual displacement with the desired displacement in the y-axis. Tracking errors are shown in figure 5.25. By integration, the velocity and the acceleration of the rear part of the robot could be obtained (see figure 5.26 and 5.27). Based on the velocity and the acceleration, the motor power used for actuating the robot was calculated and compared with the desired motor in figure 5.28.

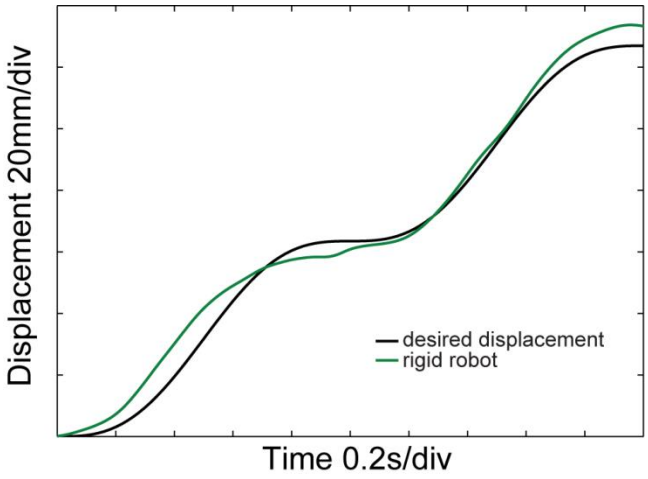

Figure 5.24 Comparison of the displacement of the rigid robot

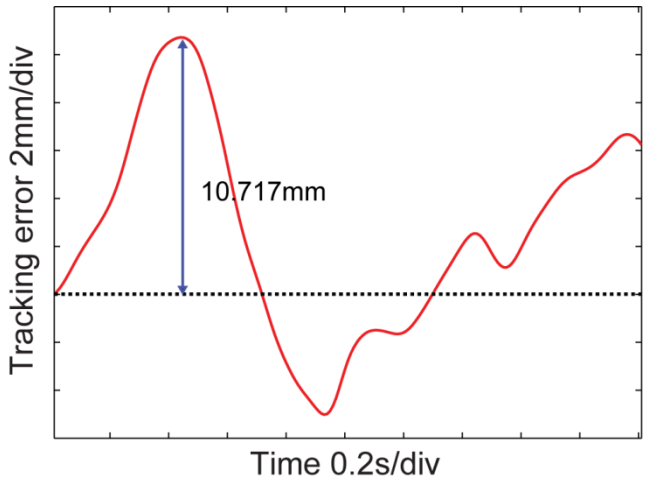

Figure 5.25 Tracking errors of the rigid robot

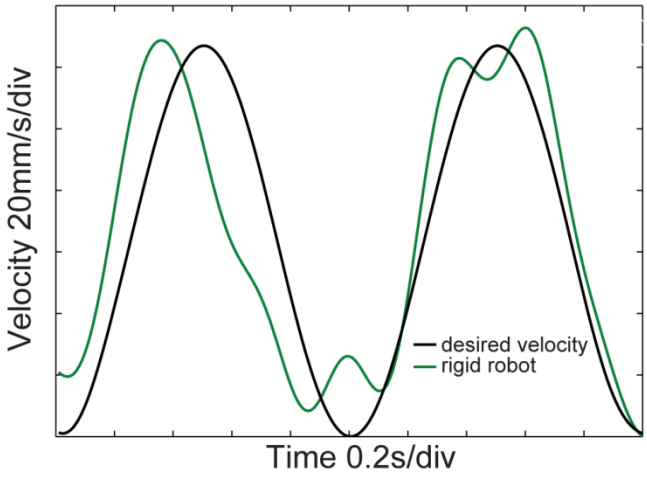

Figure 5.26 Comparison of the velocity of the rigid robot

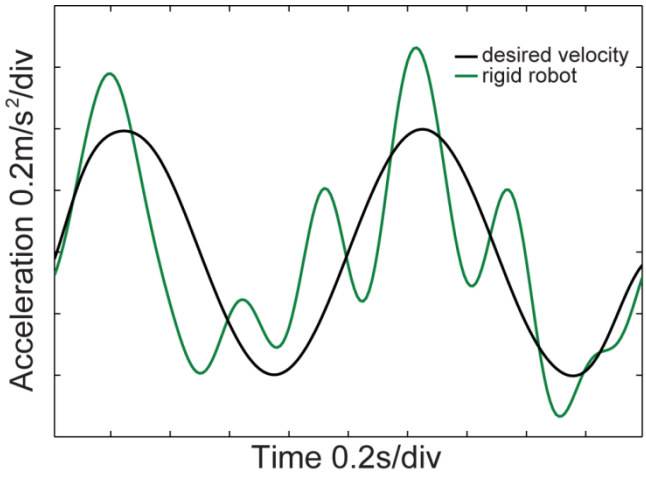

Figure 5.27 Comparison of the acceleration of the rigid robot

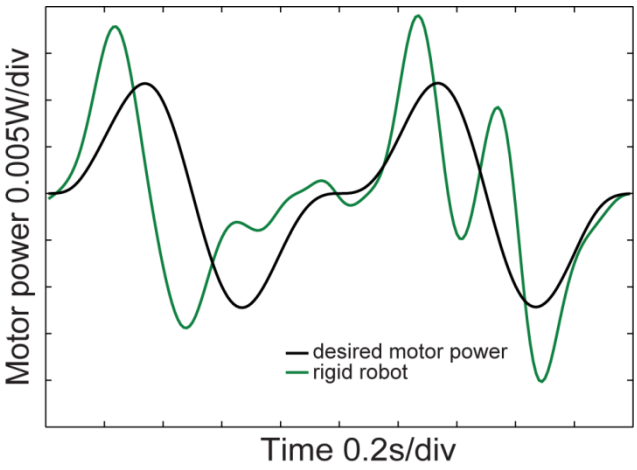

Figure 5.28 Comparison of the motor power of the rigid robot

In figure 5.24, the actual displacement has the similar variation tendency compared with the desired displacement. And the fluctuation of tracking errors is not so violent. The maximum tracking error is 10.717mm, which is acceptable. Compared with the desired velocity and the desired acceleration, the actual velocity and the actual acceleration fluctuate more frequently. Both peak values are larger than the desired peak values. So the actual peak power of the motor is larger the desired peak power.

5.4.2.2 The flexible robot (k=60N/m)

The flexible robot was programmed to follow the same desired trajectory. For this flexible robot, the displacement of both parts was recorded. Figure 5.29 illustrates the comparison of the actual displacement of the front part with the desired displacement in the y-axis. Tracking errors are shown in figure 5.30. Figure 5.31 illustrates the comparison of the actual displacement of the rear part with the desired displacement in the y-axis. Tracking errors are shown in figure 5.32. Only the rear part's velocity and acceleration are needed in this research. By integration, the velocity and the acceleration of the rear part of the flexible robot could be obtained. In figure 5.33, the actual velocity of the flexible robot is compared with the desired velocity and the velocity of the rigid robot. In figure 5.34, the actual acceleration of the flexible robot is compared with the desired acceleration and the acceleration of the rigid robot. Based on the velocity and the acceleration, the motor power used for actuating the flexible robot was calculated, which is compared with the desired motor power and the motor power of the rigid robot in figure 5.35.

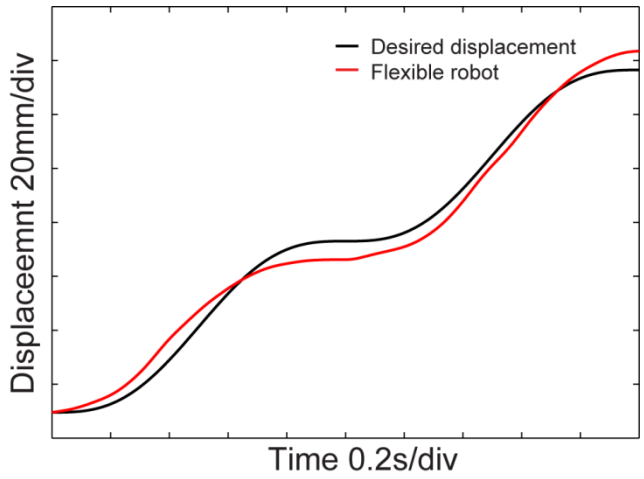

Figure 5.29 Comparison of the displacement of the flexible robot's front part

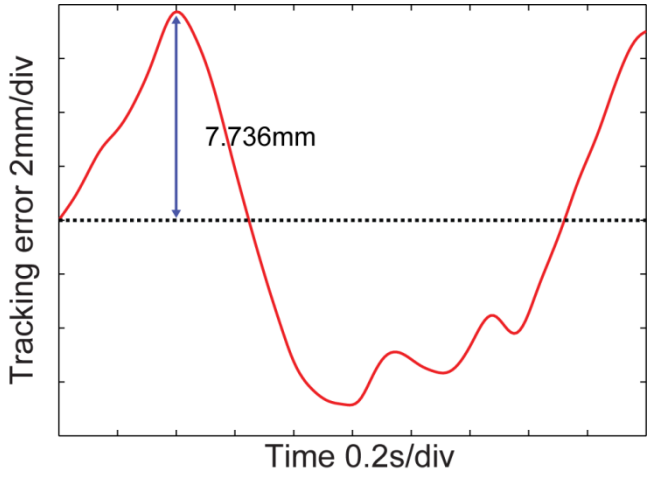

Figure 5.30 Tracking errors of the flexible robot's front part

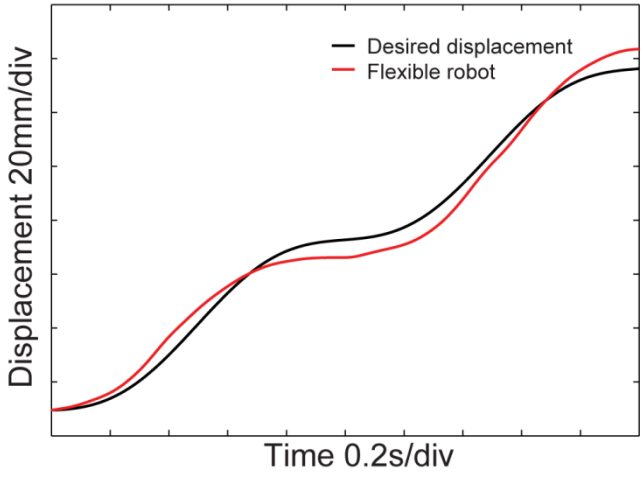

Figure 5.31 Comparison of the displacement of the flexible robot's rear part

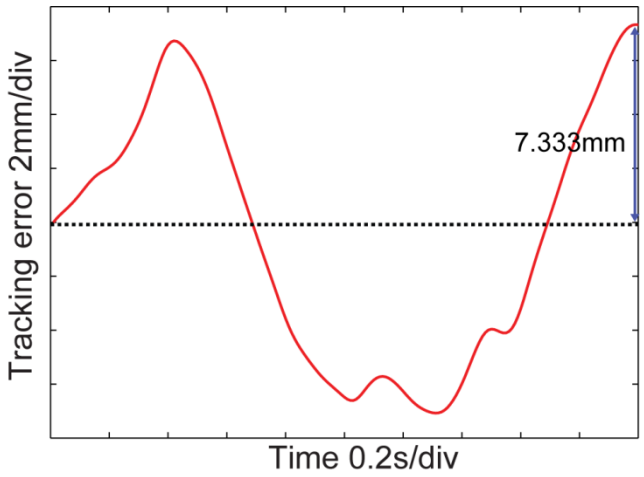

Figure 5.32 Tracking errors of the flexible robot's rear part

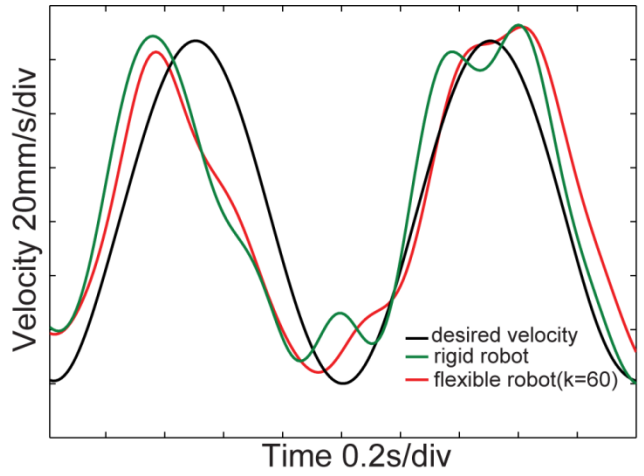

Figure 5.33 Comparison of the velocity of the flexible robot

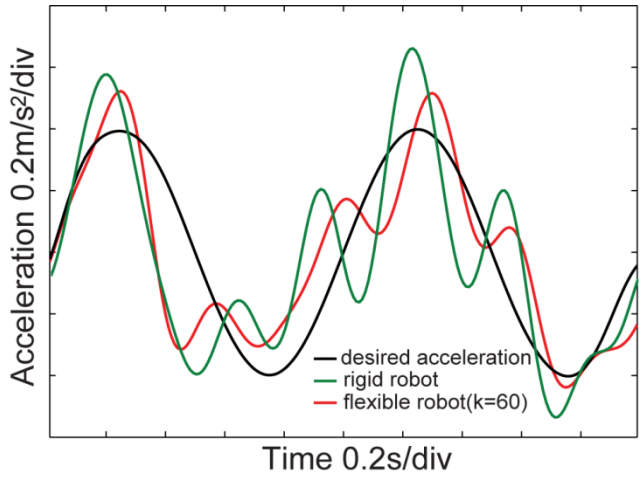

Figure 5.34 Comparison of the acceleration of the flexible robot

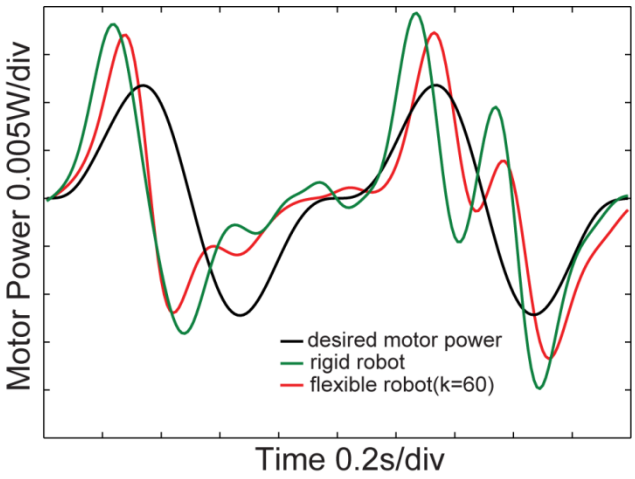

Figure 5.35 Comparison of the motor power of the flexible robot

From figures 5.29-32, we can find that both parts of the flexible are able to follow the desired trajectory respectively. Both maximum tracking errors are smaller than that of the rigid robot. So the flexible robot (k=60) has a better performance than the rigid robot at the frequency of 1 Hz. Figure 5.33 illustrates the desired velocity, the velocity of the rigid robot and the velocity of the flexible robot (k=60N/m). Waveforms of these three velocities are similar and their peak values are nearly the same. Figure 5.34 shows the desired acceleration, the acceleration of the rigid robot and the acceleration of the flexible robot (k=60N/m). Waveforms of the acceleration of the rigid robot and the flexible robot (k=60N/m) are similar, which fluctuate more frequently than the desired acceleration. The peak value of the flexible robot's acceleration is larger than that of the desired acceleration, but smaller than that of the rigid robot's acceleration. The desired motor power, the motor power of the rigid robot and the motor power of the flexible robot are compared in figure 5.35. The peak power of the flexible robot is smaller than that of the rigid robots, which is consistent with the simulation result and verify my hypothesis.

5.4.2.3 The flexible robot (k=160N/m)

This flexible robot was programmed to follow the same desired trajectory. Experiments and analysis on this robot are similar to those on the flexible robot (k=60N/m). Experimental results are shown in figures 5.36-42.

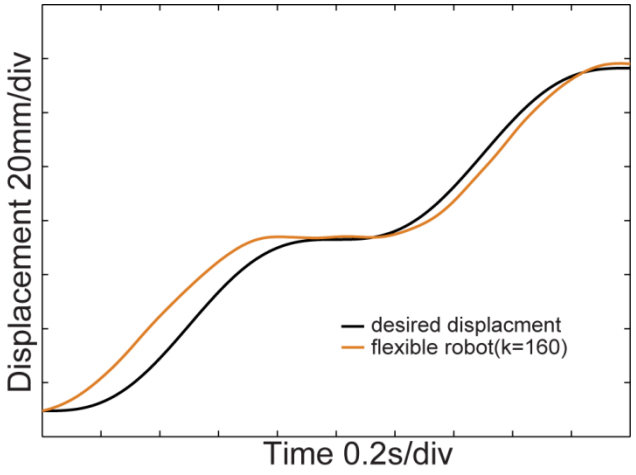

Figure 5.36 Comparison of the displacement of the flexible robot's front part

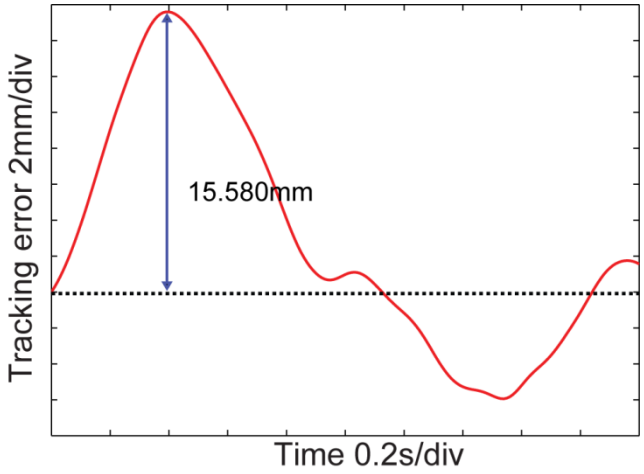

Figure 5.37 Tracking errors of the flexible robot's front part

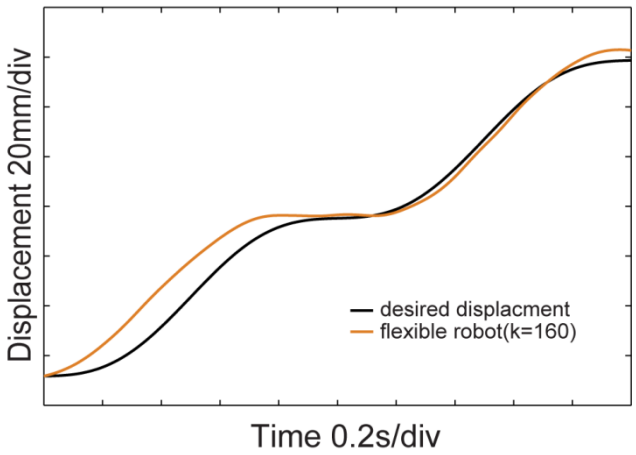

Figure 5.38 Comparison of the displacement of the flexible robot's rear part

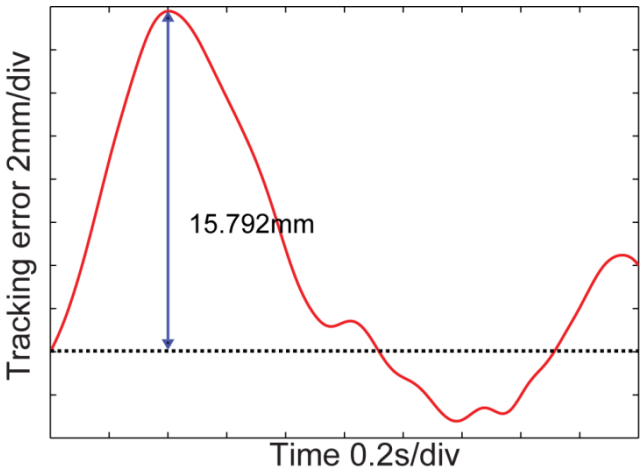

Figure 5.39 Tracking errors of the flexible robot's rear part

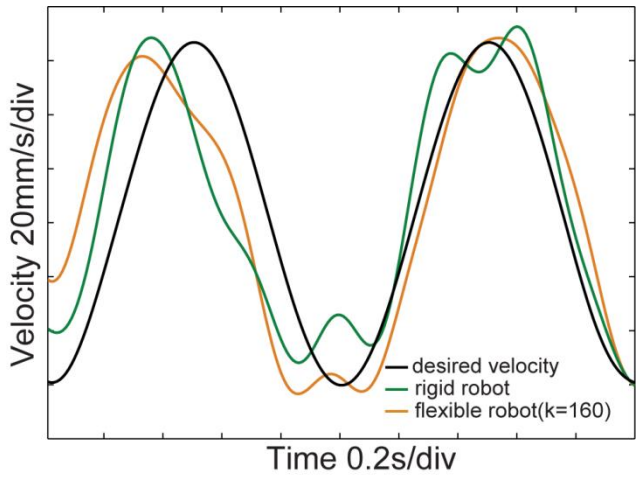

Figure 5.40 Comparison of the velocity of the flexible robot

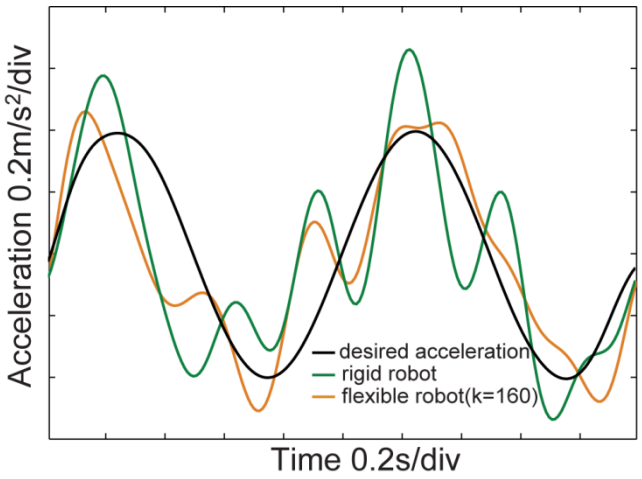

Figure 5.41 Comparison of the acceleration of the flexible robot

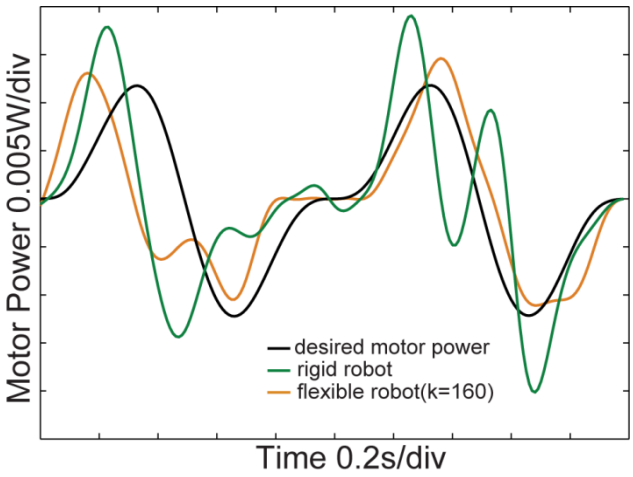

Figure 5.42 Comparison of the motor power of the flexible robot

From figures 5.36-39, we can find that both parts of the flexible robot are able to follow the desired trajectory respectively. While both maximum tracking errors are larger than that of other two robots, the performance of this robot is acceptable. Figure 5.40 illustrates the desired velocity, the velocity of the rigid robot and the velocity of the flexible robot (k=160N/m). Waveforms of these three velocities are similar and their peak values are nearly the same. Figure 5.41 shows the desired acceleration, the acceleration of the rigid robot and the acceleration of the flexible robot (k=160N/m). Waveforms of the acceleration of the rigid robot and the flexible robot (k=160N/m) are similar, which fluctuate more frequently than the desired acceleration. The peak value of the flexible robot's acceleration is similar to that of the desired acceleration, and smaller than that of the rigid robot's acceleration. The desired motor power, the motor power of the rigid robot and the motor power of the flexible robot are compared in figure 5.35. The peak power of this flexible robot is smaller than that of the rigid robots, which is consistent with the simulation result and verify my hypothesis.

5.5 Discussion

From a series of kinematic experimental results, it can be seen that the robot has a better performance when the velocity is uniform. Under the condition of uniform velocities, the curve of the actual displacement and the curve of the desired displacement are nearly coincident. All maximum tracking errors are less than 5% of their total displacement. And offsets in the x-axis are all less than 6mm. Taking into account machining errors, assembly errors, measurement errors and the performance of the motor, these tracking errors and offsets are acceptable. When the velocity is variable, the performance of the robot is not so

good compared with the performance under the condition of uniform velocities. Additionally, with the increasing of the frequency, the curve of the actual displacement becomes closer to a straight line, which can also be indicated from tracking errors. With the increasing of the frequency, the waveform of tracking errors fluctuates more violently and the maximum tracking error grows exponentially. Only when the frequency equals 1Hz, the performance of the robot is acceptable. And from simulation results, we can find that the reducing of the motor power is not obvious at lower frequencies. So the kinetic experiments were conducted at the frequency of 1Hz.

For kinetic experiments, all three kinds of robots follow a same trajectory. Figure 5.43 shows the comparison of the desired displacement with the displacement of three different robots. As shown in the figure, these three robots can achieve similar displacements.

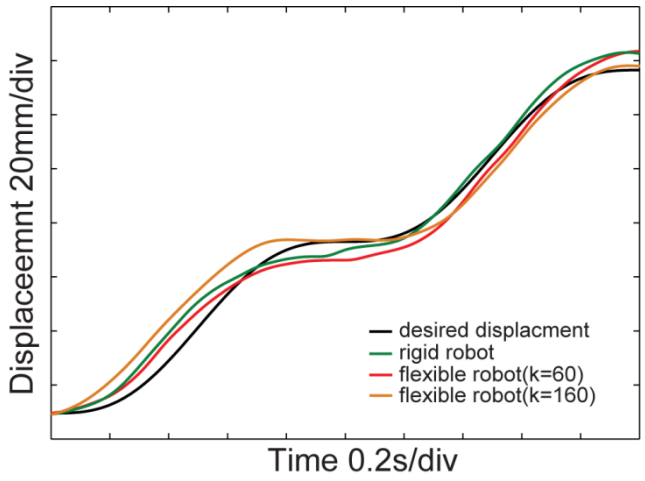

Figure 5.43 Comparison of the desired displacement with the displacement of three robots

Figure 5.44 and 5.45 illustrate velocities and accelerations of the rear part of different robots. As illustrated in figures, different trunks result in different velocities and accelerations. However, the degree of influence of different trunks on velocities and accelerations of the rear part is different. In figure 5.44, waveforms and peak values of the velocity of different robots' rear parts are similar. As a result, we get the conclusion that different trunks have little influence on the velocity of rear parts of different robots. In figure 5.45, we can find that waveforms of the acceleration of robots' rear parts fluctuate more frequently compared with the desired acceleration, which is due to the accuracy and resolution of the motor. Increasing the accuracy and resolution of the motor, the fluctuation of the waveform can be reduced. Their overall variation tendencies are similar. As to the peak value, different trunks have different influence on them. From figure 5.46, we can find that both flexible trunks have

effects on reducing the peak power of the motor. And when the stiffness of the trunk equals 160 N/m, the trunk plays a greater role in reducing the peak power, which verifies my simulation result that different trunks have different effects on reducing peak powers at the same frequency.

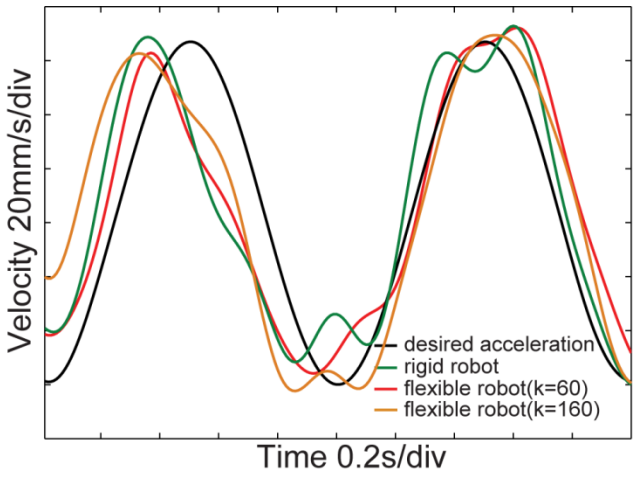

Figure 5.44 Comparison of the desired displacement with the displacement of three robots

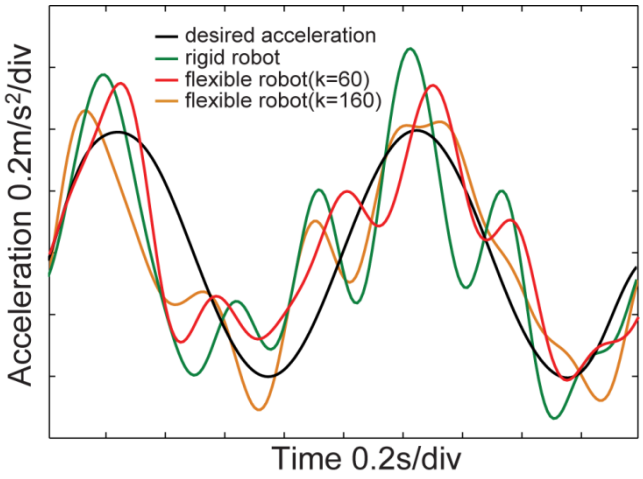

Figure 5.45 Comparison of the desired velocity with the velocity of three robots

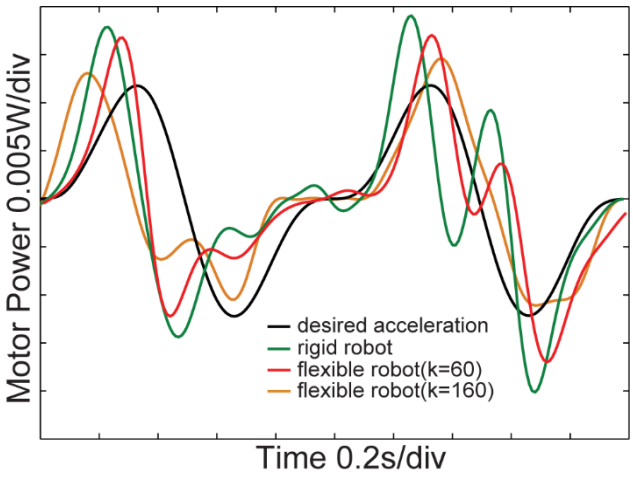

Figure 5.46 Comparison of the desired acceleration with the acceleration of three robots

5.6 Conclusion

Experiments have succeeded in evaluating the performance of the designed robot and verifying the hypothesis. From kinematic results, we can get the conclusion that the designed robot has a better performance when the velocity is uniform. From kinetic results, we can get the conclusion that robots with different trunks have different motor powers when achieving the similar locomotion. Flexible trunks are capable of reducing the peak power of the motor. Additionally, different flexible trunks have different effects. For this robot, when the stiffness of the trunk equals 160 N/m, the reducing of the motor's peak power is more obvious. By comparing velocities and accelerations of different robots, we can find that flexible trunks are able to reduce the peak vale of both the velocity and the acceleration. But the reduction rates of both peak values are different. Flexible trunks have greater influence on the acceleration.

Chapter 6 Conclusion and recommendations

6.1 Conclusion

This research aims at finding solutions from the nature to improve mobile robots' energy efficiency. Different from other researches, this research focuses on studying effects of flexible trunks on energetically efficient locomotion. By simulation analysis, robot design, and experimental verification, this research verifies the hypothesis that flexible trunks do have effects on improving energy efficiency in terms of reducing the peak power.

Lizards are a kind of animals whose locomotion involves the movement of their flexible trunks. Inspired by lizards, a simplified model has been established. And some simulations based on this model have been performed under three conditions: the trunk is rigid, the trunk is flexible but without any damping, the trunk is flexible and the damping is given. From simulation results of the latter two conditions, we can find that the damping can't change the variation tendency of results. The damping only changes the magnitude of the optimized frequencies or the optimized stiffness. From overall simulation results, we can see that flexible trunks do have effects on improving energy efficiency in terms of reducing the peak power of the motor. And the frequency of the desire locomotion and the stiffness of the trunks are two key factors which influence the reduction rate of the peak power. At the same frequency, trunks with different stiffness result in different peak powers. With the increasing stiffness, the variation tendency of the peak power is similar. When the stiffness is very small, the peak power of the motor can be extremely high. When the stiffness increases, the peak power will rapidly reduce to the minimum and then raise gain to get close to a horizontal asymptote. For each frequency, there always exits an optimized stiffness, with which the trunk can reduce the peak power to the minimum. With the same trunk, the robot running at different frequencies has different effects on the peak power of the motor. With the increasing frequency, the variation tendency of the reduction rate of the motor's peak power is similar. The reduction rate will rise to the maximum and then decrease. For each stiffness, there always exists an optimized frequency, at which the robot is able to have the maximum reduction rate of the peak power.

In order to verify the hypothesis and simulation results, a bio-inspired lizard robot was necessary. After comparing several designs, the final design had advantages in feasibility, simplicity and similarity to the simulation model. 3D printing was selected as the

manufacturing method to make the prototype. All components have been selected carefully based on the principle of cost-effect. Both hardware and software architectures have been established.

Experiments, goals of which were to evaluate the performance of the robot under different conditions and verify both the hypothesis and part of simulation results, have been carried out utilizing the motion capture system. Displacement of both parts of robots with three different kinds of trunks (rigid, stiffness equals 60N/m, and stiffness equals 160N/m) was recorded. After calculating velocities and accelerations, motor powers could be obtained. From the kinematics results, it can be seen that the robot is able to follow a desired trajectory and move along a straight line when the velocity is uniform. When the velocity is variable, the robot can only have acceptable performance at the frequency of 1Hz. As a result, kinetic experiments were conducted at the frequency of 1Hz. Robots with three kinds of trunks respectively followed the same desired trajectory. From results, we can find that flexible trunks do have effects on improving robots' energy efficiency in terms of reducing the peak power of the motor, which verify the hypothesis. Additionally, different flexible trunks result in different motor powers. The reduction rates are different because of the stiffness, which is consistent with simulation results.

6.2 Recommendations

While this research successfully achieves the desired objectives, there are still some aspects needed to be improved.

The control strategy used in this research is an open loop control strategy, by which the robot is able to follow some desired trajectories and move along a straight line. However, this robot doesn't have the ability to respond to changes in the external environment. So this robot can't work in unknown environments. In order to make the robot possess abilities to work in complex environments, more sophisticated close loop control strategies are necessary. Additionally, close loop control strategies can effectively reduce tracking errors.

Hardware also has much room for improvement. Limited by the resolution and accuracy of the motor, this robot can only follow restricted trajectories. Thus only part of simulation results has been verified. For the purpose of making the research more complete, high-performance motors are required to replace the existing motor. Besides that, the controller

and power supply are off board, which restrict applications of the robot in other areas. Compact electrical components are needed to make the robot complete more tasks.

The ultimate goal of this research is to apply findings to practical use. In this research, flexible trunks have been proved to have effects on improving energy efficiency and each frequency has its own optimized stiffness. If the robot can change its trunk's stiffness to the optimized stiffness according to the frequency of the locomotion, the robot can achieve best energy optimization. Designing a robot, the stiffness of whose trunk can be automatically adjusted to the optimum under different conditions, is surely a very interesting and challenging topic.

Bibliography

1. Pfeifer, R., M. Lungarella, and F. Iida, *Self-organization, embodiment, and biologically inspired robotics.* science, 2007. **318**(5853): p. 1088-1093.
2. Pfeifer, R., M. Lungarella, and F. Iida, *The challenges ahead for bio-inspired'soft'robotics.* Communications of the ACM, 2012. **55**(11): p. 76-87.
3. Altendorfer, R., et al., *RHex: a biologically inspired hexapod runner*. Autonomous Robots, 2001. **11**(3): p. 207-213.
4. Fukuoka, Y., H. Kimura, and A.H. Cohen, *Adaptive dynamic walking of a quadruped robot on irregular terrain based on biological concepts.* The International Journal of Robotics Research, 2003. **22**(3-4): p. 187-202.
5. Sprö witz, A., et al., *Towards dynamic trot gait locomotion: Design, control, and experiments with Cheetah-cub, a compliant quadruped robot.* The International Journal of Robotics Research, 2013. **32**(8): p. 932-950.
6. Eilam, D., *Comparative morphology of locomotion in vertebrates.* Journal of motor behavior, 1995. **27**(1): p. 100-111.
7. Ritter, R., *Lateral bending during lizard locomotion.* Journal of Experimental Biology, 1992. **173**(1): p. 1-10.
8. Edwards, J.L., *The evolution of terrestrial locomotion*, in *Major patterns in vertebrate evolution*1977, Springer. p. 553-577.
9. Jenkins, F.A. and G. Goslow, *The functional anatomy of the shoulder of the savannah monitor lizard (Varanus exanthematicus).* Journal of Morphology, 1983. **175**(2): p. 195-216.
10. Snyder, R.C., *Quadrupedal and Bipedal Locomotion of Lizards.* Copeia, 1952(2): p. 64-70.
11. Irschick, D.J. and B.C. Jayne, *Comparative three-dimensional kinematics of the hindlimb for high-speed bipedal and quadrupedal locomotion of lizards.* Journal of Experimental Biology, 1999. **202**(9): p. 1047-1065.
12. Avery, R., et al., *The movement patterns of lacertid lizards: speed, gait and pauses in Lacerta vivipara.* Journal of Zoology, 1987. **211**(1): p. 47-63.
13. Aerts, P., et al., *Lizard locomotion: how morphology meets ecology.* Netherlands Journal of Zoology, 2000. **50**(2): p. 261-277.
14. Libby, T., et al., *Tail-assisted pitch control in lizards, robots and dinosaurs.* Nature, 2012. **481**(7380): p. 181-184.
15. Jusufi, A., et al., *Righting and turning in mid-air using appendage inertia: reptile tails, analytical models and bio-inspired robots.* Bioinspiration & biomimetics, 2010. **5**(4): p. 045001.
16. Chang-Siu, E., et al. *A lizard-inspired active tail enables rapid maneuvers and dynamic stabilization in a terrestrial robot*. in *Intelligent Robots and Systems (IROS), 2011 IEEE/RSJ International Conference on*. 2011. IEEE.
17. Carlo, M. and S. Metin, *A biomimetic climbing robot based on the gecko.* Journal of Bionic Engineering, 2006. **3**(3): p. 115-125.
18. Menon, C., M. Murphy, and M. Sitti. *Gecko inspired surface climbing robots*. in *Robotics and Biomimetics, 2004. ROBIO 2004. IEEE International Conference on*. 2004. IEEE.
19. Unver, O., et al. *Geckobot: a gecko inspired climbing robot using elastomer adhesives*. in *Robotics and Automation, 2006. ICRA 2006. Proceedings 2006 IEEE International Conference on*. 2006. IEEE.

20. Floyd, S., et al. *A Novel Water Running Robot Inspired by Basilisk Lizards*. in *IROS*. 2006.
21. Floyd, S. and M. Sitti, *Design and development of the lifting and propulsion mechanism for a biologically inspired water runner robot.* Robotics, IEEE Transactions on, 2008. **24**(3): p. 698-709.
22. Qian, F., et al., *Walking and running on yielding and fluidizing ground.* 2012.
23. Li, C., T. Zhang, and D.I. Goldman, *A terradynamics of legged locomotion on granular media.* science, 2013. **339**(6126): p. 1408-1412.
24. Zhang, T., et al., *Ground fluidization promotes rapid running of a lightweight robot.* The International Journal of Robotics Research, 2013. **32**(7): p. 859-869.
25. Khoramshahi, M., et al., *Piecewise linear spine for speed–energy efficiency trade-off in quadruped robots.* Robotics and Autonomous Systems, 2013. **61**(12): p. 1350-1359.
26. Kani, M.H.H., et al. *Effect of flexible spine on stability of a passive quadruped robot: Experimental results*. in *Robotics and Biomimetics (ROBIO), 2011 IEEE International Conference on*. 2011. IEEE.
27. Bidgoly, H.J., et al. *Learning approach to study effect of flexible spine on running behavior of a quadruped robot*. in *Proceeding of International Conference on Climbing and Walking Robots*. 2010.
28. Pouya, S., et al. *Role of spine compliance and actuation in the bounding performance of quadruped robots*. in *7th Dynamic Walking Conference*. 2012.
29. Culha, U. and U. Saranli. *Quadrupedal bounding with an actuated spinal joint*. in *Robotics and Automation (ICRA), 2011 IEEE International Conference on*. 2011. IEEE.
30. Chen, D., et al., *Effect of spine motion on mobility in quadruped running.* Chinese Journal of Mechanical Engineering, 2014. **27**(6): p. 1150-1156.
31. Khoramshahi, M., et al. *Benefits of an active spine supported bounding locomotion with a small compliant quadruped robot*. in *Proceedings of 2013 IEEE International Conference on Robotics and Automation*. 2013.
32. Kani, M.H.H. and M. Nili Ahmadabadi. *Comparing effects of rigid, flexible, and actuated series-elastic spines on bounding gait of quadruped robots*. in *Robotics and Mechatronics (ICRoM), 2013 First RSI/ISM International Conference on*. 2013. IEEE.
33. Ijspeert, J.B.A.J. *A simple, adaptive locomotion toy-system*. in *From Animals to Animats 8: Proceedings of the Seventh [ie Eighth] International Conference on Simulation of Adaptive Behavior*. 2004. MIT Press.
34. Taylor, D.C., et al., *Viscoelastic properties of muscle-tendon units the biomechanical effects of stretching.* The American journal of sports medicine, 1990. **18**(3): p. 300-309.
35. Biewener, A., *Tendons and ligaments: structure, mechanical behavior and biological function*, in *Collagen*2008, Springer. p. 269-284.

Appendix A: Parameters of some robot parts

1 Servo motors

Table A1 Datasheet of SC-1251MG

Dimensions(mm):	40.8*20.2*25.4
Weight(g):	44.6
Speed(@4.8V sec/60):	0.10
Torque(@4.8V kg-cm):	7
Speed(@6V sec/60):	0.09
Torque(@6V kg-cm):	9
Gear:	Metal
Control system:	Pulse width modification
Amplifier type:	Digital controller
Pulse width range(μsec):	700-2300
Dead band width(μsec):	5
Operating travel:	100°

Table A2 Datasheet of ES09MD

Dimensions(mm):	23.0*12.0*24.5
Weight(g):	14.8
Speed(@4.8V sec/60):	0.10
Torque(@4.8V kg-cm):	2.3
Speed(@6V sec/60):	0.08
Torque(@6V kg-cm):	2.6
Gear:	Metal
Control system:	Pulse width modification
Amplifier type:	Digital controller
Pulse width range(μsec):	1100-1900
Dead band width(μsec):	5
Operating travel:	80°

2 Linear guide

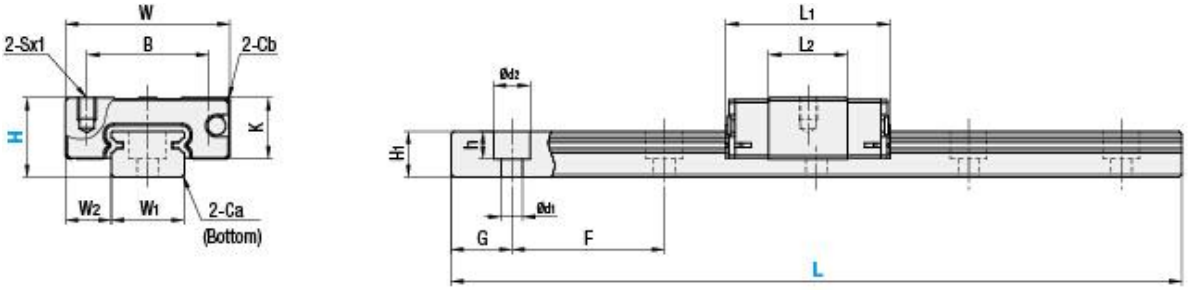

Figure A1 CAD drawing of the linear guide

Table A3 Dimensions of the linear guide

Block dimensions(mm)							
H	**W**	**L1**	**B**	**S×l**	**L2**	**K**	**Cb**
8	17	19.6	12	M2×2.5	9.6	6.5	0.3
Guide rail dimensions(mm)							
L	**W1**	**W2**	**H1**	**Ca**	**d1*d2*h**	**F**	**G**
100	7	5	4.7	0.3	2.4×4.2×2.3	15	5

3 linear springs

Table A4 Datasheet of two springs

WIRE DIAMETER	OUTSIDE DIAMETER	INSIDE DIAMETER	FREE LENGTH	MATERIAL	APPROX LOAD	SPRING RATE
0.50mm	10.30mm	9.30mm	50.00mm	Stainless steel	0.275kg	60N/m
0.60mm	8.60mm	7.40mm	50.80mm	Stainless steel	0.620kg	160N/m

Appendix B: Snapshots of the robot

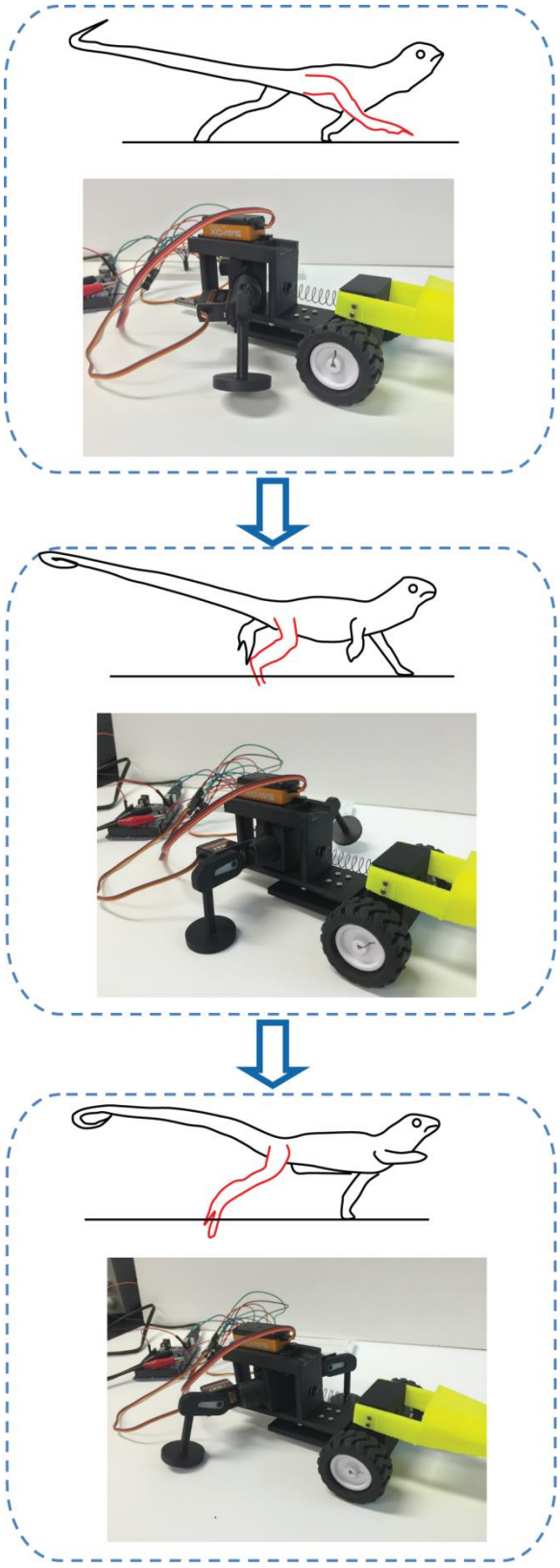

Figure B1 The propulsive stroke

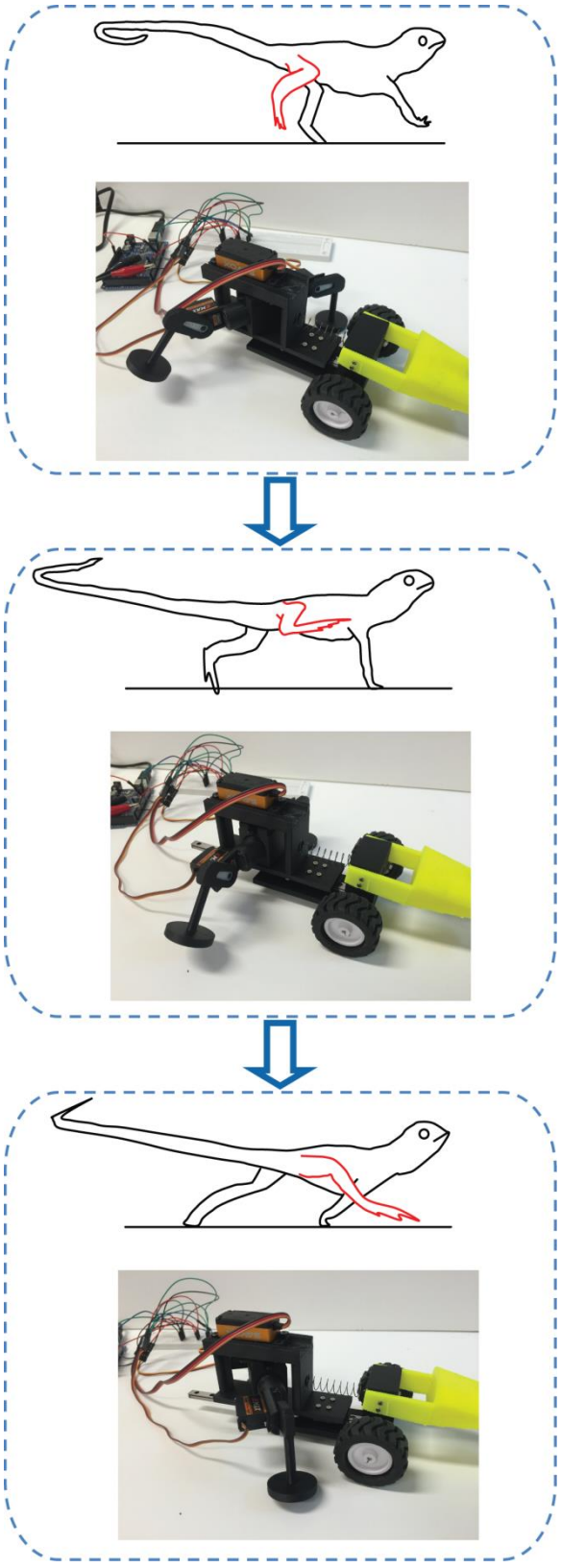

Figure B2 The recovery stroke